BERICHTE
aus dem Fachbereich Geowissenschaften
der Universität Bremen

No. 284

Kopf, A., C. Bartsch, J. Castellino, T. Fleischmann, S. Haas, C. Ioakim, K. Kirsch, S. Kufner, A. Steiner, M. Tryon, G. Wiemer, M. Zabel

REPORT AND PRELIMINARY RESULTS OF RV POSEIDON CRUISE P410: MUDFLOW (Mud volcanism, Faulting and Fluid Flow on the Mediterranean Ridge Accretionary Complex), Heraklion / Greece, 12.03.2011 – Taranto / Italy, 01.04.2011.

Berichte, Fachbereich Geowissenschaften, Universität Bremen, No. 284, 128 pages, Bremen 2012

ISSN 0931-0800

BERICHTE
aus dem Fachbereich Geowissenschaften
der Universität Bremen

No. 284

Kopf, A., C. Bartsch, J. Castellino, T. Fleischmann, S. Haas, C. Ioakim, K. Kirsch, S. Kufner, A. Steiner, M. Tryon, G. Wiemer, M. Zabel

REPORT AND PRELIMINARY RESULTS OF RV POSEIDON CRUISE P410: MUDFLOW (Mud volcanism, Faulting and Fluid Flow on the Mediterranean Ridge Accretionary Complex), Heraklion / Greece, 12.03.2011 – Taranto / Italy, 01.04.2011.

Berichte, Fachbereich Geowissenschaften, Universität Bremen, No. 284, 128 pages, Bremen 2012

ISSN 0931-0800

The "Berichte aus dem Fachbereich Geowissenschaften" are produced at irregular intervals by the Department of Geosciences, Bremen University and by MARUM.

They serve for the publication of cruise reports, PhD-theses, experimental works, and scientific contributions made by members of the department.

Reports can be ordered from:

Monika Bachur

DFG-Forschungszentrum MARUM

Universität Bremen

Postfach 330 440

D 28334 BREMEN

Phone: (49) 421 218-65516

Fax: (49) 421 218-65515

e-mail: MBachur@uni-bremen.de

Citation:

Kopf, A. and cruise participants

Report and preliminary results of RV POSEIDON Cruise P410: MUDFLOW (Mud volcanism, Faulting and Fluid Flow on the Mediterranean Ridge Accretionary Complex), Heraklion / Greece, 12.03.2011 – Taranto / Italy, 01.04.2011.

Berichte, Fachbereich Geowissenschaften, Universität Bremen, No. 284, 128 pages. Bremen, 2012.

ISSN 0931-0800

Table of Contents

Preface

The expedition P410 *MUDFLOW* is associated with two third party projects funded by DFG (Deutsche Forschungs-Gemeinschaft, entitled *MUDDY WATERS*) and NSF (US National Science Foundation). The cruise and projects aim to shed light on the dynamics of faults and mud volcanoes in the landward portion of the Mediterranean Ridge accretionary complex, Hellenic subduction zone, in the Eastern Mediterranean Sea. This area is characterised by high seismicity and efficient dewatering of the deeper portion of the forearc. Numerous mud domes are found at a distance in excess of 150 km behind the deformation front in the area between Libya and Crete. They are often, if not always, associated with backthrust faults and other structural discontinuities in the backstop area south of Crete, Greece. The study is in support of an active drilling proposal with IODP (Integrated Ocean Drilling Program, proposal 555-full3), which aims at the hydrogeology of the backstop of the Hellenic subduction zone.

Among the methods utilised during *Poseidon* Leg P410 were reconnaissance multibeam site surveys to complement existing bathymetric charts by Geosciences Azur (Villefranche-sur-mer, France), *in situ* measurements to characterise the natural state of the materials near the backstop, seafloor sampling, and deployment of long-term instruments to study sedimentological and geochemical phenomena. Part of the research strategy is to place osmotically driven flowmeter systems onto the seafloor, which will be recovered appx. 12-14 months later on a second *Poseidon* cruise (*MUDMAP*) in March/April 2012, where detailed multibeam mapping, recovery of long-term flowmeter systems, and additional coring and in situ measurements are planned.

Personnel aboard R/V *Poseidon*

1. Kopf, Achim	MARUM Univ. HB
2. Bartsch, Carolin	Univ. HB
3. Castellino, Jude	Univ. HB
4. Fleischmann, Timo	Univ. HB
5. Haas, Simon	Univ. HB
6. Ioakim, Chryssanthi	IGME
7. Kirsch, Klemens	Univ. HB
8. Kufner, Sofia	Univ. HB
9. Tryon, Mike	SCRIPPS
10. Wiemer, Gauvain	MARUM Univ. HB

Shore-based contributors to this R/V *Poseidon* report

1. Steiner, Alois	MARUM Univ. HB
2. Zabel, Matthias	MARUM Univ. HB

Participating institutions

DFG-Research Centre MARUM
University Bremen
Leobener Strasse
28359 Bremen --- GERMANY

University of Bremen
Klagenfurter Strasse
28359 Bremen --- GERMANY

IGME (Institute of Geology and Mineral Exploration)
Olympic Village
13677 Achamae-Attica --- GREECE

SCRIPPS Institution of Oceanography
University of California, San Diego
9500 Gilman Drive
92093 La Jolla --- USA

Abstract

Cruise P410 on RV *Poseidon* investigated the landward portion of the modern Mediterranean Ridge accretionary complex (MedRidge), its contact towards the InnerRidge of presumed older accreted strata, and the Cretan Margin backstop. The area is characterised by prominent deep-seated faults south of Crete, many of which are superbly imaged geophysically and some overlain by mud volcanoes at their surface (i.e. seafloor) outcrop. Earlier work has suggested that evidence for fluid (and mud) ascent from several km depth near the backstop to the accretionary prism exists, so that we used various techniques to investigate this phenomenon further: multibeam reconnaissance, gravity coring, in situ T and CPTu measurements, video surveying and long-term flowmeter deployments. The key goals were to shed light on subduction factory processes and physico-chemical interaction along the fault zones.

The study area comprised (1) the mud volcanoes in the Olimpi field, (2) the inner deformation front further north (i.e. the contact between MedRidge and Inner Ridge), and (3) the region where the Inner Ridge "deformable backstop" is backthrust onto the Cretan Margin, including a few sites where faults are believed to crop out south of the island of Crete.

The main results in the three regions can be summarised as follows:

1) From the 43 gravity cores recovered, the most interesting finding is that the grey mud, mudstone and mud breccia found in the majority of the mud volcanoes, was also recovered at a few sites at the inner deformation front and the Inner Ridge/Cretan margin boundary. The grey mud, but also the hemipelagites in the latter areas show evidence of moderate to intense deformation, indicating active backthrusting as well as mobilisation of deeper clay mineral.bearing strata as a lubricant along these faults.
2) Pore water geochemistry from the cores showed interesting phenomenae, with prominent freshening in some mud volcanoes (Milano MV, Bergamo MV) and saline fluids in others (Napoli MV). The inferred deeper mud along the faults further landward showed no pore water anomalies.
3) Shear strength of the material recovered was normal except in some moussy mud dome cores where t dropped significantly. Strength was high and core recovery low where the deep-seated, indurated mud and mudstone was found.
4) CPTu data and T data mirror the findings from geochemistry regarding the active nature of some of the mud volcanoes
5) The deployment of CAT meters went smoothly and we anticipate interesting time series data of fluid flow rate and pore water compositional transients from both mud volcanoes and one site at the Inner Ridge/Cretan Margin boundary.

2. Introduction

The Mediterranean Ridge is situated in the collision zone between Eurasia and Africa, and represents the fastest growing accretionary complex on Earth (Kopf et al., 2003a). Given the proximity of the two continental plates, processes associated with the convergent dynamics are accentuated and make this area an ideal natural laboratory for ocean drilling (see Harms et al., 2007). In Section 2, the Mediterranean Ridge will be introduced in its geological setting of initiated continent-continent collission (Ch. 2.1.). The state-of-the-art of the governing processes within the subduction zone processes will be outlined (Ch. 2.2.), with particular attention to active faulting (Ch. 2.2.1.) and mud volcanism (Ch. 2.2.2.). Chapter 2.3 illustrates the objectives of the active IODP proposal in the area, which will then be related to the objectives of this cruise and post-cruise research (Ch. 2.4.) and studies carried out earlier (Ch. 2.5.).

2.1. Introduction and Geological Setting

In the Initial Science Plan (IODP, 2001; www.iodp.org/isp/), the seismogenic zone at convergent margins has been identified as a key target by the Integrated Ocean Drilling Program. However, many of the previous subduction zone drilling legs have aimed for the frontal portion of these systems, mostly penetrating the toe area or the outer forearc (e.g. Legs 31, 56, 57, 87, 110, 112, 131, 146, 156, 160, 171, 190, 196, 204, 205). Even NanTroSEIZE (Nankai Trough Seismogenic Zone Experiment), the only active seismogenic zone drilling project, is restricted to a region between the outermost accretionary complex and the Kumano forearc basin, i.e. the frontal 50 km of the overriding plate (see Tobin & Kinoshita, 2007). Neither the hinterland close to Japan nor the exhumed Shimanto Belt accretionary complex are targeted, the latter as a result of its onshore setting (Underwood, 1993). The lack of the fundamental understanding of the geodynamic processes and physico-chemical interplay along fault zones in the area where the mechanical abutment to the accretionary complex, the so-called backstop is situated, has been the main motivation for both IODP proposal 555-full3 (Kopf et al., 1999) and this proposal. The area to be targeted is the Mediterranean Ridge accretionary complex (hereafter occasionally abbreviated as MedRidge), or more generally, the Hellenic subduction zone (HSZ).

In addition to seismogenesis along faults, which may cause a severe geohazard (e.g. megathrust earthquakes, subsequent landslides and tsunamis) and hence pose a considerable threat onto society, subduction zones are the loci of very important mass balance processes. While the downgoing plate is dewatered and altered by increasing pressure (P) and temperature (T), other constituents may be desorbed from clay, released during diagenetic and metamorphic reactions and mineral transformations, or finally melted at greater depth. Even at shallow levels, significant transfer is taking place between the hydrosphere and lithosphere (often summarised as fluid-rock interaction as

well as compaction-driven fluid release). At depth, partial melting, devolatilisation and associated processes may cause either ascent of the material towards the volcanic arc, recycling of the material in the mantle, or a combination of the two. As a consequence, this so-called big loop in the subduction factory involves the atmosphere (through volcanic degassing), lithosphere (through magma production at the colcanic arc and back-arc, as well as the asthenosphere (mantle recycling) into the mass transfer processes (see Fig. 1). The subduction zone hence provides an idiosyncratic chemical filter between surface and deep Earth reservoirs, which preferentially allows or disallows deep subduction of volatile and non-volatile components. Although there exist estimates regarding the masses and composition of downgoing materials (i.e. sediment, pore fluid, altered oceanic crust), the chemical fluxes resulting as a function of PT increase down the slab are poorly understood and rarely constrained quantitatively. With this proposal, we solicit a controlled approach of *in situ* measurements, some long-term, state-of-the-art hydrothermal deformation tests and modelling of results from the two in order to come up with a generic physico-chemical model for the HSZ forearc domain using numerical codes.

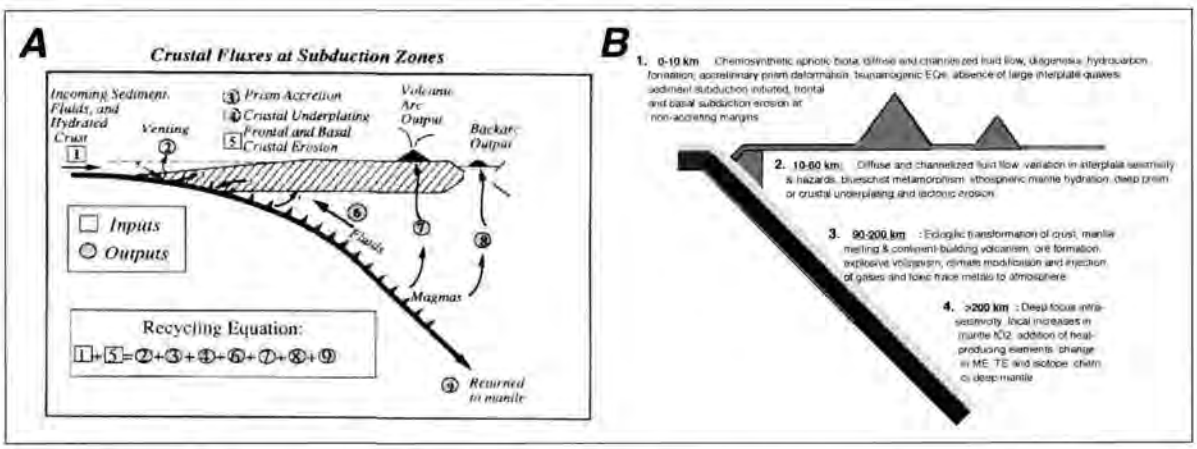

Figure 1: **a**) Schematic diagram of a subduction zone, with inputs and outputs being shown as white squares and grey dots, respectively. The three major loops in the subduction factory are #2 (the small loop with dewatering at the forearc toe and shallow subduction zone), #6 (the intermediate loop characterised by diagenetic and low-grade metamorphic processes driving deep-seated fluid release, mineral transformation, etc.), and #7-9 (the big loop with metamorphic processes and melting at high PT, causing devolatilisation and ascent of subducting materials to the volcanic arc and back-arc, as well as recycling of some components into the mantle. Figure **b**) relates these processes to depth (from Scholl et al., 1994).

The evolution of the backstop setting near Crete was summarised by Thomson et al. (1998) and Robertson & Kopf (1998), and is revisited here only very briefly. After closure of the Mesozoic Pindos Ocean to the north, sedimentary units underwent rapid subduction to approximately 35 km depth, followed by HP/LT metamorphism, and then exhumation (Thomson et al., 1998). After slab breakoff, buoyant sedimentary units underthrust the nappe pile of Crete along a shallow-dipping detachment fault, associated with tectonic uplift and formation of a forearc high which then acted as an initial 'rigid' backstop to sediment being offscraped from the Neotethyan seafloor (proposed IODP site BUTT1). Plate kinematic reconstruction suggests trench "roll-back" and accretion of a wide

accretionary prism at the leading edge of the Eurasian Plate, whilst the forearc of Crete underwent extensional deformation during the Neogene (e.g. Meier et al., 2007). This very forearc allowed accretion to be initiated some 19 Ma before present (Kopf et al., 2003a). At some stage during the Pliocene, the proto-MedRidge had undergone considerable dewatering, and this, in turn, acted as the second phase backstop ('deformable' backstop, c.f. the 'rigid', initial backstop of Cretan nappes) to the present-day accretionary prism (proposed IODP site BUTT2). Accretion was possibly accentuated after the early Miocene, in conjunction with southward "roll-back" of the Aegean arc and regional back-arc extension (e.g. Kastens, 1991). Accreted lithologies are assumed to have constructed the bulk of the northern part of the MedRidge near the backstop (proposed IODP site BUTT3). In the late Miocene (Messinian), the deep Mediterranean was overlain by thick evaporites (e.g. Ryan et al., 1973), while topographic highs between Lybia and Crete apparently remained free of salt (Chaumillon & Mascle, 1997). From the Messinian to present, the MedRidge is being thrust over its backstop domain due to incipient continental collision (Figs. 2 and 3). In the process, the backstop is faulted, and fluid flow occurs along active backthrusts and out-of-sequence-thrusts (OOSTs).

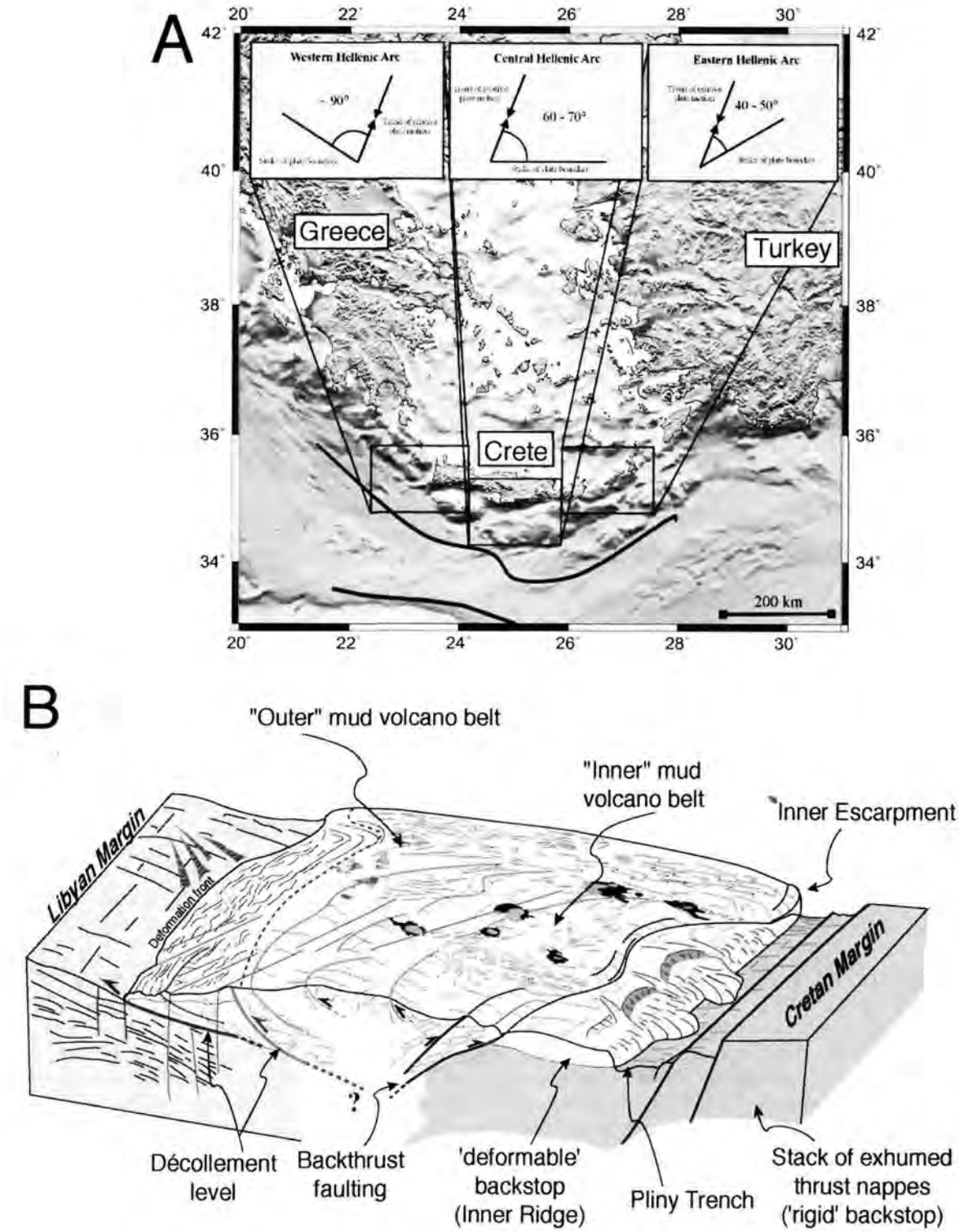

Figure 2: **a)** Location map showing the Hellenic subduction zone (HSZ) in the Eastern Mediterranean, including plate convergence vector and stress regimes along strike. **b)** Schematic block diagram of the MedRidge bordered by the Lybian margin in the south (left) and the Cretan Margin in the north (right). Green and orange pie-shaped features illustrate the occurrence of mud volcanoes. Note deep-seated faults beneath the prism and backstop.

The main features of a N-S traverse of the MedRidge and its backstop to the N are shown in Figure 2, from the North African passive margin, over a broad accretionary complex (ca. 100-120 km) and its backstop (ca. 80 km), across the forearc (Crete and adjacent islands), and the arc (e.g. Santorini), to the Aegean Sea back-arc basin. The MedRidge backstop domain is located 100-170 km behind the

deformation front, and shows an increasing northward increase in the thickness of the overriding forearc wedge/buttress (4 - >7km bsf). From MCS data, the intensity of deformation and compaction increase considerably at the transition from prism (ca. 100 km) to the Inner Ridge (ca. 150 km) behind the deformation front. Further north in the continental Cretan backstop, reverse, out-of-sequence thrusting is observed.

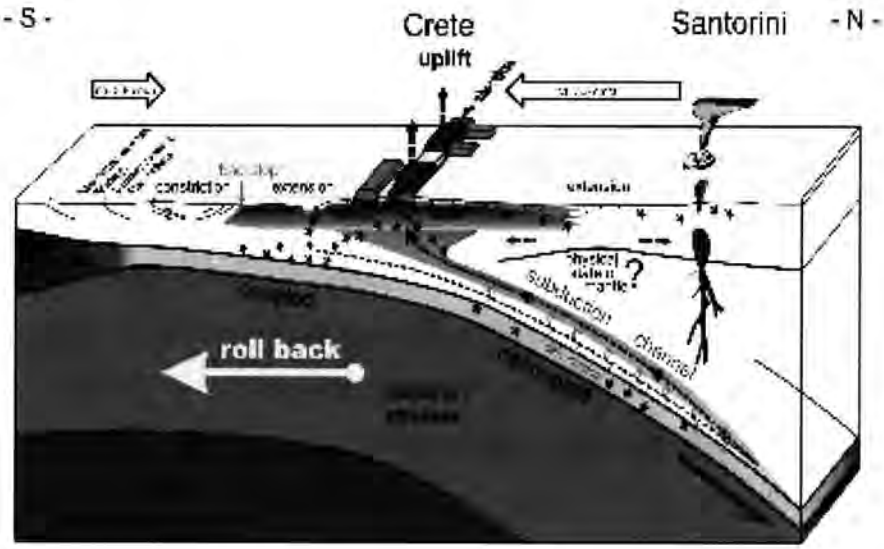

Figure 3: Schematic 3D drawing of the HSZ including the proposed pathway of hydrated mantle material, which accounts for the current uplift of Crete (see Meier et al., 2007 for details) and also which further favours migration of deep-seated fluids into the area of proposed drilling at the backstop.

The backstop of the MedRidge is located along the northern margin of a large accretionary prism created by Neogene-Recent subduction of oceanic crust of the African plate beneath the Eurasian active margin to the north (Fig. 2; Robertson & Kopf, 1998). In many accretionary complexes the imbricated wedge is backthrust over a backstop (e.g. Chile; Behrmann et al., 1992). The backthrusting is typically a response to the need to maintain a stable critical taper (e.g. Platt 1990; Lallemand et al., 1994), and in the case of the MedRidge, this can clearly be related to collision of the more rigid backstop domain in the north with an accretionary wedge to the south (Fig. 2). In the Eastern Mediterranean, exhumed and uplifted Cretan continental rock initially acted as a backstop to accrete sediment. This initial wedge, the Inner Ridge, underwent compaction and was later overridden by the present accretionary prism (the MedRidge) as a result of incipient continental collision between Africa and Eurasia (Kopf et al., 2003a). Hence, the Inner Ridge represents the transition from compacted accreted rock to rigid backstop material, allowing the study of incipient dewatering and diagenesis. It is hence possible that the backstop with its deeply rooting faults as well as the landward MedRidge with the „inner belt" MVs are very likely more significant pathways for expulsion of deep dehydration fluids than the decollement and toe of the accretionary prism (e.g. Kopf et al., 2001).

When regarding the even deeper part of the HSZ, there has been growing evidence that the processes governing both "roll back" of the subduction system as well as uplift of the island of Crete

are driven by sub-crustal dehydration (e.g. Meier et al., 2007). Based on recent geodetic, geophysical and structural data, the devolatising mantle wedge is believed to favour material transfer through the subduction channel up-dip along the plate boundary thrust (Fig. 3). This ascent of serpentinised peridotite/dunite or eclogite is likely responsible for the present-day uplift rates observed on Crete, which cause both N-S- and E-W-extension and hence decoupling of the landward forearc and the underlying downgoing slab, not dissimilar to that from the Mariana's forearc (see ODP Leg 195 drilling results; Shipboard Scientific Party 2002). Both seismological investigation and numerical simulation favour a model where return flow along a corridor of hydrated material atop of the subducting slab reaches crustal levels or even shallower (see Fig. 3, and Gerya et al., 2002; Meier et al., 2007). Along the subduction channel, partially hydrated oceanic lithosphere and trailing mantle wedge material have ascended along the wake of exhumed high pressure/low temperature (HP/LT) units and account for both present-day uplift in the landward forearc and may have rendered extension in the Cretan Sea (north of Crete) ineffective. Given that recent work in that area has lacked any evidence for fluid expulsion or gas seepage (e.g. Chronis et al., 2000; Giresse et al., 2003; Kopf et al., 2006).

In summary, drilling a backstop (or buttress) setting is now essential to elucidate fundamental deep fluid flow processes and deformation mechanisms within an accretionary prism and its buttress. The Mediterranean Ridge, being a mature zone of collision, represents an ideal natural laboratory for such an endeavour, linking marine and continental processes and providing easy access to deep-seated processes owing to its unique geodynamic evolution (slab break-off, exhumation of Crete, salt and shale diapirism, mud volcanism).

3. State-of-the-art

3.1. The subduction factory and tectonic processes

Approximately half of the sediment currently overlying the Earth's oceanic crust is traveling towards active convergent margins, part of which enters the subduction zone, is underthrust and eventually gets involved in diagenetic, metamorphic, and magma generation processes. Sediment has been shown to re-emerge in arc volcanoes based on typical geochemical signatures such as Be isotope values or depletion of high field strength elements (HFSE) relative to light rare earth elements (LREE) and large ion lithophile elements (LILE) at the volcanic arc (e.g. Tera et al., 1986; Morris et al., 1990; Brenan et al., 1995; Plank & Langmuir, 1998; Elliot et al., 1997). Afterwards, part of the sediment residue continues to sink into the mantle and becomes one of the potential sources of mantle plumes and/or heterogeneities (e.g., Kogiso et al., 1997; Kamber & Collerson, 2000). Despite the improvements of geophysical investigation techniques and numerous DSDP and ODP expeditions, there is a clear lack of understanding of the physico-chemical processes attendant to the subduction of sediment. This is particularly true for the mechanical processes controlling the location and frictional behaviour of the plate boundary fault, but also regarding processes of fluid-rock interaction, mineral transformation, and devolatilisation that affect chemical cycling as well as effective strength of these materials (e.g. Hawkesworth et al., 1991; Dia et al., 1995; Johnson & Plank, 1999; Bebout et al., 1999; Kopf, 2009). In the subduction factory, there is a fundamental difference between the inputs (i.e. incoming sediment and crust as well as material from frontal and basal subduction erosion) and outputs, most importantly accretion, underplating, fluid release, and arc and back-arc magmatism (Fig. 1a). During cruise P410, the focus was mostly on the fault-driven fluid release originating from the frontal and intermediate loop (#2, 6 in Fig. 1a), which will be quantified in situ (using CAT fluxmeter systems; see Ch. 6.5) and calibrated by means of hydrothermal geotechnical experiments and geochemical analyses of natural pore fluids at the backstop drillsites and pore water extracted during the geotechnical tests. The wealth of data gained will be crucial to support the active drilling proposal 555-full3 for SPC (Science Planning Committee) ranking and OTF (Operations Task Force) scheduling, but also to provide important data for the Geochemical Earth Reference Model (GERM, see www.earthref.org/GERM).

3.2. Active faulting and physico-chemical processes

The backstop concept

The picture of an accretionary system of a pile of granular material in front of a "bulldozer" (e.g. Davis et al., 1983), is oversimplified, because it implies a non-deformable back-stop which does not

interact with the prism in front of it. Following the Mohr-Coulomb theory, the mechanical stability of an accretionary wedge has been debated at length on the basis of analytical and mathematical approaches (e.g. Chapple, 1978), or analog experiments (e.g. Malavieille, 1984) that do or do not consider cohesion (e.g. Davis et al., 1983) have been developed for the prism. Strong rheological contrasts between prism and (more rigid) backstop may favour deformation of the latter, which occurs in a complex interaction between mechanical (strength within prism and backstop, coupling/friction between the plates, etc.), hydraulic (porosity, pore fluid pressure, permeability) and thermal (e.g. conductivity, T-gradient) parameters (e.g. Lallemand et al., 1994; Kukowski et al., 1994; and most recently in a dynamic Coulomb wedge theory by Wang & Hu, 2006). Along a fair number of margins the seaward-leading edge of the continental crust is the backstop, however, as demonstrated for the Alaskan margin, old compacted accreted strata may act as the mechanical abutment to non-cohesive material above the downgoing slab (von Huene et al., 1998). Similarly, in the Mediterranean, the Inner Ridge represents the active backstop and is overthrusted landward by the accretionary prism (Fig. 2). In addition to this major suture, there is a large number of deep-seated out-of-sequence faults in the accretionary complex, many of them traceable to several km depth on MCS lines (see Chaumillon & Mascle, 1997; Kopf et al., 2003a). A large number of them is juxtaposed by mud volcanoes, with an estimated volume of fluid discharge that exceeds that at the frontal prism where fluid-rich trench deposits get deformed (Kopf et al., 2001; see also Ch. 2.2.2. below). Fluids may play a major role along the fault separating the MedRidge from the Inner Ridge backstop, but also separating the Inner Ridge from the Cretan Margin (see Fig. 6a), as evidenced from inverse polarity seen in MCS reflection profiles (see examples in Figs. 6b-d). Hence we plan to collect shallow gravity cores at the outcrop of the faults proposed in 555-full3, just considerable up-dip. Those samples will be subjected to major stress and elevated temperature, with fluids to be collected and analysed (see Ch. 3.1.). This way, the PT-controlled effects on both strength, pore pressure evolution and geochemistry can be identified and quantified, and then can be related to the natural environment (Ch. 3.2.) and used to constrain numerical models (Ch. 3.3.).

Physico-chemical processes and hydrology driving fault strength

The interaction between solid sediment particles and trapped pore water has profound physical and chemical repercussions and starts immediately after deposition on the seafloor. Consolidation may only occur if the fluid pressure from the pores can dissipate; otherwise pore pressures build up and counteract cohesion and reduce the mechanical strength of the sediment. This has first been described by Hubbert & Rubey (1959) and ever since has been a matter of controversial debate (see e.g. Byerlee [1978] vs. Rice [1992]). In addition to the physical properties, chemistry of the solids and fluids is also affected after deposition (in particular the ad-/desorption processes on clay minerals). Both mechanical pore space reduction and diagenetic reactions cause a decrease in permeability. Processes

active include clay mineral dehydration, alteration of biogenic opal, zeolite formation, dissolution of metastable mineral phases, to name just a few (see summary in Moore & Saffer, 2001). Such diagenetic to low-grade metamorphic processes may mobilise major (such as K, Na, Ca, Mg, Fe, S, and Si) and minor components (e.g. Cl, Ba, B, Sr, Cs, Li, Rb) as well as many other trace elements as a result of dissolution and mineral transformation processes (see summary in Guangzhi, 1996). The resulting supersaturated pore fluids may cause precipitation and hence significantly modify the fabric (Kawamura & Ogawa, 2004) as well as the strength and permeability of the sediment (Bjorlykke & Hoeg, 1997; Dewhurst et al., 1999), its mineralogy, and chemical composition of the pore fluid residue. Examples of "healed" fractures and deformation bands, but also of authigenic cements in hydrofractures are abundant in cores from the DSDP and ODP. Examples include the Cascadia, Japan Trench, Nankai or Barbados subduction systems, but are not restricted to them. However, it is yet undecided whether these precipitates contribute to an increase in fault strength, or whether they form after fault slip as a result of stress release and a drop in solubility as a consequence.

3.3. Mud volcanism, fluid budgets and geochemical cycling

Mud volcanism has been demonstrated to be a global phenomenon, which is commonly associated with compressional tectonics and sediment accretion at convergent margins (see review by Kopf, 2002). Mud domes and diapirs frequently occur in marine subduction zones at the plate boundary near the toe of accretionary prisms (Henry et al., 1996), further landward in the forearc (Mascle et al., 1999), but also on land where collisional processes and deformation are more accentuated (Lavrushin et al., 1996). Irrespective of the tectonic compression, the main driving force of mud extrusion is the negative buoyancy of the clay-rich material at depth. Fluids may either be trapped as a result of high sedimentation rates or lateral influx into clay-bearing sediments, or may be generated *in situ* owing to processes such as mineral dehydration reactions and hydrocarbon generation at greater depth (e.g. Hedberg, 1974). Quiescent as well as catastrophic emission of greenhouse gases (mostly methane) accompanies extrusion and may contribute significantly to climate change (Higgins & Saunders, 1974; Kopf, 2002). The Mediterranean Ridge is one of the areas where mud volcanism is most common globally (e.g. Kopf et al., 1998a, 2001), with estimated dewatering rates exceeding that at the frontal toe of the prism. Together with the enigmatic fluid chemistry of such fluids (Deyhle & Kopf, 2001; Dählmann & De Lange, 2003), this attests a profound influence on geochemical cycling and fluid budgets in subduction zones (Kopf et al., 2001). Ascent of the mud may be rather rapid in the MedRidge area (Kopf & Behrmann, 2000), and hence allows the preservation of chemical (and biological) signatures over time. Extrusive activity has been shown to be episodic from ODP Leg 160 drilling (Emeis et al., 1996), and may be coupled to deep-seated processes (e.g. seismicity in the HSZ, realease of brines from Messinian formations containing evaporates, etc.).

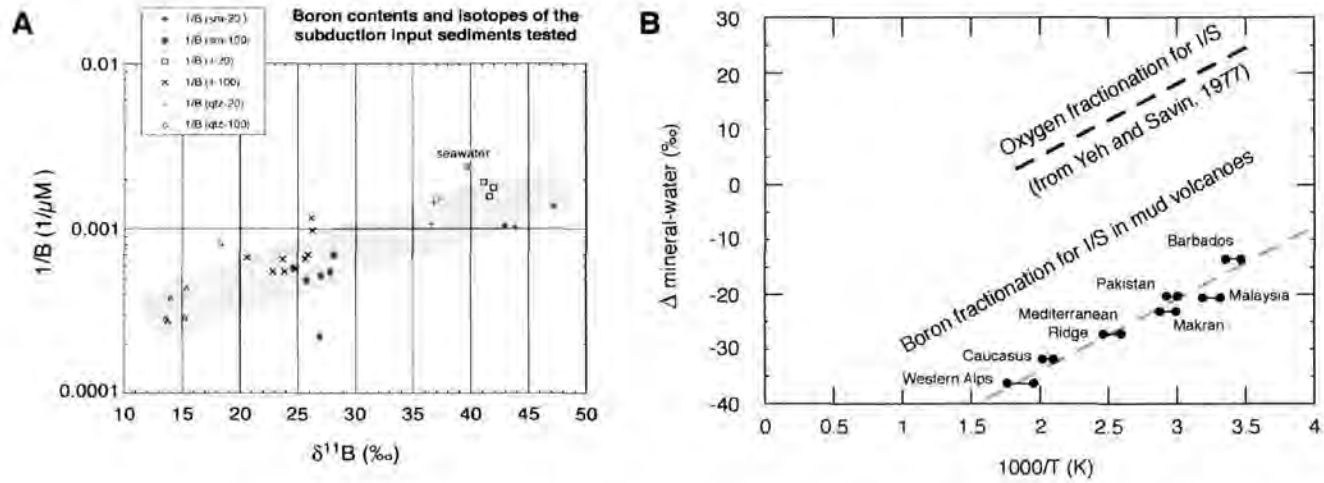

Figure 4: **a)** Results from B analysis on fluids and solid particles from hydrothermal deformation tests of smectite (sm)-, illite (il)- and quartz (qtz)-rich endmember sediments off Japan (from Kopf et al., 2002); b) Data compilation from MV study using B fractionation and paleo-T to estimate the depth of mud- and fluid mobilisation (from Kopf & Deyhle, 2002). See text.

Active mud volcanoes provide a tectonic window into the deeper subduction system and hence carry geochemical and potentially biological signals inherited from depth. Core as well as long-term fluid flowrates complementing existing data will provide a solid basis for numerical modelling and to test hypothesis concerning mud extrusive episodicity and possibly microbial activity. The episodic extrusion or fluid seepage could be quantified by in situ flowmeter deployments at the drill sites proposed.

3.4. Geochemical cycling

When returning to the subduction factory cycles (Fig. 1), mud volcanism and deep-seated faults may help illuminate the intermediate loop. Numerous authors have used the mobile element Boron and its stable isotope ratio ($d^{11}B$) to illuminate processes in the moderate T window of subduction zones (Spivack et al., 1987; You et al., 1993, 1996; Kopf et al., 2000; Deyhle & Kopf, 2001, 2002). These studies on natural samples and from hydrothermal experiments suggest that B is a powerful proxy with a wide variety of $d^{11}B$ values for different subduction inputs and related diagenetic reactions. Examples of the proponent's evolvement in these studies are given in Figure 4 and have been wrapped up in various publications (oral and as manuscripts; see Kopf et al., 2002; Kopf & Deyhle, 2002; Deyhle & Kopf, 2001, 2002, 2005). The work attested that there are well-defined trends for B processes in selected silica systems such as clay-dominated ones (Kopf & Deyhle, 2002), but not in all of them (Deyhle & Kopf, 2005). However, the wealth of these results indicates that a thorough analysis of physico-chemical processes at moderate PT-conditions may identify the key processes in fault zone mechanics (see Hüpers et al., 2011), shed light on the source depth of mud volcanoes (Kopf

& Deyhle, 2002), and characterise more clearly what processes dominate the "intermediate loop" in the subduction factory.

In 2006, existing fluid flow models from accretionary complexes similarly large than the HSZ (Barbados, Costa Rica and Japan) have been combined with geochemical data to establish a conceptual model for an active forearc. The preliminary results of this modelling approach, which utilised the mobile element Boron as a powerful tracer, were presented at AGU fall meeting 2006 (Saffer & Kopf, 2006). A refined version was introduced at the following Goldschmidt conference (Saffer & Kopf, 2007), and could demonstrate that for all three margins, the simulated desorption of B due to deformation and clay mineral transformation can generate the B concentrations observed in the pore waters recovered during earlier ODP drilling (Legs 110, 156, 170, 186). In fact, for Costa Rica and Japan, simulated B contents in source regions below the sampling locations are higher than required, which is consistent with the possibility of mixing during transport up-dip. The locus of peak clay dehydration in these systems also coincides with low Cl pore waters recovered during the ODP expeditions in question. An example is given in Figure 5; for details, refer to Saffer & Kopf (2007), which is currently wrapped up into a manuscript.

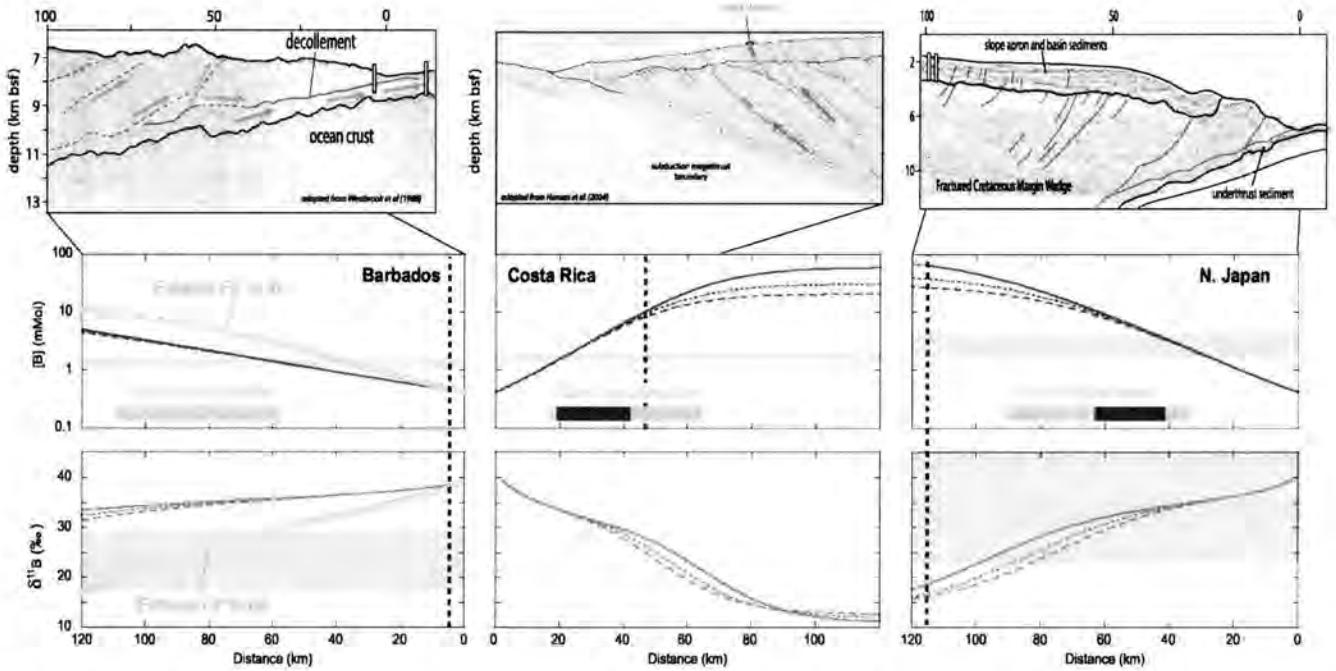

Figure 5: Simulated B concentration and stable isotope signature based on fluid flow models across the Barbados, Costa Rica and Japan forearcs. For details see text and Saffer & Kopf (2006, 2007).

If we now translate those models to the Mediterranean Ridge, we face two main problems. First, there is only limited information on the overall permeability structure of the huge accretionary complex owing to the lack of DSDP and ODP drilling, so we are limited to physical property data from only a few detailed studies (e.g., Neuzil, 1994; and Kopf et al., 1998b, which seems appropriate for the region around BUTT3, but cannot easily be extrapolated to the entire prism and backstop rocks). Second, the

model needs a major adaptation if flow from depth along deep-seated thrusts and backthrusts (BUTT1, -2) is to be simulated, because rather little is known about these regimes. We are currently working on such a model, which uses B and Cl geochemical data (concentrations and stable isotope ratios) from the proponents group's earlier work (Deyhle & Kopf, 2001; Dählmann & de Lange, 2003). *In order to overcome these shortcomings and lack of knowledge, we are proposing the* Muddy Waters *project as well as a resarch expedition with RV* Poseidon *to collect some of these critical data/samples at sites BUTT1 and –2.*

Another path we are following feeds well into the geochemical modelling. The proponent has worked extensively on hydrothermal deformation experiments including fluid chemistry monitoring (up to 150°C and up to 80 MPa overburden stress). Initial results indicate enrichment in mobile phases (Ba, B, Li, etc.), but also of HFSEs and LILEs may be released from the sediment into the fluid phase (Kopf et al., 2002; Hüpers et al., in press), a process previously attributed to much larger depth levels. There is also a number of elements with interesting behaviour, which nicely links the physical changes (thermal consolidation of the sediment; Hüpers & Kopf, 2009) and chemical variations. For instance, profiles of Ca, Ba and S over the hydrothermal deformation test indicate that barite and anhydrite may be formed, a process in agreement with earlier drilling results at the toe of the MedRidge (Emeis et al., 1996, and 972 and 973 site chapters in there). Systematic testing of sediments at moderate PT and measurement of the fluid chemistry will be fed into fluid-rock interaction modelling using COMSOL Multiphysics (formerly Femlab) including the Earth Science module to simulate the high-temperature effects. These data further get incorporated into the existing fluid flow models (see Fig. 5) once they have been adapted for the Hellenic subduction system.

For ground-truthing the models, the CAT meter data and samples from deployments on the surface traces of the faults to be drilled (BUTT1, -2; see IODP proposal 555-full3, Ch. 2.3), the crestal portion of *Lich, Napoli and Milano* mud volcano (BUTT3 and ODP Sites 970 and 971; see Emeis et al., 1996). The CAT meters record flux rate over months and also collect fluids (spiked with a tracer) using an osmotic approach. Previous data with these systems indicate a correlation between distinct variations in fluid outflow and nearby seismic noise off Middle America (Brown et al., 2005). In active mud domes in collisional settings, *in situ* heat flow and CPTU measurements show an increase in temperature (Grevemeyer et al., 2003) and pore pressure (Kopf et al., 2009) when the structure is hydraulically active.

IODP drilling and monitoring of chemical flux and composition across the Mediterranean Ridge backstop, for instance with osmosamplers in a CORKed hole, will represent a big step forward in understanding the shallow part of the subduction zone (intermediate loop) and its temporal variability. The proposed Muddy Waters*-study is an essential step towards that overarching goal, with valuable geochemical and fluid flow information fed into numerical subduction cycling models for the HSZ and, with little adaptation, to other convergent margin settings (see above and Fig. 5).*

3.5. Backstop drilling proposal #555-full3: Drilling objectives and proposal history

Drilling proposal into backstop domain

The buttress to the MedRidge is suggested to be drilled along a N-S transect of three sites from the Cretan margin (parallel to the direction of shortening) to the northern margin of the accretionary prism (Fig. 6a). In the south, the hinterlandward accretionary prism is peppered with deep-seated mud volcanoes (Fig. 2b), one of which (a small, cone-shaped dome called "Lich"; Fig. 6b) is the target of site BUTT3. Both the crest, the flank, and the surrounding seafloor down to the active backthrust connected to the edifice will be sampled (Fig. 6b). Further north, the main backthrust along which the accretionary complex is overriding the „Inner Ridge" backstop domain of ancient accreted strata, is the objective of site BUTT2 (Fig. 6c). The northernmost site BUTT1 is situated north of the „Inner Ridge" at the Cretan margin, where a stack of thrust nappes got exhumed approx. 19 Ma ago, then forming the initial backstop to Neothethyan sediments which now build up the „Inner Ridge" (Kopf et al., 2003a). The northward dipping succession can be subdivided into HP-LT metamorphic units made of plattenkalk and phyllite-quartzite (PQ), and the overlying succession of low-grade metamorphic, largely sedimentary nappes (Pindos, Gavrovo, Tripolitza, etc.) from the contrast in seismic properties (most prominently a strong series of reflectors caused by a jump of 1500 m/s in p-wave velocity when entering the HP/LT units; Fig. 6d). This boundary is interpreted to be the former seismogenic detachment plane along which the metasedimentary units got exhumed and is the key target of the proposal to unravel the complex tectonic evolution (see Thomson et al., 1998; Meier et al., 2007; Brix et al., 2008).

In addition to the hydrotectonic objectives, proposal 555 provides rich opportunities for deep-seated fluid chemistry and deep biosphere. Marine sediments hold the majority of all microorganisms on our planet, with up to one third of the living biomass on Earth thriving beneath the seafloor, and microbial cells are recorded down to a sediment depth of 1.6 kilometers with an age of up to 116 million years (e.g. Parkes et al., 1994). The discovery of a diverse and active sub-seafloor microbial community, both in deep sediments and in crustal rocks, has fundamentally changed our perception of life on Earth and represents one of the last major frontiers in natural science exploration. Drilling deep-seated faults and mud volcanoes will provide a window to depths inaccessible by conventional drilling, possibly exceeding 10 km and tapping into areas where at the boundary between domains 1 and 2 in Figure 1b (see Scholl et al., 1994 for details), with fluids from both diagenesis and low-grade metamorphism in and beneath the landward prism and backstop, but also from dehydrated mantle material ascending along permeable faults of inverse polarity (see Figs. 6b-d).

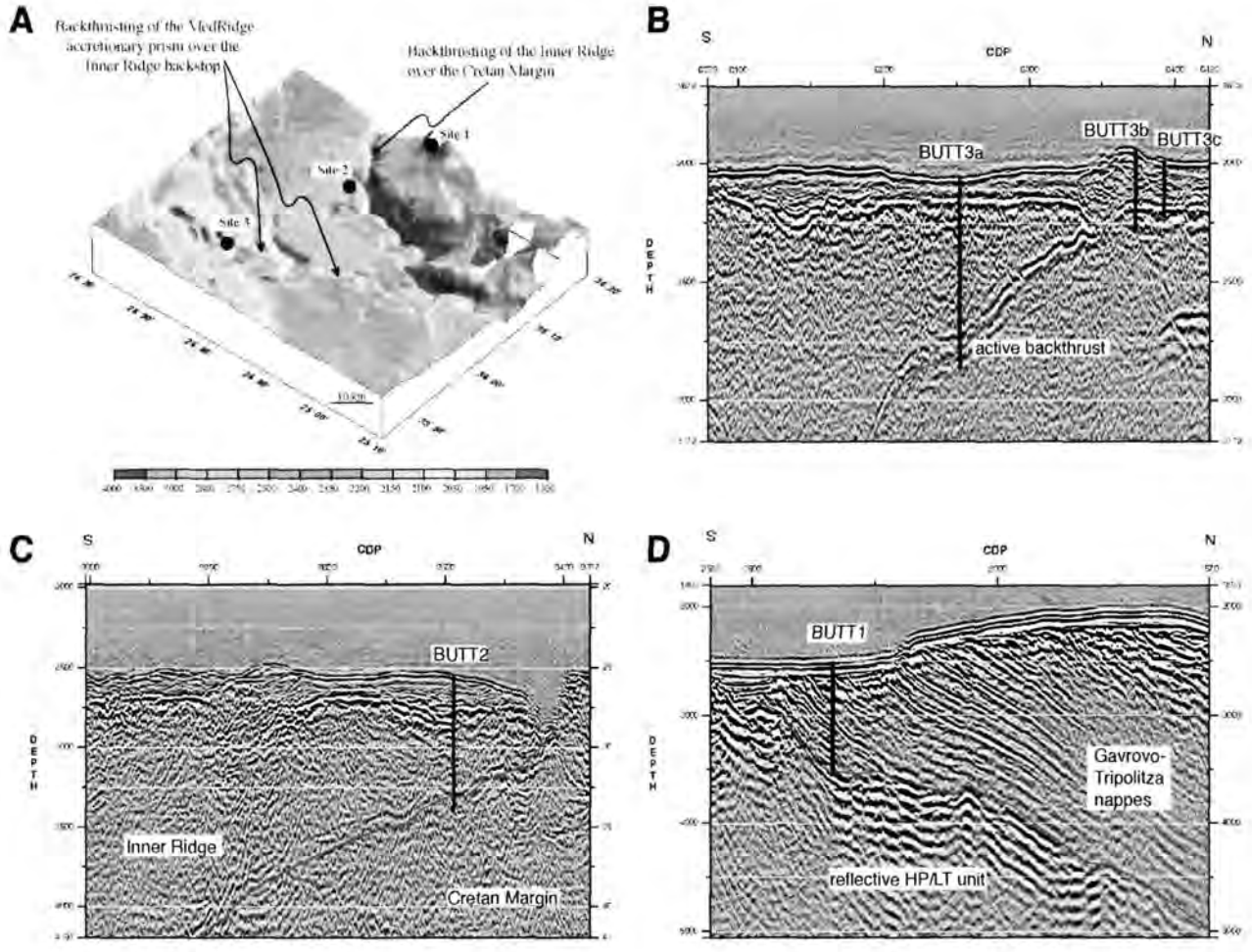

Figure 6: Drilling strategy of proposal 555-full3: **a**) Bathymetric map of the HSZ backstop domain with the Inner Ridge and Cretan Margin and the three drill sites. Depth-migrated MCS profiles across the drill sites illustrate the deep-seated faults in each location (red line for clarity): **b**) BUTT3 targets "Lich" mud volcano, where a transect of shallow holes aims for the edifice as well as the fault feeding it; **c**) BUTT2 penetrates the deep-seated backthrust that separates the active prism from the "Inner Ridge" backstop; **d**) BUTT1 at the Cretan margin, where the former detachment along which HP/LT units got exhumed is overlain by low-grade nappes; the seismogenic detachment is the target of drilling. See text and Kopf et al., 1999.

In more detail, the key objectives of drilling and logging the three sites proposed include:

BUTT3 –mud volcano juxtaposing active backthrust fault

(i) To investigate the sedimentology, biostratigraphy, and mud volcanism on the southernmost part of the accreted part of the MedRidge;

(ii) to compare microbial activity in nutrient- (sapropels in the sedimentary cover) and methane-rich sediments (mud breccia) regarding their genetic code, AOM efficiency, etc.;

(iii) to core the base of a mud volcano to quantify its duration of extrusive activity, and potentially intervals of quiescence in the sedimentary record above;

(iv) to determine if the backthrust fault is the main dewatering pathway, and hence controlling the mud volcanic driving process;

(v) to measure pore fluid pressures over long periods of time (by conventional CORK) and to test whether hydrofracture (due to elevated fluid pressures in the backstop) or brecciation (due to fault movement) generate the clasts found in mud breccias;
(vi) if possible utilise PCS, geochemical CORK, or other state-of-the-art devices to recover pristine gas and pore water samples in order to constrain and quantify fluid flux and fluid composition to test the hypothesis of a deep generated fluid phase and the presence of microbes;
(vii) to measure *in situ* permeability by Packer test to allow comparison to such data gained from the toes off Barbados and Cascadia (Screaton et al., 1990, 1999), or more recent hydrological results from Legs 190/196 off Japan (Moore et al., 2001) and 308 in the Gulf of Mexico (Expedition 308 Scientists, 2005);
(viii) to relate short-term episodicity of fluid flux and pore pressure transients (the latter as a proxy for strain; e.g. Davis et al., 2001, 2004, 2006; Ge & Screaton, 2005; Kopf et al., 2005) to mud volcanic activity, and
(ix) to relate variations in fluid geochemistry due to deep biosphere processes and/or todiagenetic/low-grade metamorphic reactions down-dip in the deeper portion of the prism and buttress.

BUTT2 - Inner Ridge/deformable backstop domain
(i) to study the sedimentology, biostratigraphy, deformation and deep biosphere at the Inner Ridge of the Mediterranean Ridge;
(ii) to characterise the old accreted rock overlying the backthrust (see Fig. 6c), and to identify and quantify deformation and dewatering mechanisms;
(iii) to penetrate the backthrust that carried the Mediterranean Ridge accretionary wedge onto the Cretan margin „rigid" backstop, and to investigate the nature and rheology of the overridden rock;
(iv) to test whether mineral dehydration may account for the expected, enigmatic fluid chemistry, due to tectonic shortening and burial; and
(v) investigate deep biosphere and fluid flow at the transition between the Inner Ridge and Cretan continental backstop.

BUTT1 - Exhumation/'rigid' backstop domain

We propose to drill the northernmost site on the Cretan margin (Figs. 6a, d) where a sharp contact is seen between the well stratified unit (Tripolitza-Gavrovo) above and a highly reflective unit (PQ?) underneath (se Fassoulas et al., 1994); both units are overlain discordantly by a thin cover of hemipelagic Plio-Quaternary sediment. The highly reflective contact shows a p-wave velocity contrast of 1600 m/s, and has been interpreted to represent the an old, reactivated detachment fault plane along which HP/LT units (plattenkalk and PQ) got exhumed (see Fig. 6d, and Kopf & Bohnhoff, 2007).

The primary objectives of this site are

(i) to study the sedimentology, biostratigraphy, and vertical motion history related to Neogene extensional tectonics of a thin sedimentary cover, and to determine the nature of the discordant contact of these Neogene sediments to the northward-tilted block beneath;

(ii) to test whether out-of-sequence faulting, as suggested by analog modelling (Gutscher et al., 1998), affects the 'rigid' part of the backstop, for instance by reactivation of a former detachment (Fig. 6d);

(iii) to penetrate Tripolitza-Gavrovo limestone, through a former low-angle detachment, and into HP/LT metamorphics (anticipated to be PQ; see Fig. 6d);

(iv) to study the contact, both geochemically and structurally, in order to investigate physical and chemical processes (e.g. migration of deep fluids, etc.) along this deeply rooting out-of-sequence thrust fault, which is inferred to tap into an area beneath Crete which is influenced by ascent of dehydrated mantle wedge material (see Fig. 3 and Meier et al., 2007).

4. Objectives and strategy of the cruise P410 and post-cruise research

Traditionally, many European research institutions consider the Eastern Mediterranean a natural laboratory for the study of climate change, collisional tectonics, life in extreme environments, landslide processes, to name just a few. A large number of IODP drilling proposals has been put forward, however, very few of them resulted in scheduled expeditions. Still, both national and pan-European (EU, ESF, etc.) initiatives have focused on the Eastern Mediterranean, and ongoing research includes multi-disciplinary projects such as HERMES-HERMIONE, MOCCHA, ESONET, or MARBEF. IODP proposal 555-full3 stands in this line since it combines many fields of geosciences and biogeosciences, and most importantly all three major aspects of the ISP (namely Geodynamnics, Deep biosphere, and Paleoclimate; see IODP, 2001) although it was written and submitted in 1999 (i.e. prior to writing the new science plan; see above). The timely 555-drilling strategy (see Ch. 2.3. above) led the SSEP expert group to a 5* rating, which in the plenary discussion was adjusted to a strong 4* rating, which makes this proposal a candidate for drilling in the current phase, or taken across to be drilled soon in the program beyond 2013.

Second, the two major topics addressed in proposal 555 have been major themes in NSF Margins: Seismogenesis (i.e. SEIZE) and the Subduction Factory (see www.nsf-margins.org). The proponent has been in close contact with the key players in NSF Margins, which form a significant portion of the NanTroSEIZE team where drilling deep out-of-sequent-thrusts is equally the key strategy. The cruise P410 (Mudflow) and the associated DFG (*Muddy Waters*) and NSF projects hence try to incorporate partners from national, European and US institutions, which are leading in the field and provide the technical or regional expertise (see Ch. 3.4 and 5.2). On cruise P410, this is achieved by a Greek and US scientist participating.

Third, there is a demand by the IODP Environmental Protection & Safety Panel (EPSP) to ground-truth at each of the three proposed sites (i.e. 5 holes; see Kopf et al., 1999) that there is deep fluid seepage, but equally low to moderate concentrations of free gas in the core. In addition, SPC asked for further evidence of freshened diagenetic or metamorphic fluid (i.e. hydrological activity of the backstop system). Most of these geochemical analyses will necessarily take place shore-based after the cruise, but both fluid and headspace gas sampling will be carried out.

After a pre-scruise compilation of existing data, cruise P410 aims at collecting:

- gravity cores to ground-truth fluids from depth at each IODP drill site, its vicinity, and other targets of potential interest in the context of this research,
- characterise *in situ* data on shear strength, pore pressure (both from CPTU deployments),
- measure the governing geotechnical parameters in the laboratory (shipboard as well as shore-based),
- gather *in situ* temperature data together with the gravity core sampling using MTLs,

- measure composition of headspace gas from gravity cores to identify potential safety hazard prior to drilling,
- longer term fluctuations in geochemical signature of expelled waters and knowledge of flow rate.

The three main parts of the suggested approach will be outlined in more detail in Chapters 4.1 - 4.3. below.

4.1. Sampling and analytical goals

Ground-truthing

Coring: One of the major goals during the planned RV *Poseidon* cruise is multiple gravity coring at the three sites. For BUTT1 and –2, the sampling strategy is to move up-dip along the deep-seated faults and recover core at the seafloor outcrop of the fault several times while the ship is minimally offset. In contrast, at BUTT3 we plan to collect a transect of cores from the base of the flank to the crest and all the way to the opposite base of the flank. This way we can ensure that we identify the hydrologically most active region on the dome. Getting core is critical for the geotechnical and geotechnical work in the proposed study, and to fulfil safety requirements by the EPSP for hydrocarbon detection (by headspace analysis).

Geotechnical testing: A small number of the suite of multiple gravity cores will be left unopened on the cruise and are preserved for hydrothermal deformation experiments (up to 80 MPa effective stress and 150 °C) and permeability as well as standard oedometer tests. Permeability variation with increasing normal stress is the key parameter for the proposed study, because it is governing the fluid flow modelling across the entire accretionary complex and backstop domain.

Pore water geochemistry: Major and trace elements will be measured routinely on pore fluids from the gravity cores, the hydrothermal deformation experiments, and also from cut tubing coils after recovery of the CAT meters (see below). We also plan to analyse B isotopes on selected samples from these three groups of fluids.

Gas composition: Collecting headspace gas from each section of the gravity core is a straightforwartd means to identify enrichment in methane and higher hydrocarbons. Analysis will be carried out the shore-based using gas chromatography for hydrocarbon (CH_4, C_2-C_6) concentration. Determination of $\delta^{13}C$ of subsamples after separation will be done on a mass spectrometer to distinguish between biogenic and thermogenic origin

In situ measurements

CPTU: The dynamic (i.e. free-fall) deployment of CPTU (Cone Penetration Testing with pore pressure measurement [U]) has been proven to be a time-efficient way to collect geotechnical parameters such as tip resistance and sleeve friction (as a measure for bearing strength and cohesion),

pore pressure and temperature (Stegmann et al., 2006, 2007; Kopf et al., 2007). These parameters may then be used to estimate permeability and undrained shear strength based on empirical solutions from extensive studies (Bennett et al., 1985; Song et al., 1999). For soft marine sediments, Bennett et al. (1985) suggest the relationship: $Cu = U\text{max}/6$, where $U\text{max}$ is the maximum insertion pressure. The decay of excess pore pressure produced by the insertion is governed by the consolidation process around the probe and can be modelled as radial consolidation. Bennett et al. (1985) predict the coefficient of horizontal consolidation (Ch) from the time taken for 50% of $U\text{max}$ to dissipate, and Ch can then be used to determine the permeability (k), using the expression: $k = Ch\ \mu\ m\text{u}$, where $m\text{u}$ is the compressibility and μ is the viscosity of the pore water. We will compare in situ permeability estimates to data gathered in the geotechnical laboratory on gravity core specimens (see above).

HF: The *in situ* measurement of temperature monitoring is an irreplacable parameter for identifying fluid flow processes or anomalies owing to frictional heating at depth. Using violin bow-HF probes (e.g. Gennerich et al., 2002) developed at Univ. Bremen will help to identify such processes, similar to earlier work in collision zones (e.g. Grevemeyer et al., 2003 offshore Costa Rica, where elevated heat flow hinted towards mud volcanic activity; and Grevemeyer et al., 2009 at the Gibraltar Arc where thrust ramps in a wedge of olistostromes and other clastic series attested active thrusting of coarse-grained, strong material). We will apply the same pogo-style deployment strategy and will measure HF transects prarallel to plate convergence across the two faults (BUTT1, -2) and the across the entire mud volcano and its vicinity (BUTT3) during the *Poseidon* cruise.

The key questions and testable hypotheses based on sampling, *in situ* measurements and chemical analyses include:

- Can authigenic precipitates and/or free hydrocarbon gases provide evidence for active fluid flow or venting along the fault outcrops and at the crest of the *Lich* mud dome?
- Are there inherited "deep" signatures, sulfate depletion or free hydrogen (i.e. the strongest electron donor) that indicate microbial activity and/or evidence for life at extreme depth?
- The permeability of surface and subsurface sediment, in particular in the shallow fault or on top of the mud dome, are sufficiently high to allow active venting.
- $\delta^{11}B$ signatures of the fluids found at the coring sites will be depleted relativ to seawater because of deep-seated dehydration processes and other diagenetic reactions (see Kopf & Deyhle, 2002).
- Will other elements be mobilised, e.g. Li, Mg, Ba or K in the deep HSZ, as is indicated from the controlled hydrothermal deformation tests we carried out so far?
- How well do the permeabilities estimated from in situ CPTU tests correlate with permeameter experiments at various confining stresses in the geotechnical laboratory?
- Do HF measurements give evidence for deep-seated fluid flow, e.g. when measuring across

the mud dome (see Grevemeyer et al., 2003 for comparison)?

The answers to these questions and hypotheses will be compared to the monitoring data (see next paragraph), and will be fed into numerical models.

4.2. Monitoring goals

Monitoring fluid flow: Monitoring pore fluid composition over extended periods of time has been shown a powerful approach in subduction forearcs to identify and quantify chemical processes (Kastner et al., 2005). Chemical and Aqueous Transport (CAT) meters (Tryon et al., 2001) have been in use for over a decade and have played a major role in quantifying the flux of water from benthic seeps, its impact on geochemical cycles and biological systems, and the nature of the driving forces of seepage in a wide range of settings (e.g., Füri et al., 2010; Tryon et al., 2010). The CAT meter systems are capable of measuring diffuse fluid flow through the sediment surface on the order of 0.1 mm yr^{-1} - 15 m yr^{-1} when the flow is through sediments with permeabilities of less than 10^{-8} cm^2 (typical seafloor sediments). The instrument measures fluid flow by determining the degree of dilution of a chemical tracer that is injected by an osmotic pump at a known rate into the fluids venting into or out of a collection chamber situated on the seabed. The pump also withdraws a subsample of this tracer/fluid mix into sample coils allowing a serial record of the flow rates to be determined over several months. The coil's diameter is sufficiently low to promote plug flow so that sections of defined length may be cut and analysed after recovery to get time series with a resolution of <1 hr. (Tryon et al., 2001). The CAT meters will be deployed at the locations of each BUTT drill site which are found to be most hydrologically active (based on gravity coring) at the end of the *Poseidon* cruise. The instruments will be recovered during a later cruise.

Monitor temperature transients: Downhole high-resolution temperature monitoring is an irreplacable parameter for the integrity of downhole packers and sea floor borehole seal as proven by records from CORKs in ODP Holes 1253A and 1255A off Costa Rica, an erosive convergent margin. The 700 days long record shows very clearly that the MTLs (miniature temperature loggers; Pfender & Villinger, 2002) are reliable and drift-free sensors with enough resolution to resolve small temperature signals associated with transient pressure events (Davis and Villinger, 2006; Heesemann et al., 2006). Also HF across active mud volcano off Nicaragua (Grevemeyer et al., 2003) the flux through the mud dome is elevated by 10-20 mW/m^2. In general, T and HF data provide important clues regarding fluid flow activity without much time for the deployments (see section 5.5 and 6.5). Both MTLs and HF measurements are a key component during RV *Poseidon* operations in the 555 backstop area.

The testable hypotheses based on long-term data include:

- Positive correlations exist between temperature transients and changes in flow rate (to be tested with an additional MTL on the CAT meter at each site).

- T gradients in the wider area around the drill sites reflect coupling (and hence frictional heating) beneath the MedRidge prism, and drop in the landward part in the north where older rock and also basal decoupling at the plate boundary are thought to dominate (see Gerya et al., 2002); some of those T data match long-term measurements at the CAT meter sites.
- Fluid chemistry in the spiked coil collected after CAT meter deployment shows distinct temporal variability, which reflects variation in fluid flow activity.
- Enrichment in mobile phases as well as enrichment-depletion patterns typical for diagenetic fluids from several km depths will likely be found at all three BUTT drill sites.

4.3. Post-cruise numerical modelling goals

Several workers have shown that the discrete element method (DEM; Cundal & Strack, 1978), which is based on a compartimentalised (or particle) approach, can be successfully utilised to simulate the behaviour of non-cohesive systems in shear experiments under high stress conditions and build-up of orogenic wedges (e.g. Morgan & Boettcher, 1999; Strayer et al., 2001). Other workers used finite element kinematic thermal models of specific subduction zones in order to test our models against seismological and magmatic observations (Peacock, 1990). In accretionary prisms, and namely their drillable frontal part, numerous studies related to ODP were conducted successfully (Bekins et al. 1995; Bekins & Saffer 1998, 2002; Ge & Screaton, 2005). Some of this work is neatly summarised for the Barbados accretionary wedge and attests that numerical simulation is a powerful means to set up a hypothesis, which can later successfully be confirmed by drilling (see details in Bekins & Screaton, 2007). Their models are based on steady-state pore pressures, a hydrostatic boundary at the ocean, and a permeability-depth relation as constraints. We here want to extend sich models by incorporating non-steady state data (from CAT meters) and geochemical signatures characteristic for a certain depth range (as in Saffer & Kopf, 2006, 2007; see Fig. 5 as an example) to come up with a comprehensive model for the MedRidge accretionary complex all the way to its backstop domain in 150-200 km behind the deformation front.

In order to achieve this challenging goal, the COMSOL Multiphysics code with the Earth Science module has been identified as the most promising approach. A variety of specialiced interfaces are available for easy application of the Richards and Navier-Stokes equations, Darcy's law, and Brinkman's extension of Darcy's law (which will allow us to directly incorporate our permeability laboratory results). In addition, the module handles the transport and reaction of solutes as well as heat transport in porous media, two other sets of parameters, which will be collected long-term (using the CAT meters; see section 5.5 and 6.5) and from gravity cores (see section 5.6 and 6.6) during this project.

The questions and hypotheses to be tested by numerical modelling include:

- What is the "deep" fluid signature beneath the MedRidge and HSZ backstop domain, and how is that signature altered during ascent of mud and/or fluid migration along faults?
- Based on what is believed a "deep" (i.e. diagenetic) geochemical fluid signature, a thorough forward modelling approach using all geotechnical data available and the HSZ forearc geometry will allow us to proof such a composition to be likely, or not.
- Vice versa, our models, which are based on our earlier work (Saffer & Kopf, 2007), could be turned backward so that geochemical signatures near the seafloor (pore fluid from gravity core) can be modeled backward based on chemical variation in the hydrothermal deformation tests. This way we can estimate the chemical fluid composition in several km below the seafloor beneath the MedRidge or Crete by taking e.g., Boron ad-/desorption and B isotope fractionation into account. This will allow us to test the Meier et al. (2007) model shown in Fig. 3, i.e. whether a mantle wedge/subduction channel fluid source is possible or likely.
- We can further answer questions regarding the fluid flow and permeability patterns in a mature thrust wedge for the first time, and use those results for pore pressure estimates and the frictional strength of the HSZ system in the collision zone between Africa and Eurasia.

5. Methods

5.1. Seafloor surveys

(S. Kufner)

During cruise P410, a site survey was carried out in order to identify adequate spots for the gravity cores and to complement the existing bathymetric charts by Geosciences Azur (J. Mascle, Villefranche-sur-mer, France). For this purpose, the multibeam sonar system *Multibeam 3050* from *L-3 Communications ELAC Nautik* (1) was used. This system has been installed on RV *Poseidon* in October 2010 and was still in the testing phase.

To determine the structure and depth of the sea floor, a short pulse of sound (ping) is generated by a projector. The created signal travels as compressional wave through the water. The local speed of sound depends on salinity, pressure and temperature. As the wave front is interrupted by the sea bottom, a certain factor of the energy is reflected. This reflected signal (echo) has the same frequency than the source wave and is recorded by hydrophones which measure the oscillations in pressure as the pressure front of a sound wave passes. Knowing the travel time and the speed of the sound in water the depth of the sea bottom can be calculated.

A multibeam sonar allows to map more than one location of the sea floor with one single ping. The bottom locations are arranged to map a contiguous strip perpendicular to the path of the survey vessel. The dimension of this stripe is the swath width. The advantage of a multibeam system in comparison to a singlebeam system is a higher survey speed.

In order to determine the exact position of the echoes occurring along the ship, the projector and hydrophone array are installed perpendicular to each other (Mills cross arrangement). Using this arrangement, the area of the ocean floor ensonified by the projectors intersects with the area observed by the hydrophones only in a small area. The dimensions of this area correspond approximately to the projector and hydrophone array beam widths.

The range of the instrument is limited by the amount of attenuation and by the noise level. Errors that would occur due to yaw and pitch motion of the vessel are fully compensated by a transmit technique of the *Seabeam 3050* by splitting the transmitted fan in several sections which can be steered individually.

The *Multibeam SB 3050* system on *Poseidon* is designed to operate in depths from 3 m to approximately 3000 m. The operating frequency is in the 50 kHz band. Maximum ping rate is 50 swaths per second and the maximum number of beams is 315. The maximum across-ship swath coverage sector is 140 degrees.

The hardware components of the *Seabeam 3050* system include a motion sensor, a positioning system, a sound velocity profiler and a surface sound velocity sensor. An operating computer receives

the preprocessed data stream. Bathymetric data can be visualised in real time using the *Hypack* (2) mapping tool. A schematic diagram of these different components can be seen in Figure 7.

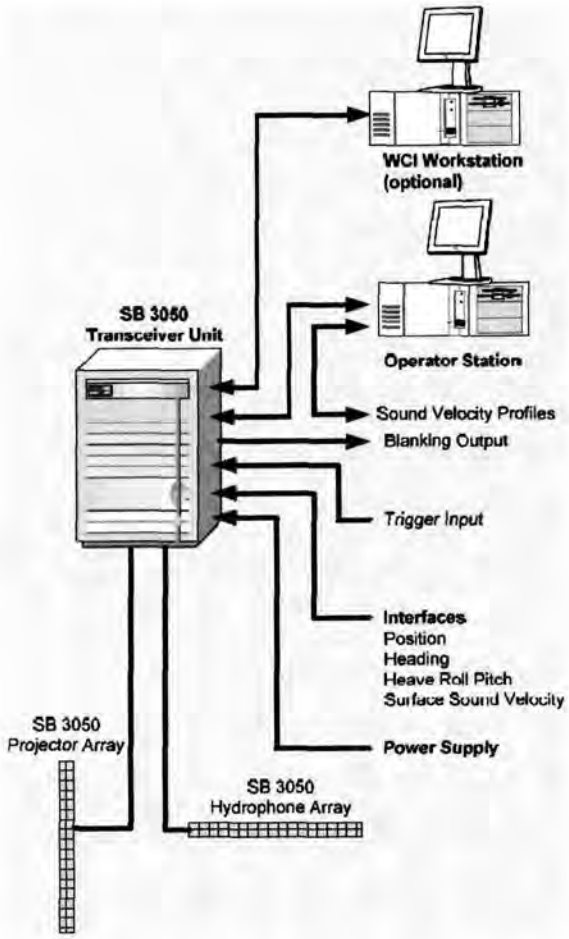

Fig. 7: Layout of the Multibeam system recently installed on RV *Poseidon*. See text.

5.2. Underwater video surveys (Video-MUC)

(M. Tryon, A. Kopf)

In order to identify the most active areas on the mud valcanoes (and potentially also active fault zones), a video system developed by Oktopus (Kiel, Germany) was mounted to the metal frame of a multi-coring device (Fig. 8a). The system comprises the following components:

- a telemetric unit for real-time control and observation (one deck unit, one underwater unit)
- two High-Intensity-Discharge lights
- a 2.5mm / f 2.0 colour video camera plus 3 laser pointers to measure distances.

All components are connected via deep-sea cables and Subconn connectros. The individual components are shown in Figure 8b.

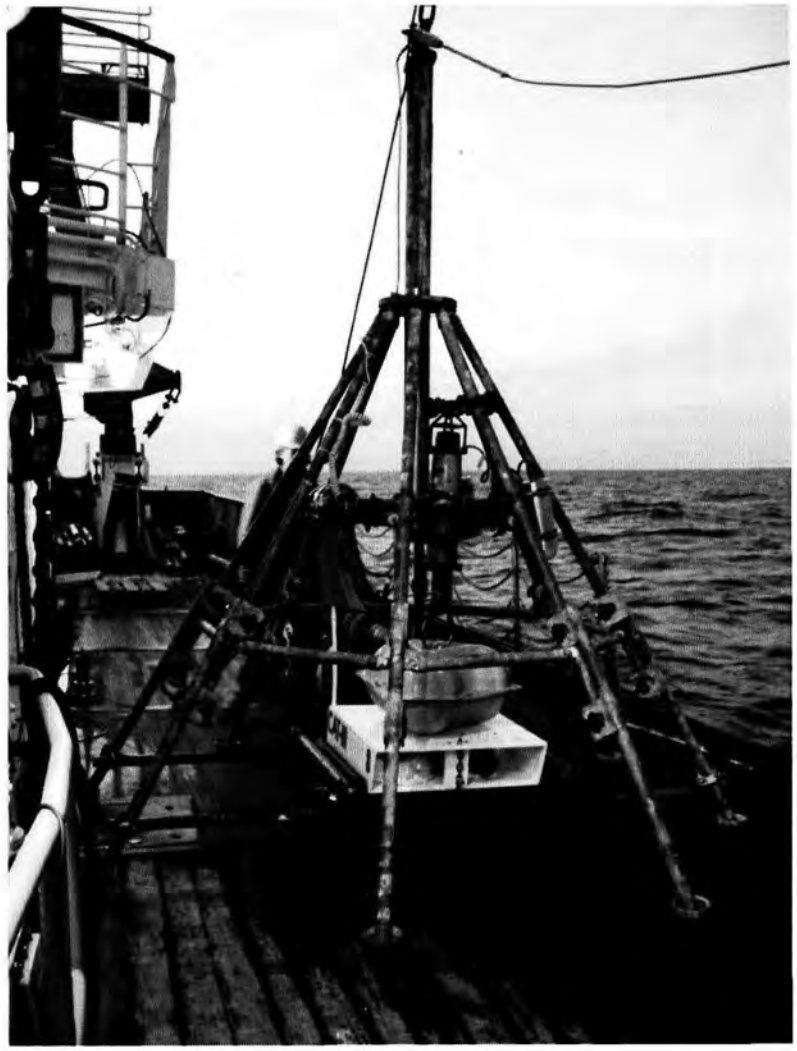

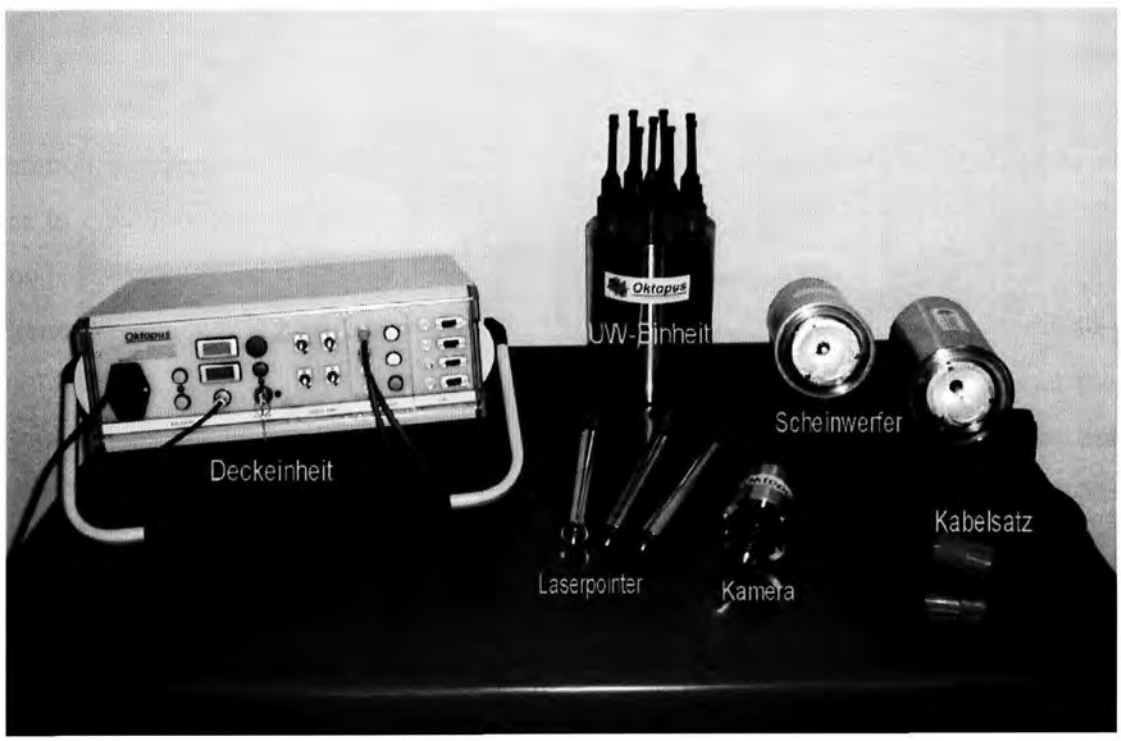

Fig. 8: (a) Multi-Corer frame with video system and underwater lights for surveying the seafloor. In the bottom centre, a CAT meter is mounted for future deployment (see also section 5.5 below); (b) Individual components of the Video system.

5.3. *In situ* temperature measurements

(M. Tryon)

On cruise P410 the *in situ* temperature gradients were measured with miniaturised autonomous Miniature Temperature Loggers (MTLs, Fig. 9). For technical specifications and detailed information, refer to Pfender & Villinger (2002).

Parameters of autonomous temperature data loggers:

Instruments serial no.:	sediment and water temp. logger: 18543-65C, -67C, -68C, -70C, -75C, -77C, -78C, -79C
Sample rate:	1 sec
Spacing:	usually 1 m, 2 m, 3m, etc. below the weight set; sometimes variable spacing depending on length of gravity corer; one water temperature sensor at weight set with sensor tip looking up.

Measurements (seafloor penetration) were realised by mounting the MTLs to gravity core barrel using fins and receptacles and get gradient at the chosen spacing as well as reference temperature in the water column. The probe remains in the seafloor sediment for several minutes to allow for some dissipation of artificial frictional heat from inserting the gravity corer.

Fig. 9: MTL prior to deployment of the gravity corer on cruise P410. The pointy end with the thermistor is facing downward.

5.4. *In situ* CPT testing

(A. Steiner, G. Wiemer, A. Kopf)

On R/V *Poseidon* cruise P410 , we used the MARUM deep-water free-fall CPTu probe (see Fig. 10, and Stegmann et al., 2007). Cone Penetration Testing (CPT) is an effective method for *in situ* measurements of these geotechnical parameters with one instrument (Lunne et al., 1997), namely sedimentary strength (tip resistance, sleeve friction), pore pressure, tilt and acceleration. For these measurements, the CPT system relies on 15 cm^2 cone with only pore pressure tubing in the tip (u1 and u3 positions) and a pressure housing containing a all other sensors and the microprocessor at the top. In addition, deceleration and tilt are monitored for vertical profiling of the penetrated sediment column.

Instrument

The free-fall CPT (FF-CPT) instrument for deep (up to 4000 m water depth) marine use consists of a 15 cm^2 piezocone and a water-proof housing containing a microprocessor, volatile memory, battery, and accelerometer (see Fig. 10a; and Stegmann and Kopf, 2007 for details). Two pore pressure port (u_1 and u_3) are equipped with differential pressure transducers. The stainless steel pressure-tight housing containing a microprocessor, standard secure digital memory card (SD), tiltmeter, accelerometer, power supply (battery packages), absolute and differential pore-water sensors as well as power and data interface module (PDIM). The tiltmeter (dual-axis tilt sensor) monitors the penetration angle at +/- 45° relative to vertical. Five different accelerometers with different ranges (+/- 1.7g, +/- 18g, +/- 35g, +/- 70g and +/- 120g) provide information about the descent de/acceleration behaviour of the DWFF-CPTU instrument upon penetration. These data allow the researcher to calculate penetration velocity and depth during multiple deployments by 1st and 2nd integration.

The reference pore-water pressure port at the pressure-tight housing is equipped with an absolute 40.0 MPa (400 bar) pressure sensors (WIKA ECO-1). The pore-water pressure ports at the tip (u_1) and 0.75 m behind the tip (u_3) are connected to the differential pore-water pressure transducers (VALIDYNE P55D) via stainless steel tubing. Pore-water pressure changes can be monitored over a range of 85 kPa (12.5 PSI) to 140 kPa (20.0 PSI) with a resolution between 8.0 - 15.0 Pa (Fig. 10b). The sensors are protected with valves if high excess pore-water pressures are met (e.g. owing to blocked hydraulic tubes). They are further used to bleed the tubing in case of gas is trapped inside, especially during the initial phase of deployment when the instrument is lowered through the water column.

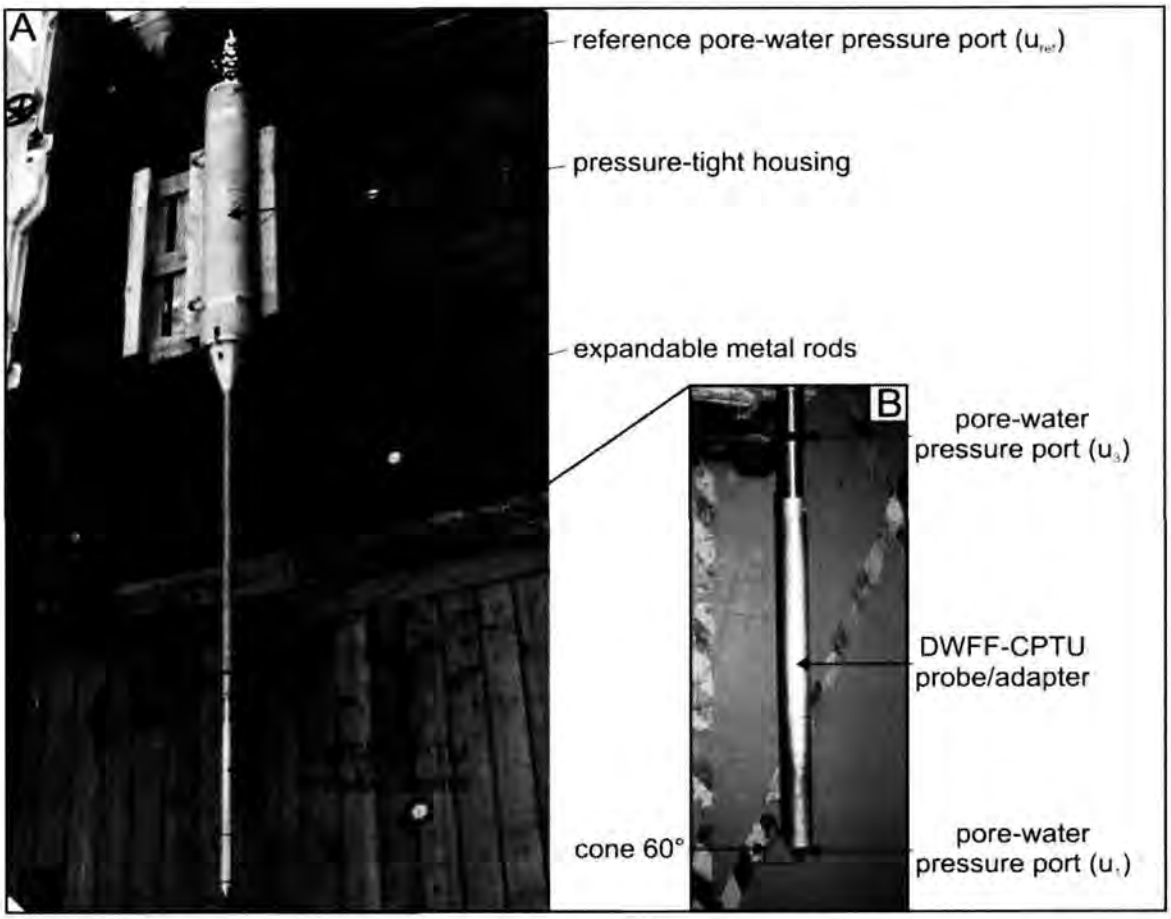

Fig. 10: Deep-water FF-CPTu instrument (a). Panel (b) shows blow up of the frontal portion with the pore pressure ports.

The DWFF-CPTu instrument is used in an autonomous mode, at which all sensor and transducer information will be stored on a standard secure digital memory card (SD) with a very high sampling frequency (1 kHz). In addition, a data transmission telemetry system (Seabird Electronics SBE36 CTD) is used to monitor all sensor and transducer parameter on board the research vessel in real-time (lower sampling frequency 1 Hz). The telemetry system consists of a deck unit (SBE36 CTD) and a PDIM. A schematically sketch of the telemetry system is shown in Figure11. It provides real-time data acquisition and control of the instrument (e.g. operation of the valves) via an attached personal computer (PC) using a self-developed LABVIEW control software.

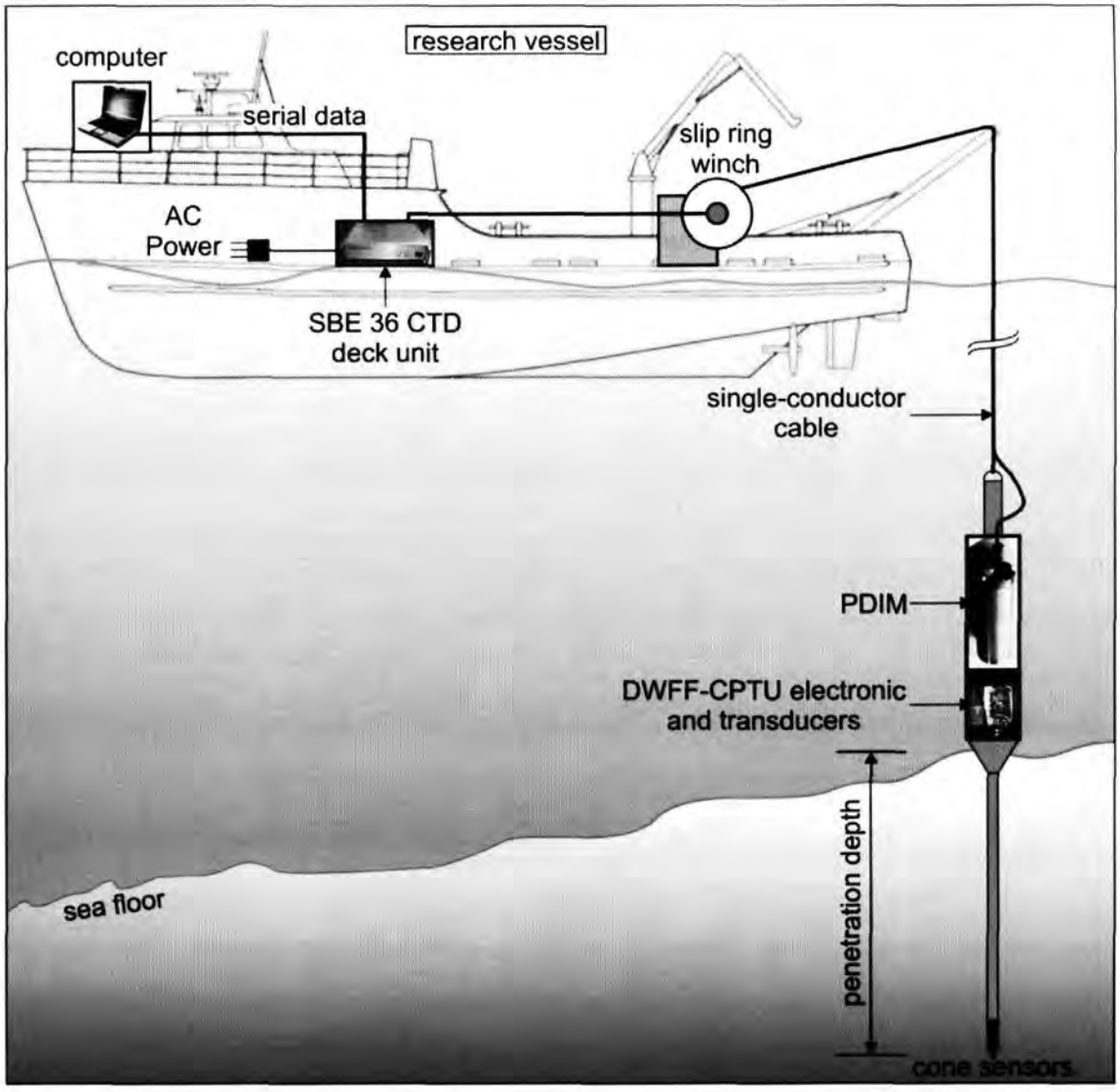

Fig. 11: Schematic of SBE36 CTD and PDIM telemetry system.

The frequency of data acquisition is variable and depends on the operation purpose of the DWFF-CPTU instrument (e.g. sub-seafloor profiling or pore-water pressure dissipation). Binary data are temporarily stored on a standard secure digital memory card (SD) and then downloaded via W-LAN to a PC. The two non-volatile battery packs available provide performance times of about eight to twelve hours, respectively. A self-developed deck interface box is used to download the recorded data and to charge the battery packs.

The length of the DWFF-CPTU instrument is variable from 4.1 m to a maximum length of 6.8 m depending on what type of sediment is anticipated. The extension is accomplished by adding 1.4 m long metal rods and internal extension data/power cables as well as steel tubing within them. Hence, the weight of the DWFF-CPTU instrument ranges from approx. 500 kg to max. 550 kg. The DWFF-CPTU instrument is deployed as individual measurement or pogo-style and remains in the sub-seafloor for about 20 to 30 minutes.

The DWFF-CPTU instrument was used with a self-developed piezocone probe/adapter (Fig. 11b) equipped with pore-water pressure ports at two locations (at the tip - Δu_1 and 0.75 m behind the tip - Δu_3). During RV *Poseidon* cruise P410, the DWFF-CPTU instrument was generally deployed in 4.1 m long mode (CPTU probe/adapter + 1 rod + pressure-tight housing).

A 1 kHz microprocessor data recording unit (AVISARO microcontroller) was utilised during deployments, focusing at the shape of the pore-water pressure dissipation curve (> 20 min deployment time according telemetry real-time data) and aiming at the sub-seafloor profiling of the sedimentary succession. The sub-seafloor profiling takes less than 7.0 sec and at the high sampling rate, provides the user with data of a vertical resolution < 5.0 $x10^{-3}$ m thickness.

The deployment mode aims (i) at a high-resolution vertical record (1 kHz logging frequency) of crucial in-situ sediment physical properties and (ii) at the recording of the excess pore-water pressure evolution once the DWFF-CPTU instrument is stuck in the sediment (dissipation test). Pore-water pressure dissipation is usually recorded for 20 to 30 min. The DWFF-CPTU instrument was veered at 1.2 m/s winch speed to a level 30 – 50 m above the seafloor, then the winch speed was varied between 0.5 - 1.2 m/s until the DWFF-CPTU probe hits the seafloor and dynamically decelerated until its penetration depth of several meters sub-seafloor (a fix winch speed for each location). The instrument is recovered after the dissipation test.

5.5. CAT-meter deployments

(M. Tryon)

The Chemical and Aqueous Transport (CAT) meter (Fig. 12) (Tryon et al., 2001) is designed to quantify both inflow and outflow rates on the order of 0.05 cm/yr to 100 m/yr. At high outflow rates, a time series record of the outflow fluid chemistry may also be obtained. These instruments have been in use since 1998 and have been successful in monitoring long term fluid flow in both seep and non-seep environments (e.g. Tryon et al., 2004, Tryon, 2010).

The CAT meter uses the dilution of a chemical tracer to measure flow through the outlet tubing exiting the top of a collection chamber (Fig. 13). The pump contains two osmotic membranes that separate the chambers containing pure water from the saline side that is held at saturation levels by an excess of NaCl. Due to the constant gradient, distilled water is drawn from the fresh water chamber through the osmotic membrane into the saline chamber at a rate that is constant for a given temperature. The saline output side of the pump system is rigged to inject the tracer while the distilled input side of the two pumps are connected to separate sample coils into which they draw fluid from either side of the tracer injection point (Fig. 13). Each sample coil is initially filled with deionized water. Having two sample coils allows both inflow and outflow to be measured. A unique pattern of chemical tracer distribution is recorded in the sample coils allowing a serial record of the flow rates to

be determined. Upon recovery of the instruments the sample coils are subsampled at appropriate intervals and analyzed using a Perkin-Elmer Optima 3000XL ICP-OES. Both tracer concentration and major ion concentration (Na, Ca, Mg, S, K, Sr, B, Li) are determined simultaneously.

Fig. 12: CAT flowmeter systems on deck of RV *Poseidon* prior to deployment.

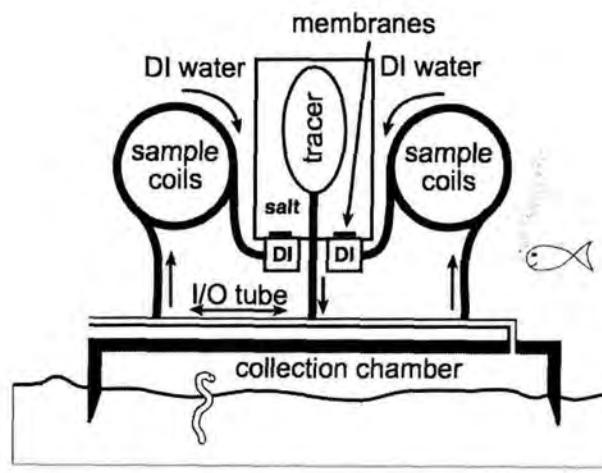

Fig. 13: CAT flowmeter schem,atic (from Tryon et al. 2001).

As explained in Tryon et al. (2001), diffusion in the sample coils is negligible. Typical sample sizes are 25-75 cm of tubing, many times the characteristic diffusion length for typical seawater ions at ocean bottom temperatures. Our data has shown that we typically achieve resolutions of ~0.5% of

the deployment time in the latest portions of the record and ~2% in the oldest portion for deployments of a year.

During Poseidon cruise P410, 2 CAT meters each were deployed on mud volcanoes Milano and Napoli, and and another deployed in a valley south of a large detached block between the inner and outer Mediterranean Ridge. These site were determined to be our best strategy for detecting and sampling fluid flow and fluid chemistry, based on the cores retrieved at each site and the temperature gradients measured. The locations and times of deployments are tabulated at the end of this section. Deployment was accomplished for the first two meters (Milano, Napoli) by installing each instrument into the video-guided deployment frame (Fig. 14), lowering to the sea floor, surveying for an appropriate site, and releasing the instrument on the sea floor at the site. Since we observed no biological indicators of fluid flow and no obstructions to sealing the collection chamber to the sea floor such as rocks or carbonate pavements, we deployed the other three meters using only the acoustic release on the hydro-wire without the video frame.

Fig. 14: CAT meter in video guided deployment frame.

5.6. Gravity coring and sediment description

(A. Kopf, S. Haas, T. Fleischmann, C. Bartsch, J. Castellino, C. Ioakim)

In order to recover sediment cores, a gravity corer with tube lengths of 3 to 6 m and a weight of approximately 1.5 tons was used during cruise P410 (Fig. 15). Before using the coring tool, the plastic

liners were marked lengthwise with a straight line in order to retain the orientation of the core for potential paleomagnetic analyses and then placed inside the steel tube of the gravity corer.

Fig. 15: Gravity corer on board RV *Poseidon*.

Once back on deck, the sediment cores were cut into sections of 1 m length, closed with caps on both ends and labelled according to a standard scheme (Fig. 16). By definition, the half core with the marked line was stored as archive half (after having passed the Multi-Sensor Core Logger – see Ch. 5.7.3), while description, sampling, etc. were carried out on the remaining half. For the detailed procedures each working half core underwent, see below.

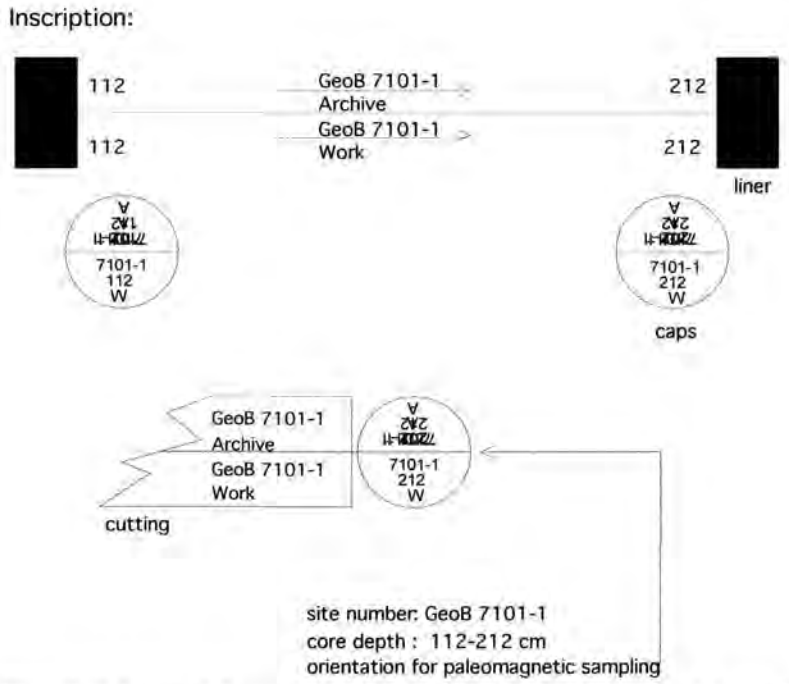

Fig. 16: Scheme of the inscription of gravity core segments used during P410.

Sediment description

Split gravity cores were photographed and described from a largely sedimentological standpoint. Grain size and composition of sediments were determined mainly visually using a simple hand-lens, HCl-testing and analyzing smear slides of dominant lithologies under a cross-polarizing microscope in accordance with Rothwell (1989). The size of grains was assessed based on Wenthworth's (1922) classification. The colour of the material was determined visually on board using Munsell's colour chart nomenclature, and also has been studied spectrophotometrically after the cruise on the Multi-Sensor Core Logger (MSCL; see Appendix 9.3). For each core, a composite one-page core log sheet was compiled. It shows core photographs next to a graphical core log and gives information on redeposition-/event layers (i.e., sand layers, volcanic ash layers or clear evidence for mass movement deposits, such as mud clasts in muddy or sandy matrix, tilted beds and repetition of strata), bioturbation and the assigned lithological units in three different columns. The core log is combined with results from the fall cone penetration test (see below). A wide variety of features, such as sediment lithology, primary sedimentary structures, bioturbation, soft-sediment deformation, and coring disturbance is indicated by patterns and symbols in the graphic logs. A key to the full set of patterns and symbols used on the barrel sheets is shown in Figure 17. The symbols are schematic, but they are placed as close as possible to their proper stratigraphic position. All core photographs are provided in Appendix 9.2 (see below).

Lithologies

- homogenouse to motteled yellowish brown (ochre) sandy to silty mud
- faintly laminated grayish to yellowish brown (ochre) sandy to silty mud with little Corg content
- motteled light (olive) gray to grayish sandy to silty mud
- olive gray silty mud with higher abundance of dispersed volcanic material
- dark olive gray silty mud with high Corg content (Sapropels)

Lithological Boundaries:

- clear, sharp boundary within few centimeters
- diffuse transition over several centimeters

Symbols (Physical structures and lithologic accessories):

- sand layer
- sand patch
- dispersed sand
- volcanic ash layer
- Pumice
- pieces of carbonate concretions
- fine grained black spots (high C-org)
- mud clasts
- slump folds
- fault (normal)
- cylindric hole filled with sandy to silty mud with circluar halo -- ? fluid conduit ?
- cylindric channel filled with sandy to silty mud ? fluid conduit ? or bioturbation ??
- cylindric void / channel (? fluid conduit?)
- void
- ?? ~5mm long fine hard, dark brown, elongeted components that look like wood remains but does not burn, no HCL raction. Agglutinated benthic formaminiferas or Concretions??

Biorubation:

- weekly bioturbated
- bioturbated / motteled - structurless
- absent bioturbation / laminated

Fossils

- coral (Caryophyllia)
- mussel shell (??)

Event Layer:

- clear evidence for redepostion event
- assumed redepostion event

Fig. 17: Key of symbols for barrel sheets of gravity core description.

5.7. Physical properties

(G. Wiemer, S. Haas)

During cruise P410, shipboard physical properties measurements were restricted to falling cone penetration tests and vane shear tests on the working half of the core. Since no container with a Multi-Sensor Core Logger (MSCL) could be placed on board RV *Poseidon*, these measurements on the undisturbed archive half of the cores were carried out immediately after the cruise at MARUM Bremen. A description of the instrument is given below (Ch. 5.7.3.).

5.7.1. Cone penetrometer

The geotechnical properties along the sediment cores were determined according to British Standards Institutions (BS1377, 1975). A Wykeham-Farrance cone penetrometer WF 21600 (Fig. 18a) was used for a first-order estimate of the sediment's stiffness. For the measurement, the metal cone was brought to a point exactly on the split core face (Wood 1985). A manual displacement transducer was then used to measure the distance prior to and after release of the cone (i.e. penetration after free fall of the cone). Precision is 0.1 mm of displacement. The distances measured can then be translated into sediment strength (see Hansbo, 1957).

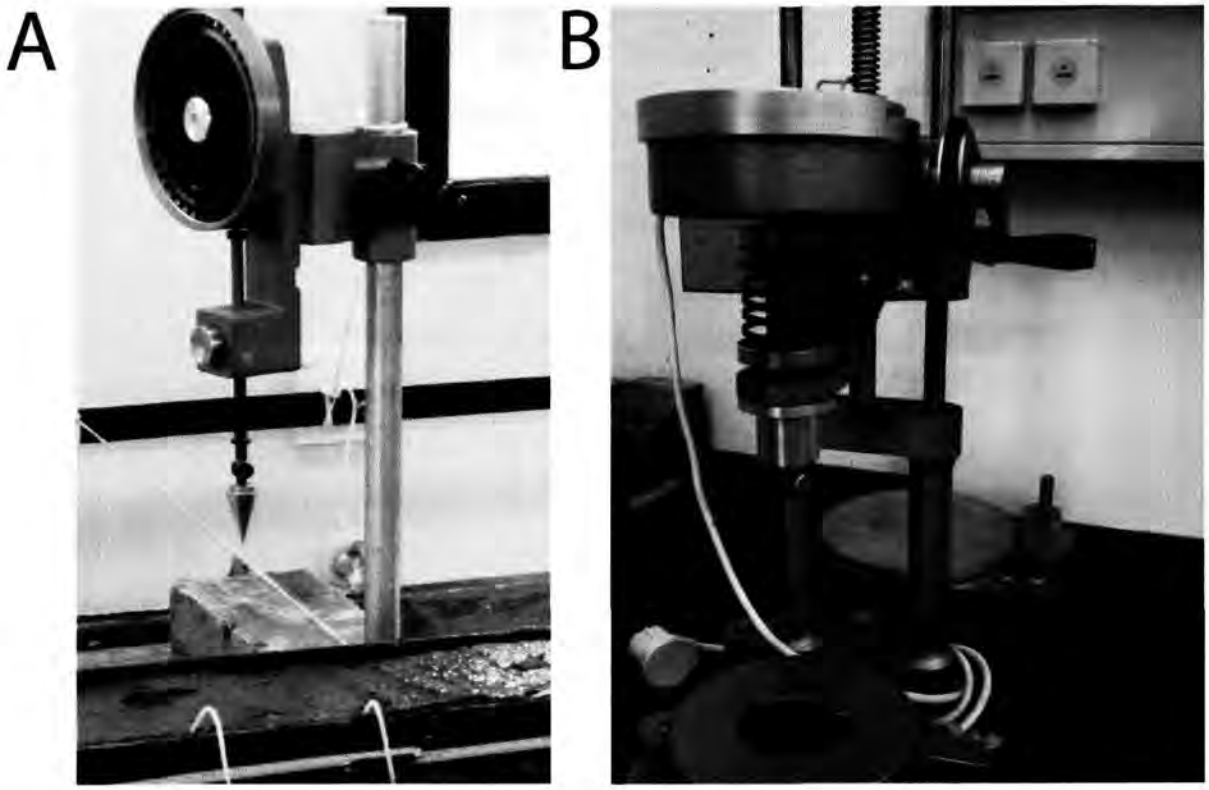

Fig. 18. (a) Falling cone penetrometer and (b) vane shear device used on the split core surface.

A falling cone penetrometer with a defined weight (80.51 g) and geometry (30° cone) was used by Hansbo (1957) during a detailed study of the relationship between the cone penetration and soil strength. The undrained shear strength s_u can be calculated from the variables mass and tip angle of

the falling cone, gravity g, penetration depth d and the cone factor k via the "cone factor". Wood (1985) calculated from fall-cone and miniature vane tests average values of cone factors (in our case k=0,85 for a 30° cone). The undrained shear strength can then be calculated using the equation $s_u = (k*m*g)/d^2$.

Shore-based laboratory testing will include ring shear experiments as well as dynamic triaxial shear tests to obtain residual strength and rate-dependent frictional properties as well as the liquefaction potential of the materials recovered.

5.7.2 Vane shear testing

In addition to the Cone Penetrometer a double vane shear apparatus by GSC ATLANTIC was used for more information about sediment stiffness and residual shear strength (Fig. 18b). The distance between the two vanes is 15 cm. For the measurements, four-bladed vanes (L = 12.5 mm, h = 6.25 mm, d = 12.5 mm) were inserted into the split undisturbed core faces and rotated at a constant rate of 90°/min. Data are logged via an interface module (GSC ATLANTIC) using the Testpoint software package.

A spring transmits the rotation at the vane. The torque required shearing the sediment along the vertical and horizontal edges of the vane. The undrained shear strength, s_U depends on the torque T, the vane constant K, the maximum torque angle at failure σ and the spring constant B that relates the deflection angle to the torque (Blum, 1997). The vane constant, K is a function of the vane size and geometry and was used during the measurements with $K=\pi*d^2*(h/2)+\pi*(d^2/6)$ for full dipping vanes. The undrained shear strength can then be calculated using the equation $s_U= T/K$. Shore-based laboratory testing will include ring shear tests to obtain residual strength and rate-dependent frictional properties of the materials recovered.

5.7.3 Multi-sensor core logger

The *GEOTEK* MSCL device at MARUM Bremen combines three sensors on an automated track (see schematic diagram in Fig. 19). The P-wave velocity, gamma ray attenuation (bulk density), and the magnetic susceptibility were recorded, and from this data the fractional porosity and impedance were calculated. RGB images were also produced with a full color digital line scan imaging system. Magnetic susceptibility, bulk density, and line scan photography were generally measured on all cores.

Magnetic Susceptibility

Magnetic susceptibility was measured with a Bartington point sensor MS2 using an 80-mm internal diameter sensor loop (88-mm coil diameter) operating at a frequency of 565 Hz and an alternating field of 80 A/m (0.1 mT). The sensitivity range was set to the low sensitivity setting (1.0

Hz). The sample period and interval were set to 2 s and 4 cm, respectively, unless noted otherwise. The mean raw value of the measurements was calculated and stored automatically. The quality of these results degrades in XCB and RCB cores, where the core may be undersized and/or disturbed. Nevertheless, general downhole trends are useful for stratigraphic correlations. The MS2 meter measures relative susceptibilities, which have not been corrected for the differences between core and coil diameters.

Gamma-Ray Attenuation

Bulk density was estimated for split core sections as they passed through the GRA bulk densiometer using sampling periods and intervals of 2 s and 4 cm, respectively, unless noted otherwise. A thin gamma beam from a Caesium-137 source with energies around 0.662 MeV is passed through the core and the relative intensity of this beam can be used to measure the gamma density. These photons are scattered by electrons in the core and loose some of their energy. To determine the gamma density the number of unscattered electrons is measured by counting photons with the same principle energy as the photon source. The gamma density of an aluminum billet of stepped thickness is used to obtain calibration equations to convert gamma density into actual density values.

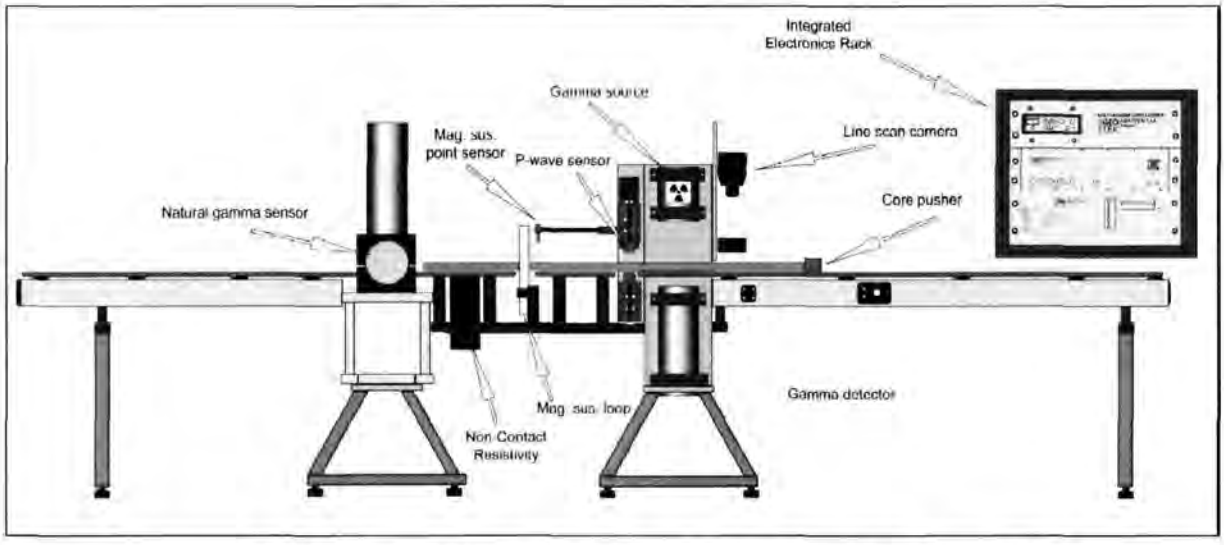

Fig. 19: Schematic drawing of the Geotek Multi Sensor Core Logger (MSCL).

P-Wave Velocity

The P-wave velocity is measured at 4-cm intervals and 2-s periods using two PWL transducers. The PWL measured P-wave velocity across the unsplit core sections. In order to determine the P-wave velocity, the PWL transmits 500-kHz P-wave pulses through the core at a frequency of 1 kHz. The transmitting and receiving transducers are aligned perpendicular to the core axis while a pair of displacement transducers monitors the separation between the P-wave transducers. Variations in the outer diameter of the liner do not degrade the accuracy of the velocities, but the unconsolidated

sediment or rock core must completely fill the liner for the PWL to provide accurate results. During this measurement good acoustic coupling between the core liner and transducer is achieved by adding water to the contact points.

5.8. Pore water geochemistry

(M. Zabel, K. Kirsch)

The composition of pore water in marine sediments is one of the most suitable indicators to characterize the benthic system. Thus, vertical, horizontal and temporal changes in concentrations of dissolved constituents can be used for identification and quantification of specific transfer processes, regardless of whether these are mircobially mediated or caused by abiotic reactions. Furthermore, pore water signatures and profiles can reveal the importance fluid transport mechanisms. In the majority of deep sea-sediments molecular diffusion is by far the dominate process, which controls the transport of dissolved components. When advection becomes important at a specific location (e.g. seep sites), the modeling of pore water profiles allows the calculation of the corresponding flow rates. Last but not least, pore water compositions can also indicate to the history of the waters of even to their primary source.

During this cruise, pore water geochemistry was conducted mainly to find indications for the upward transport of fluids from deeply buried formations, caused by the deformation and subduction of the African plate moving northward below the European plate. In this context salinity, mainly expressed by the concentrations of chloride, sodium, sulfate, magnesium, calcium and potassium, is of particular interest. Inorganic geochemical analyses were manifold, and usually started by measuring electrical conductivity (as a first-order measure of salinity) and pH (see Fig. 20a). For the extraction of pore water rhizon samplers (~0.4 µm; Seeberg-Elverfeldt et al., 2005) were used on the split core (Fig. 20b). The vacuum necessary to operate the rhizon samplers was created by pulling up 10 ml plastic syringes. The amounts of pore water retrieved by this method were between 5 and 10 ml. In general, the depth resolution varies approximately between 20 and 30 cm.

Fig. 20: (a) pH measurement and (b) rhizon pore water extraction in split working half of the gravity core.

Subsamples of 40 µL were diluted with 3960 µL deionized water for anion analysis, 1 mL aliquots were diluted with 9 mL of 1% HNO_3 for cation analysis. 0.5 to 1.5 mL of some sample preserved with zinc acetate for sulfide determination. The remaining original samples were kept without addition of preservatives. Analysis took place in the shore-based laboratory at MARUM, Bremen University. Cations were measured using ICP-OES (Agilent 720 Simultan; precision 1%). Anions were detected by ion-chromatography. We used a Metrohm ion-chromatograph equipped with a conventional anion-exchange column and carbonate-bicarbonate solution. For all measurements the standard deviation were found to be less than 2%.

5.9. ARGO floats

(A. Kopf)

Argo floats are built in specialist factories in the USA, France and Germany. They are built very carefully to work reliably for four years. A float is about 1.1 m tall and weighs around 25kg. Its body (the pressure case) is made of aluminium tubing sealed at the ends, and is strong enough to withstand pressures of more than 200 atmospheres - the pressure at 2000m depth. At the top are the sensors that measure temperature, salinity and pressure (depth), and an antenna to transmit the data back via satellite. At the bottom there is a rubber bladder, which can be deflated to make the float sink, or inflated to make it rise. The pressure case contains electronics, pumps and many batteries. The electronics include

- a microprocessor that stores the data from the sensors until it can be transmitted,
- a programme that controls when the float sinks and rises,
- and a position fixing and data transmission system that controls the interaction with the satellite.

A hydraulic system adjusts the buoyancy of the float, by inflating or deflating the external rubber bladder. Each float has a unique number that allows it to be recognised and distinguished from all the

other floats. A schematic of how a float looks is given in Figure 21. Figure 22 shows a float after having been deployed on cruise P410.

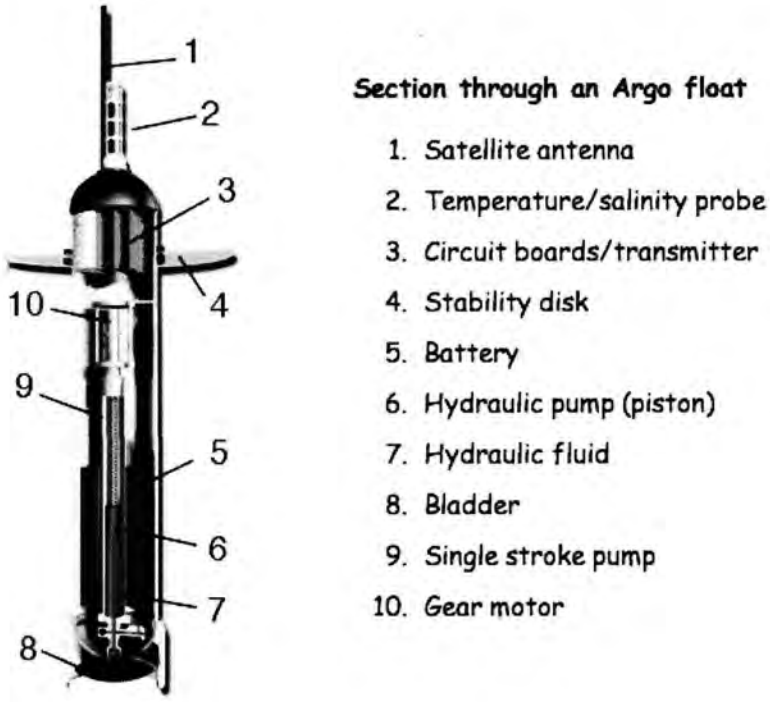

Fig. 21:. Cross-sectional view of an ARGO float and its components. See text.

Fig. 22: ARGO float after to deployment and prior to sinking to its operation depth below sealevel. See text.

When an Argo float is launched its bladder is inflated to keep it floating at the surface. After a few minutes the float sends a test message, then the pumps deflate the bladder and the float sinks. The float is designed to be a bit less compressible (squashy) than sea water, so as it sinks it becomes increasingly buoyant.

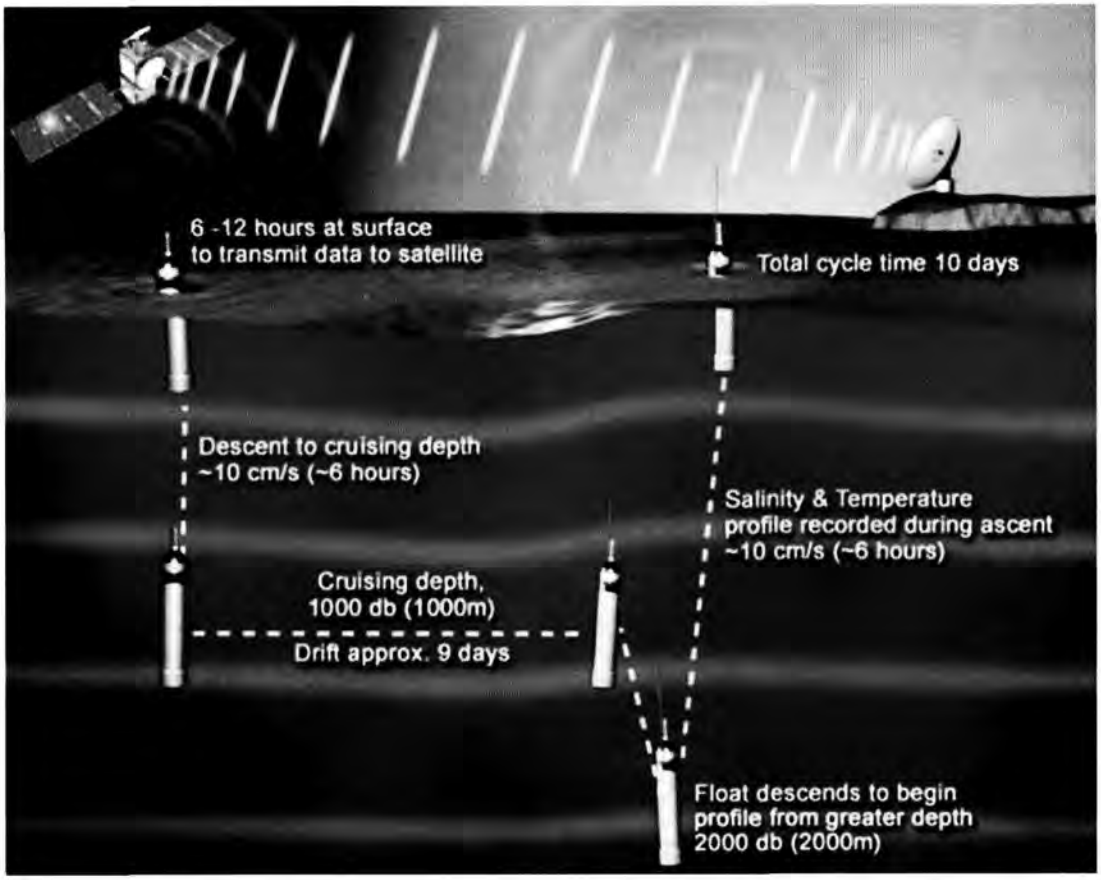

Fig. 23: Typical types of operations of an ARGO float. See text.

At about 1000m depth the float's density is the same as the density of the surrounding water,and so it stays at that level, drifting slowly with the currents. After a while the bladder deflates again, and the float sinks to 2000m (see Figure 23). There oil is pumped into the bladder; the float becomes buoyant and rises, measuring temperature and salinity on the way up. Some six hours later it reaches the surface and starts to transmit its data via satellite to an Argo ground receiving station. The position of the float is calculated from the Doppler shift of the transmitted message. Finally the bladder deflates and the float sinks to start all over again. This measurement cycle is repeated every 10 days. After 150-200 repeats (3-4 years) the batteries are exhausted. With no energy to bring it to the surface, the float drifts until the pressure case corrodes and leaks, and the float sinks to the seafloor.

6. Preliminary Results

6.1. Seafloor surveys

(S. Kufner, A. Kopf)

Given the fact that the Multibeam system on RV poseidon was installed rather shortly before cruise P410, seaflor mapping was not part of scientific tasks the research permission to the Greek authorities asked for. We hence had the system running for navigation purposes and to find the correct features on the seafloor (and to match them with existing bathymetric charts provided by Geosciences Azur), but did not record anything.

Figure 24 shows a screen shot obtained during the on-board bathymetric survey, which gives an example of the data quality.

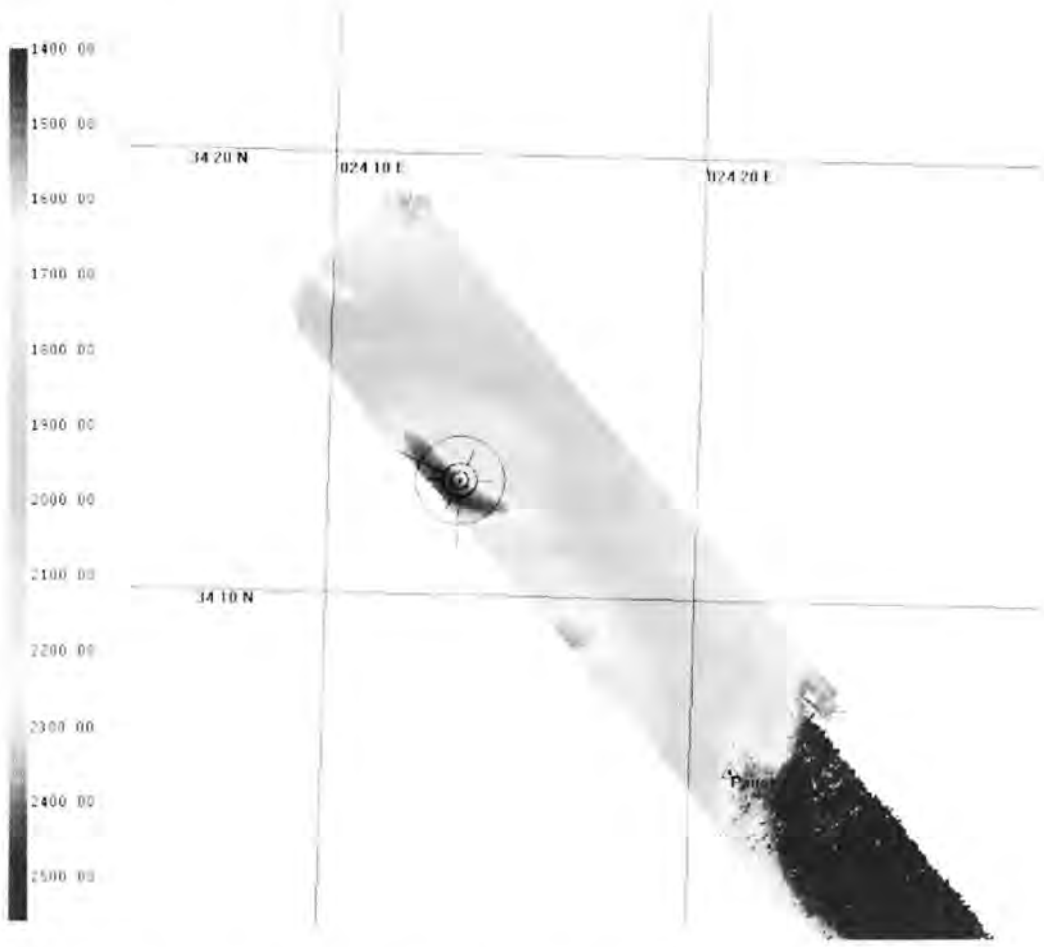

Figure 24: Screen shot showing the bathymetric data obtained during the Pos410 cruise using the *Hysweep* mapping tool (2).

6.2. Underwater video surveys (Video-MUC)

(M. Tryon, A. Kopf)

The camera system and underwater lights attached to the Multicorer frame provided rather dissappointing views of the mud volcano surface in terms of quality. One could see that there were no boulders or carbonate crusts or other obstacles, so for the purpose of steering clear of those when deploying the CAT meters the system was OK. However, it was rather demanding to focus the attention on the unsteady, low resolution video stream and the idea of using the MUC as a deep-towed camera system was abandoned after two attempts. In fact, even the CAT meters were deployed without video-guidance towards the end of the cruise (see station list, Appendix 9.1)

6.3. *In situ* temperature measurements

(M. Tryon, T. Fleischmann)

In order to obtain thermal gradients that may be helpful in identifying sites of active fluid flow or mud volcanism, and to place the sediment and pore fluid samples in the appropriate thermal regime, 3 or 4 Antares miniture temperature loggers (MTLs) were installed on outriggers on the core barrels for most coring operations (Fig. 9). These sensors have a resolution of approximately 0.001°C and accuracy of ±0.1°C and are programmed to record at 1 Hz (see section 5.3 above). On insertion a temperature spike is caused by friction that rapidly dissipates. The loggers were allowed to equilibrate after core penetration for 7 minutes before core retrieval. This was adequate for equilibration for all but the highest temperature changes at Milano MV. In this latter case a qualitative extrapolation was made that indicated only minor changes in temperatures and gradients (<5%) from that at the end of the record before extraction. The results are shown below (Table 1 and Fig. 25), organized by target feature or geologic province.

date	*station*	*gradient deg/km*	*gradient type*	*target feature or province*	*note*
110327	15362	1521	linear	Milano MV	970D, thick mud flow
110315	15306	1224	linear	Milano MV	970D
110315	15307	10	linear	Milano MV	970C
110327	15363	29	linear	Bergamo MV	
110318	15323	17	linear	Bergamo MV	
110317	15318	16	~linear	Bergamo MV	
110319	15325	8	linear	Bergamo MV	bent barrel
110317	15317	0	linear	Monza MV	
110317	15314	78	linear	Napoli MV	on plateau W of 971D
110318	15321	26	linear	Napoli MV	NE flank
110318	15320	8	linear	Napoli MV	on plateau S of 971D
110327	15366	37	linear	Leipzig MV	
110320	15332	24	linear	Leipzig MV	
110327	15367	24	linear	Maidstone MV	
110328	15370	23	linear	Maidstone MV	

110328	15369	20	~linear	ridge WNW of Maidstone	"Moscow MV"
110320	15330	16	linear	Lich MV	BUTT3 crest
110314	15303	11	linear	Lich MV	BUTT3 crest
110314	15302	-	not linear	Lich MV	BUTT3 NE flank
110320	15329	-	not linear	Lich MV	BUTT3 NW flank
110320	15331	-	not linear	Lich MV	2 km E of crest
110323	15345	50	linear	outer to inner ridge border	
110323	15343	25	linear	outer to inner ridge border	
110323	15344	11	~linear	outer to inner ridge border	
110326	15358	123	~linear	inner ridge to Crete margin	valley S of large block
110324	15347	59	linear?	inner ridge to Crete margin	BUTT2 only 2 loggers
110325	15353	25	linear	inner ridge to Crete margin	Spider mound
110325	15352	7	linear	inner ridge to Crete margin	Cat's eye
110324	15348	-	not linear	inner ridge to Crete margin	trench N of BUTT2
110326	15356	13	linear	Crete margin	BUTT1
110326	15357	0	linear	Crete margin	ridge
110325	15354	0	~linear	Crete margin	

Table 1: Results from MTL measurements at various GeoB stations.

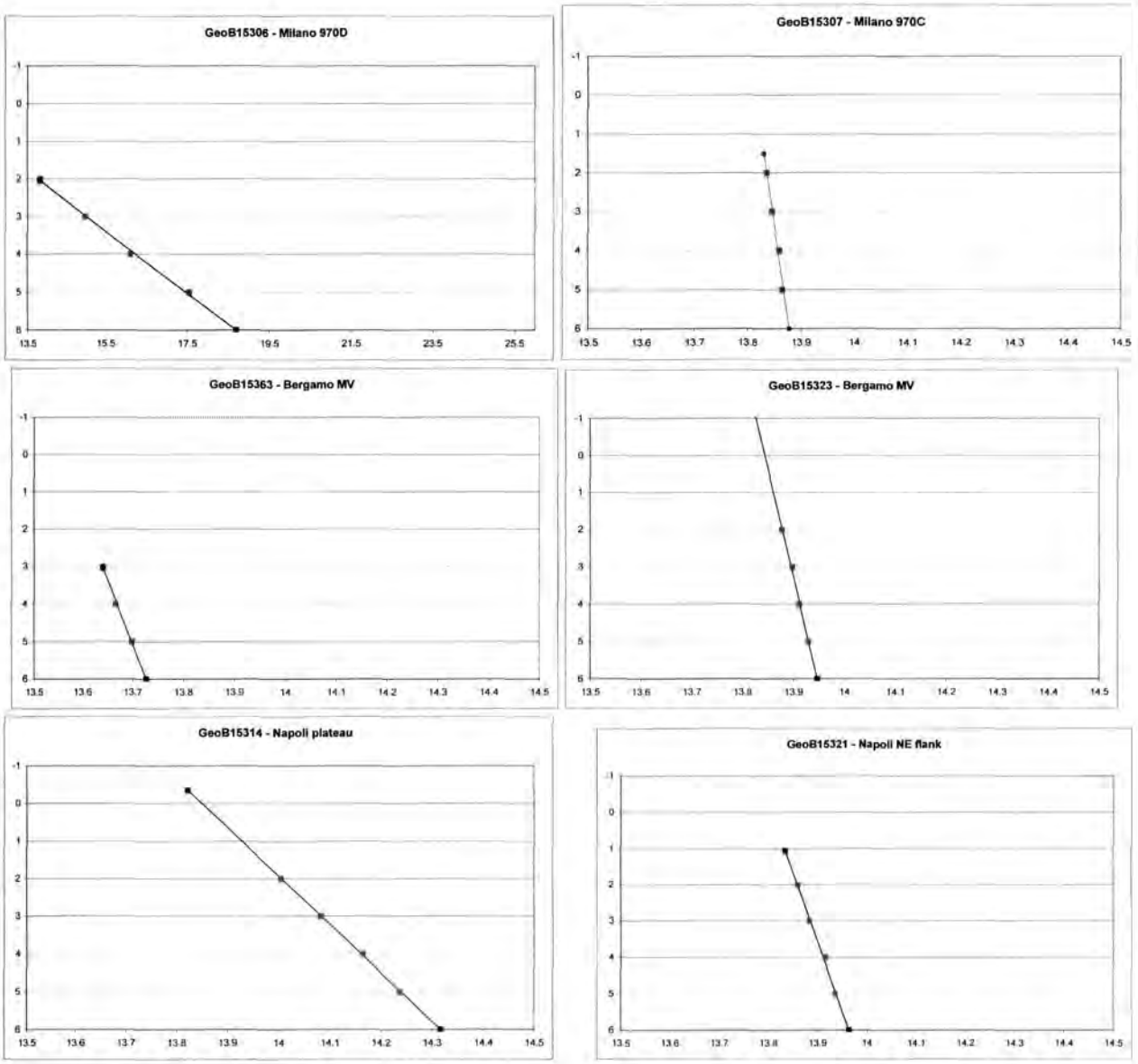

Fig. 25: T data (dots) and calculated gradients using the linear best fit function. Examples show Milano MV (top row), Bergamo MV (middle row) and Napoli MV (bottom row). See text.

6.4. *In situ* CPT testing

(A. Steiner, G. Wiemer, A. Kopf)

During Poseidon cruise P410, a total of 9 deep-water free-fall Piezocone Penetrometer measurements (DWFF-CPTU) were conducted (Fig. 26).

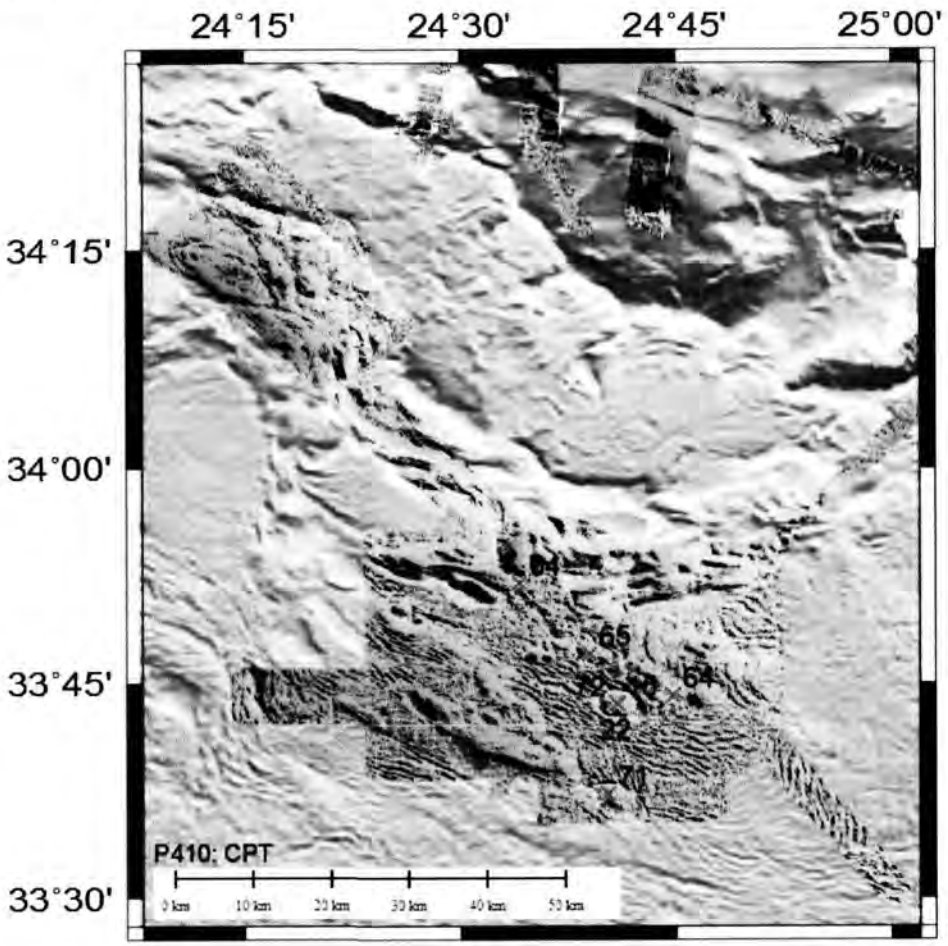

Fig. 26: Map showing all DWFF-CPTU deployments during the Poiseidon cruise P410. The deployments are represented with the last two digits of the GeoB nomenclature. The bathymetric chart underlying the map is courtesy of J. Mascle, Geosciences Azur, Villefranche-sur-Mer, France.

The water depth varies between 1950 and 2050 mbsl (meter below sea-level). The penetration depth ranges between 1.5 and 3.0 m. The DWFF-CPTU measurements address following strategies:

- operational checkout of the DWFF-CPTU equipment for water depth >1500 mbsl.
- Comparison between DWFF-CPTU measurements and gravity core data (vane shear and fall-cone tests) with respect to the strain-rate correction of the in-situ data.
- In-situ characterization of the background sediments close-located to the different MV's.
- In-situ characterization of the MV shallow sediment succession in order to evaluate the fluid/gas conditions, consolidation settings (active or not active MV) and strength properties.

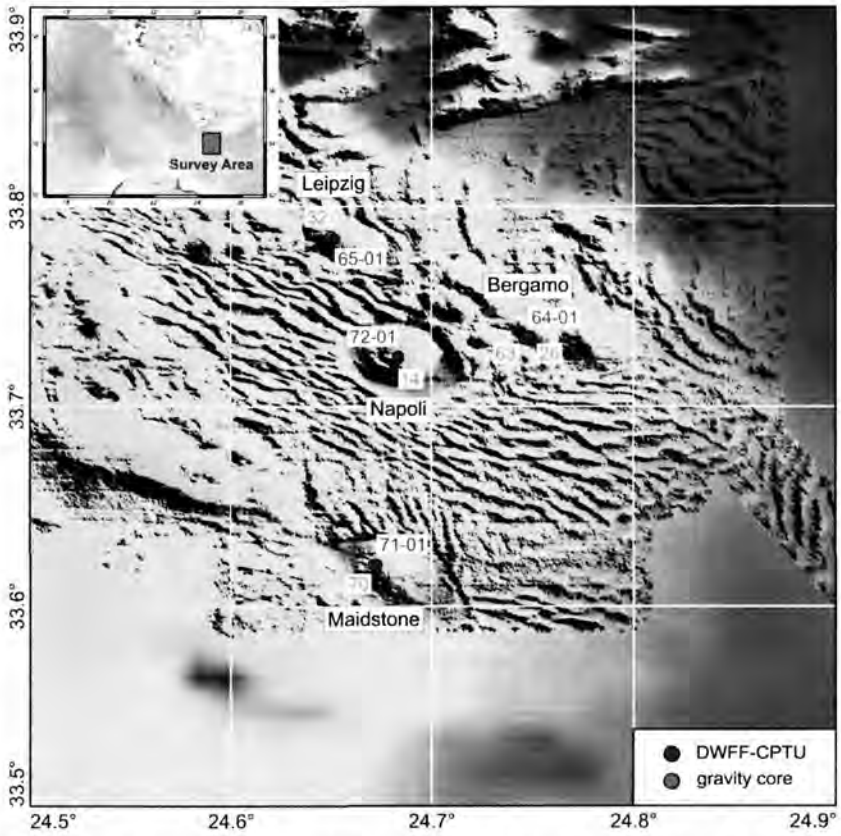

Fig. 27: Measured and corrected excess pore-water pressure at the tip (Δu_1) and 0.75 m behind the tip (Δu_3) for the Leipzig MV. Additionally, the derived undrained shear-strength (s_u) of the DWFF-CPTU measurements (GeoB15365_01) compared with the laboratory tests (GeoB15332) are shown. The green line represents the measured (dynamic) parameters. The red, blue and orange lines show corrected (quasi-static) parameters based on empirical strain-rate solutions (Dayal & Allen 1975, Mitchell 1976, A. Steiner, unpubl. data). Map is base don seafloor survey by J. Mascle, Geosciences Azur, Villefranche-sur-Mer, France.

Due to performance and electronic problems the first five tests failed (GeoB15304_01-02, 15315, 15322_01-02). However, those got sorted out and the subsequent five measurements gathered good results concerning the characteristic of the sub-seafloor sediments (GeoB15364, 15365, 15371, 15372). These tests are located at Leipzig, Bergamo, Napoli and Maidstone MVs, all located adjacent gravity coring sites (Fig. 27). The comparisons of the undrained shear-strength, measured in-situ and in the laboratory, show good accordance (Figs. 28 through 32).

The excess pore-water pressure of the sediments for MVs Leipzig, Bergamo and Maidstone varies between 20 and 60 kPa and the derived undrained shear-strength is between 5.0 and 15.0 kPa (Figs. 28, 29, 30, 32). Hence, these sediments are characterized as highly over-consolidated with an undrained shear-strength ratio (s_u/σ_0') of 0.5 to 1.5. The results indicate that the above mentioned MV's are not active.

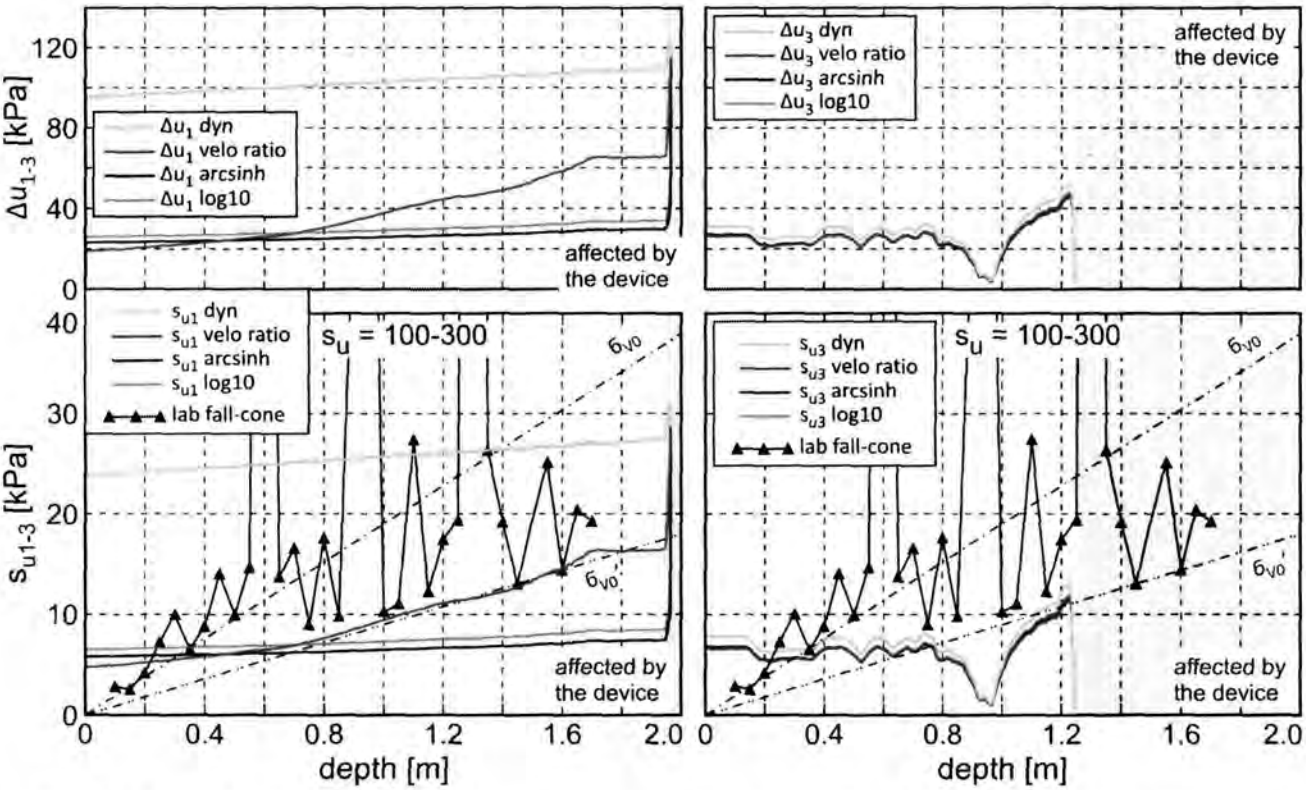

Fig. 28: Measured and corrected excess pore-water pressure at the tip (Δu_1) and 0.75 m behind the tip (Δu_3) for the Leipzig MV. Additionally, the derived undrained shear-strength (s_u) of the DWFF-CPTU measurements (GeoB15365-01) compared with the laboratory tests (GeoB15332) are illustrated. The green line represents the measured (dynamic) parameters. The red, blue and orange lines show corrected (quasi-static) parameters taking into account the empirical strain-rate solutions (Dayal & Allen 1975, Mitchell 1976, A. Steiner, unpublished data).

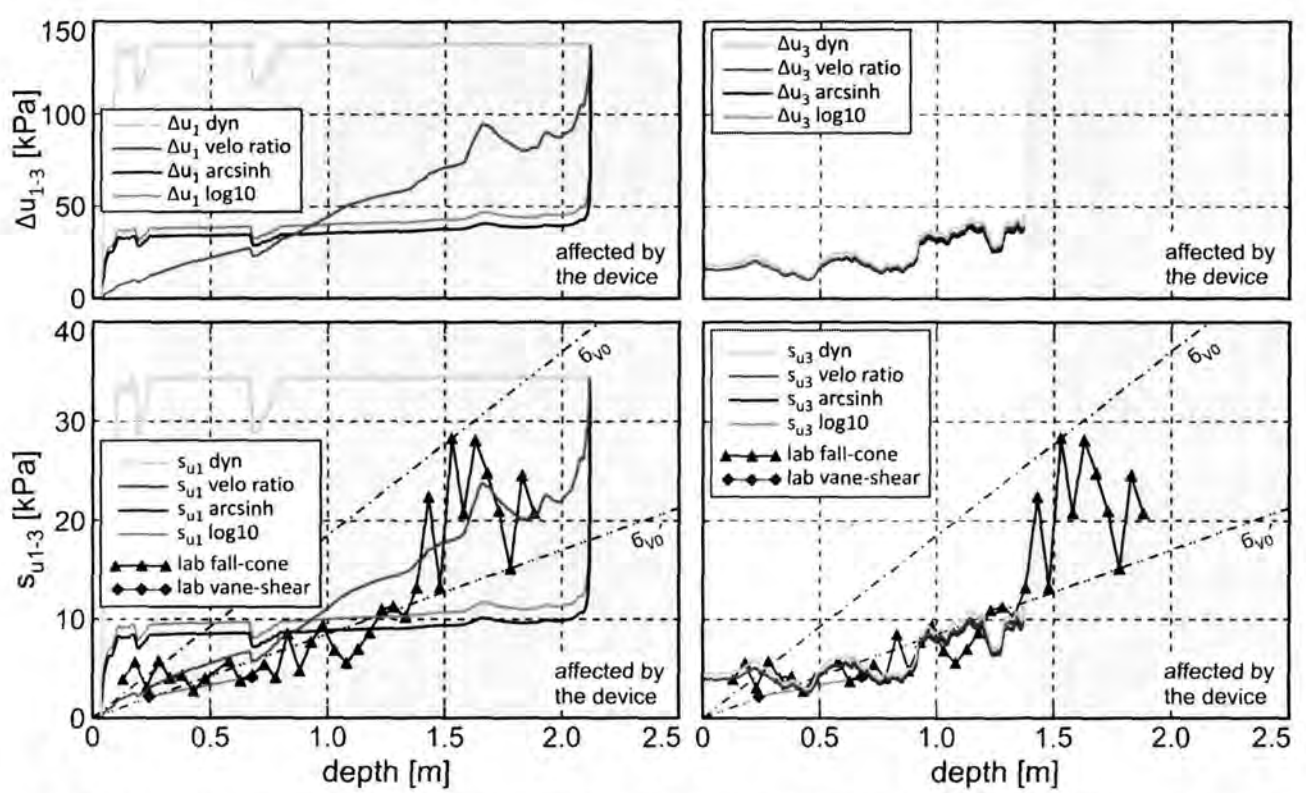

Fig. 29: Measured and corrected excess pore-water pressure at the tip (Δu_1) and 0.75 m behind the tip (Δu_3) for the Bergamo MV. Additionally, the derived undrained shear-strength (s_u) of the DWFF-CPTU measurements (GeoB15364-01) compared with the laboratory tests (GeoB15363) are illustrated. The green line represents the measured (dynamic) parameters. The red, blue and orange lines show corrected (quasi-static) parameters taking into account the empirical strain-rate solutions (Dayal & Allen 1975, Mitchell 1976, A. Steiner, unplished data).

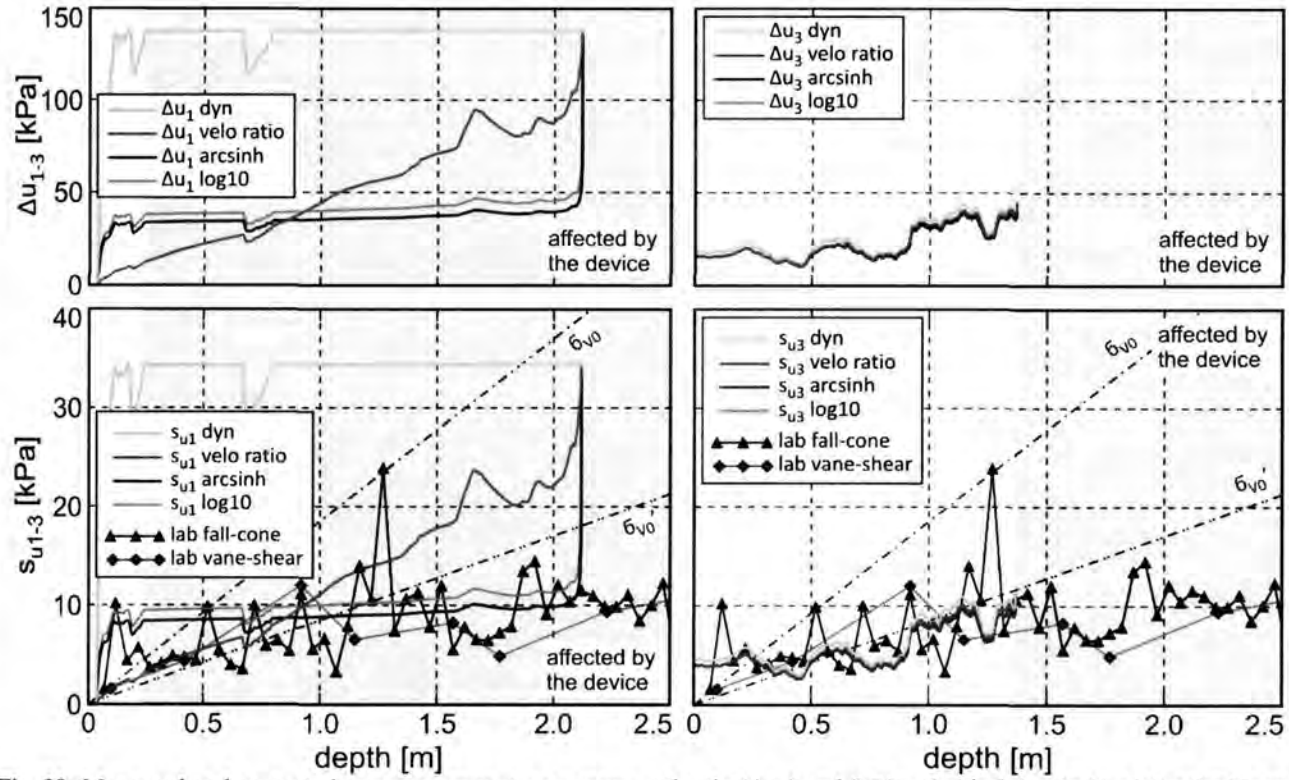

Fig. 30: Measured and corrected excess pore-water pressure at the tip (Δu_1) and 0.75 m behind the tip (Δu_3) for the Napoli MV. Additionally, the derived undrained shear-strength (s_u) of the DWFF-CPTU measurements (GeoB15372-01) compared with the laboratory tests (GeoB15314) are illustrated. The green line represents the measured (dynamic) parameters. The red, blue and orange lines show corrected (quasi-static) parameters taking into account the empirical strain-rate solutions (Dayal & Allen 1975, Mitchell 1976, A. Steiner, unplished data).

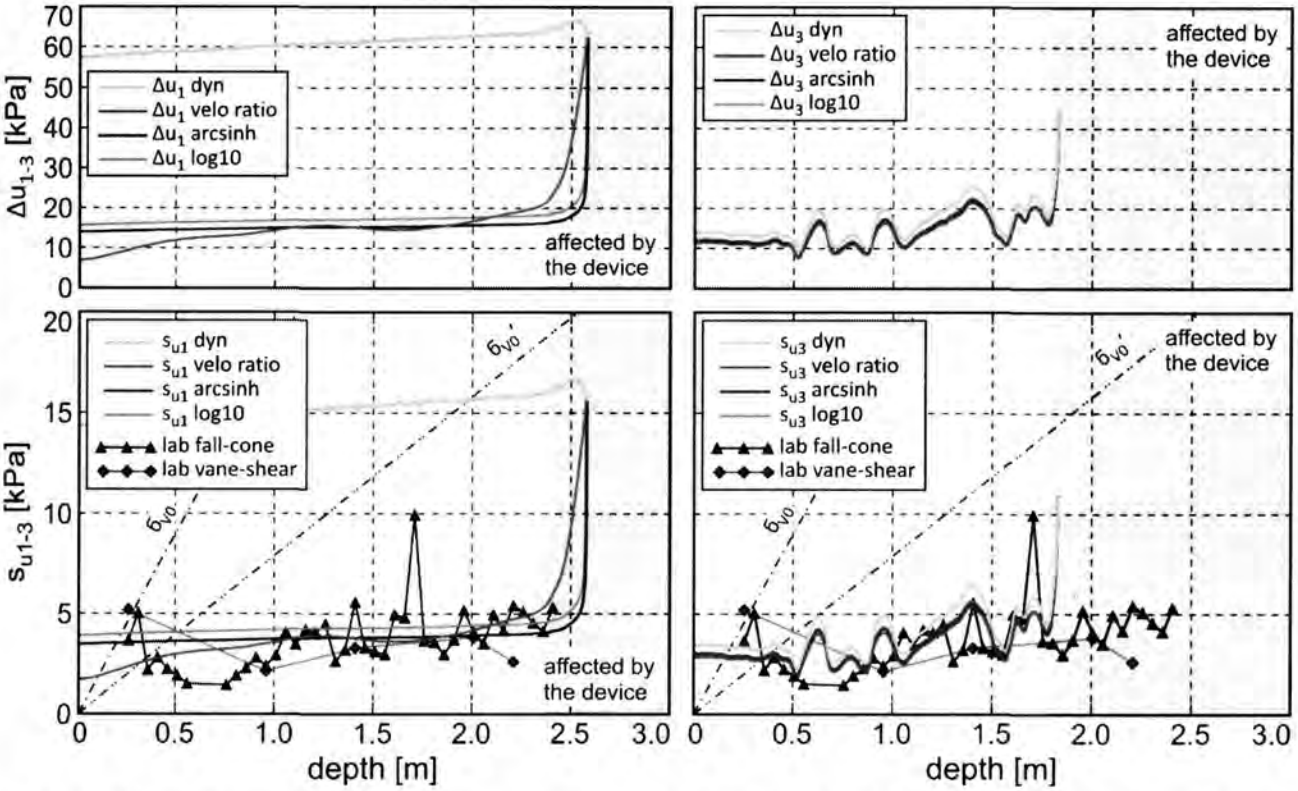

Fig. 31: Measured and corrected excess pore-water pressure at the tip (Δu_1) and 0.75 m behind the tip (Δu_3) for the Bergamo MV. Additionally, the derived undrained shear-strength (s_u) of the DWFF-CPTU measurements (GeoB15364-01) compared with the laboratory tests (GeoB15363) are illustrated. The green line represents the measured (dynamic) parameters. The red, blue and orange lines show corrected (quasi-static) parameters taking into account the empirical strain-rate solutions (Dayal & Allen 1975, Mitchell 1976, A. Steiner, unplished data).

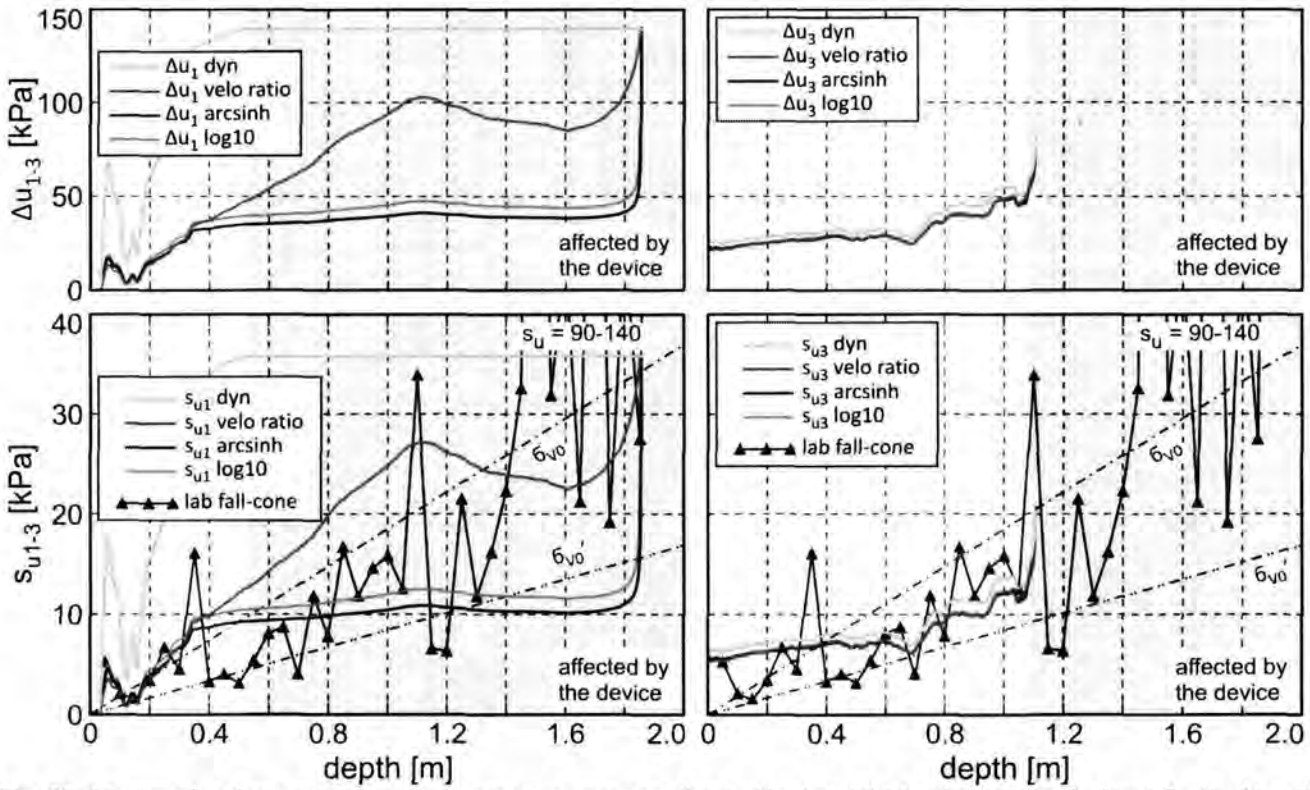

Fig. 32: Measured and corrected excess pore-water pressure at the tip (Δu_1) and 0.75 m behind the tip (Δu_3) for the Napoli MV. Additionally, the derived undrained shear-strength (s_u) of the DWFF-CPTU measurements (GeoB15372-01) compared with the laboratory tests (GeoB15314) are illustrated. The green line represents the measured (dynamic) parameters. The red, blue and orange lines show corrected (quasi-static) parameters taking into account the empirical strain-rate solutions (Dayal & Allen 1975, Mitchell 1976, A. Steiner, unplished data).

The measurements for the MV Napoli show excess pore-water pressures between 10 and 20 kPa and an undrained shear-strength of 2.0 to 5.0 kPa (Fig. 31). Characteristic for these sediments is the normally- to slightly over-consolidated behavior with an undrained shear-strength ratio (s_u/σ_0') of 0.2 to 0.5. Consequently, this mud volcano is clearly active (see also section 6.3 above).

In all tests, fluid/gas structures, coarser sediments and angular to well rounded clasts are scattered along the sediment succession. These features are identified by a significant drops of the excess pore-water pressure and an increase of the laboratory parameters (i.e. Figs. 28 and 30). More data will be acquired during post-cruise geological/geotechnical laboratory measurements (standard- and advanced tests).

6.5. CAT-meter deployments

(M. Tryon)

From the six CAT meters initially prepared for cruise P410, five got deployed. The locations are given in Figure 33 and Table 2, showing that four ended up on mud volcanoes while the fifth was placed at the potential outcrop of the backthrust fault separating the "modern" MedRidge from the Inner Ridge.

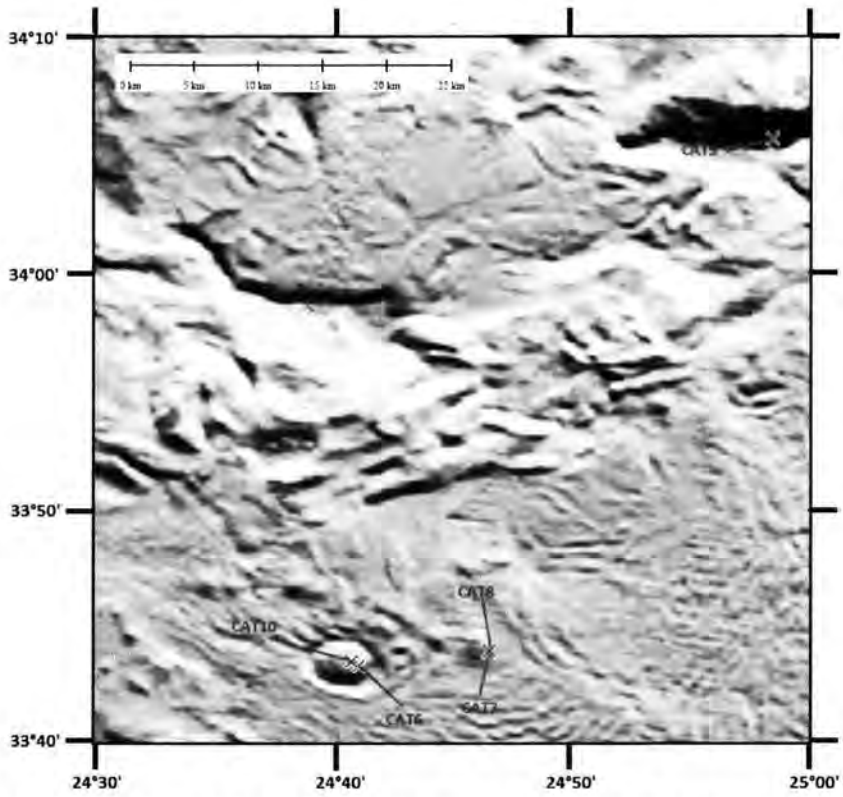

Fig. 33: Map showing the locations of the CAT meter deployments. Background bathymetry courtesy of J. Mascle, Geosciences Azur, Villefranche-sur-Mer, France.

meter	release serial #	deploy date	time (UTC)	Latitude	Longitude	location
CAT 6	34152	28-Mar-11	1420	33°43.45	24°41.15	center of Napoli mud volcano
CAT 7	34149	28-Mar-11	1550	33°44.02	24°46.56	center of Milano mud volcano
CAT 8	34151	15-Mar-11	2220	33°44.10	24°46.61	center of Milano mud volcano
CAT 9	34150	26-Mar-11	1830	34°05.65	24°58.44	valley S of large ridge on inner-outer ridge border
CAT 10	34147	17-Mar-11	1400	33°43.64	24°40.86	center of Napoli mud volcano

Table 2: Positions of CAT meter stations during cruise P410.

In spring 2012, cruise P429 with RV Poseidon is setting out to recover the flowmeters.

6.6. Gravity coring and sediment description

(A. Kopf, S. Haas, T. Fleischmann, C. Bartsch, J. Castellino, C. Ioakim)

A total of 43 gravity cores were taken during cruise P410. Usually, either the 3m or 6m long version was used, sometimes equipped with outriggers containing MTLs (see sections 5.3 and 6.3 above). The cores can be divided into three subgroups on a regional basis:

- Mud volcanoes on the active MedRidge
- Inner deformation front / Inner Ridge
- Inner Ridge-Cretan Margin transition.

The subdivision of the cores into these three categories is listed in Table 3. The cores will be described as subgroups in the following.

Region	Core GeoB153-	Length (cm)	Comments
Inner deformation front			
	41	0-138	strong, brownish sediment, coarse-grained layer
	43	0-538	light brown-grey, similar to -44 and -45
	44	0-200	light greyish brown, contains large clast
	45	0-255	grey-brown, partly dry and mottled
	40	0-79	
	34	0-50	grey-brownish, high shear strength
	39	0-320	contains white, broken up material
	35	0-250	various colours, two harder layers, contains sapropel
	37	0-89	brownish hard material, old accreted strata??
Inner Ridge – Cretan Margin			
	47	0-187	background sediment, layered, brittle, high shear strength
	48	0-56	background sediment
	49	0-265	background sediment with several sapropels
	51	0-148	yellowish-brownish sediment
	52	0-458	background sediment with sapropel
	53	0-367	background sediment with sapropel
	58-1	0-73	hard, brittle greyish material, old accreted strata?
	58-3	0-134	hard, brittle greyish material, old accreted strata with some clasts
	54	0-440	multi-coloured layered sediment, with sapropels
	56	0-300	multi-coloured layered sediment, with sapropels
	57	0-244	multi-coloured layered sediment, contains white layer
Mud Volcanoes			
Lich	2	0-139	grey and brownish hemipelagic sediment
	3	0-485	bioturbated background sediment, greyish
	29	0-280	layered sediment, no mud breccia
	30	0-150	grey and brownish colours mixed
	31	0-291	grey and brownish hemipelgic sediment, indurated, contains sapropel
Leipzig	32	0-187	top grey mud with white bands, below moussy mud
Napoli	11	0-299	grey fine-.grained mud, layered
	12	0-319	grey indurated material, high strength, similar to -26
	14	0-260	similar to -12 or -26
	20	0-47	top brownish hemipelagite, below grey mud breccia/flow
	21	0-263	top brownish hemipelagite, below grey mud without clasts, high shear strength
Monza	17	0-59	grey mud with clasts, less homogeneous than -12 and -14, similar to 26
Bergamo	63	0-180	-
	23	0-300	fluid rich mud, moussy, grey
	25	0-77	grey, strong mud with dark clast, similar strength as 25 or 26

	26	0-300	interlayering between background sediment and mud breccia/extruded grey mud
Milano	6	0-30	mud matrix with large clast (fills entire core liner), also smaller angular clasts
	9	0-50	grey, inhomogeneous mud with clasts, brownish in places, low shear strength
	10	0-110	grey, inhomogeneous mud with clasts, similar to 62
	62	0-291	matrix-supported mud breccia
	7	0-200	grey, inhomogeneous mud with clasts
Maidstone	67	0-315	-
	70	0-200	top brownish hemipelagite, below mud breccia with large clast, top bioturbated
mud ridge	69	0-315	layered (background?) sediment

Table 3: List of gravity core stations during cruise P410.

6.6.1 Mud volcanoes on the active MedRidge accretionary complex

On the various mud volcanoes and ridges studied during cruise P410, 24 gravity cores were taken altogether. The mud domes included Milano and Napoli (which were also drilled during ODP Leg 160 (Emeis et al., 1996) as well as Leipzig, Maidstone, Lich, Bergamo and an unnamed mud ridge in the southern portion of the Olimpi field area (Fig. 34). Table 3 specifies how many cores were taken on which feature, and also provide a short summary of the lithological observations plus the length of the recovered section.

In general, the group of features sampled can be broadly divided into active and dormant ones, with the recovery of grey mud or mud breccia having been the main criterion. Based on the observations in the sediment plus additional data (T data from MTLs [section 6.3], pore pressure from CPTu [section 6.4], physical properties [section 6.7] and pore water geochemistry [section 6.8], and results from former studies), we suggest that the recently active features include Milano, Napoli, Leipzig and Bergamo whereas the mud ridge, Lich and Maidstone.

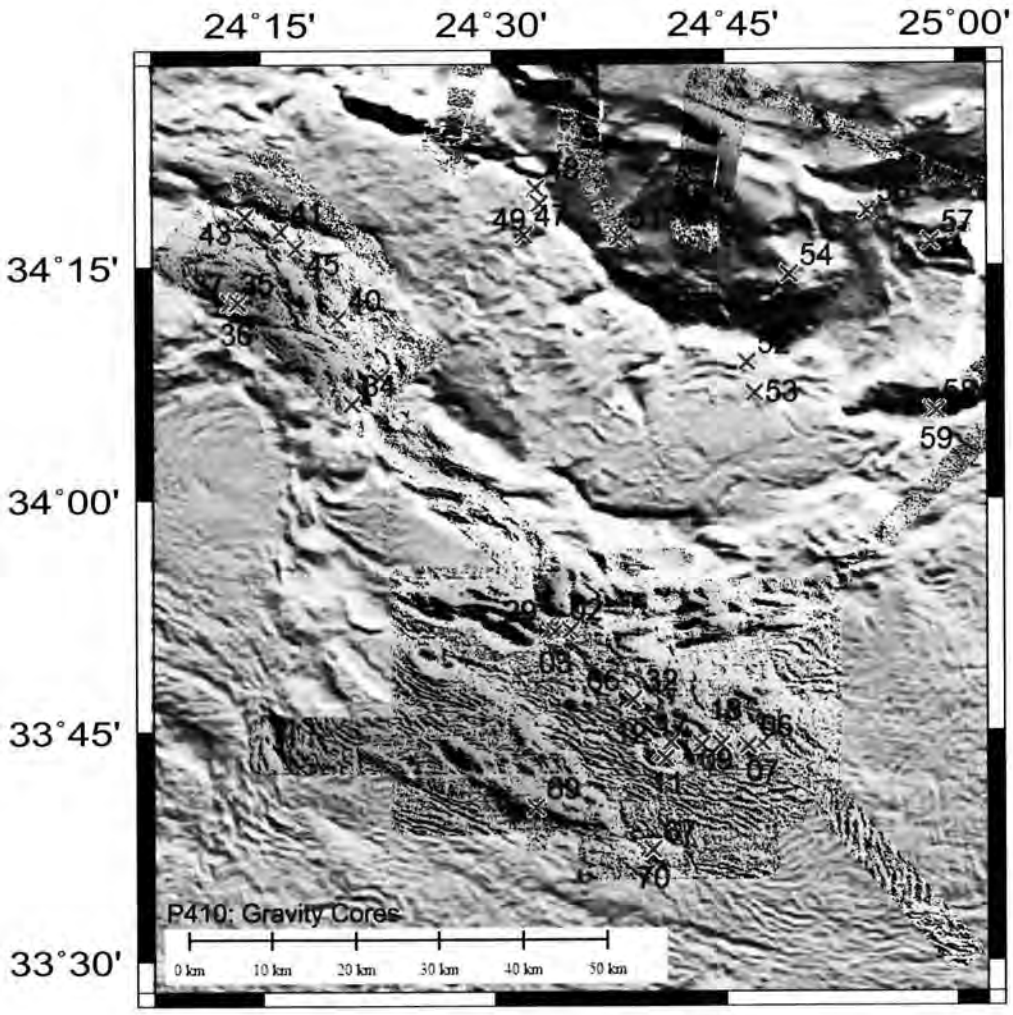

Fig. 34: Map showing the gravity core locations visited during cruise P410. Background bathymetry courtesy of J. Mascle, Geosciences Azur, Villefranche-sur-Mer, France.

Among the active ones containing grey mud/mud breccia, only Napoli is actively seeping fluids while all others are temporarily dormant, but in places show a mousse-like texture rich in waters and (inferred, since we did not sample this) gas. Moussy sediment was found at MV Bergamo (only core GeoB15323) and Napoli (GeoB15312 has gas voids in many places, ODP Leg 160 holes 971D and 971E at the crest have gas pockets of variable size throughout; Emeis et al., 1996), which then also indicated where the conduits reach the seafloor.

Bergamo MV has otherwise a brownish thin cover of background sediment, which is underlain by mud breccia (GeoB15325). Core GeoB15326 is very interesting as it mirrors the episodic activity in mud flows. An interlayering between multi-coloured bakgroudn sediment with mud breccia or extruded mud is found, with grey mud lenses at 55-64 cm bsf (below sea floor), 121-127 cmbsf, 140-149 cmbsf, 164-167 cmbsf, and then from 192 cmbsf until terminal depth of the core at 300 cmbsf (see example in Fig. 35, right; refer also to complete lithologs in Appendix 9.2). The background hemipelagites contains brownish to reddish mud, dark grey to black sapropels of several decimeters in thickness, and almost white to brown patches and layers of fine-grained mud. Dating will shed light

on the timing of the various phases of mud volcanic activity/extrusion in post-cruise research. It can be assumed, however, that Bergamo has either been actively venting methane gas so that oxidation of organic matter was hampered, or that the dark deposits associated (and sometimes amalgamated with the grey mud (GeoB15323, -25, -26) are not sapropels, but assoiated with mud extrusion (post-cruise XRD analyses will hopefully clarify this aspect). The clasts found within the mud breccia are claystones of various degree of hardness, but also lithified sedimentary rocks (mudstones, polymictic sandstones and gravels).

Leipzig MV is similar to Bergamo MV in the sense that the mud breccia recovered is overlain by 6-8 cm of red to brown clayey background sediment (GeoB15332). The mud breccia contains abundant clasts, some of which are several cm in diameter and comprise well indurated material from the deeper accretionary complex.

Maidstone MV is also not so dissimilar from Leipzig and Bergamo MVS given that a dm-thick cover of hemipelagic sediment is overlying mud breccia, with the contact being diffuse (see zone between 10 and 30 cmbsf in core GeoB15370, Fig. 35 centre; Appendix 9.2). The clasts are mm- to cm-sized, subangular, and usually soft and altered. In the lower part of the core, the clasts are light olive grey, disggregated, and smeared out horizontally.

Monza MV is also similar to Maidstone and Leipzig MVs, i.e. the core recovered (station GeoB15317) shows a cm-thick cover of reddish brown background sediment that overlies an inclined, cascading surface of grey mud breccia. The core was aiming at the crestail area of the dome, however, the inclined surface suggests some flank processes including creep or sliding.

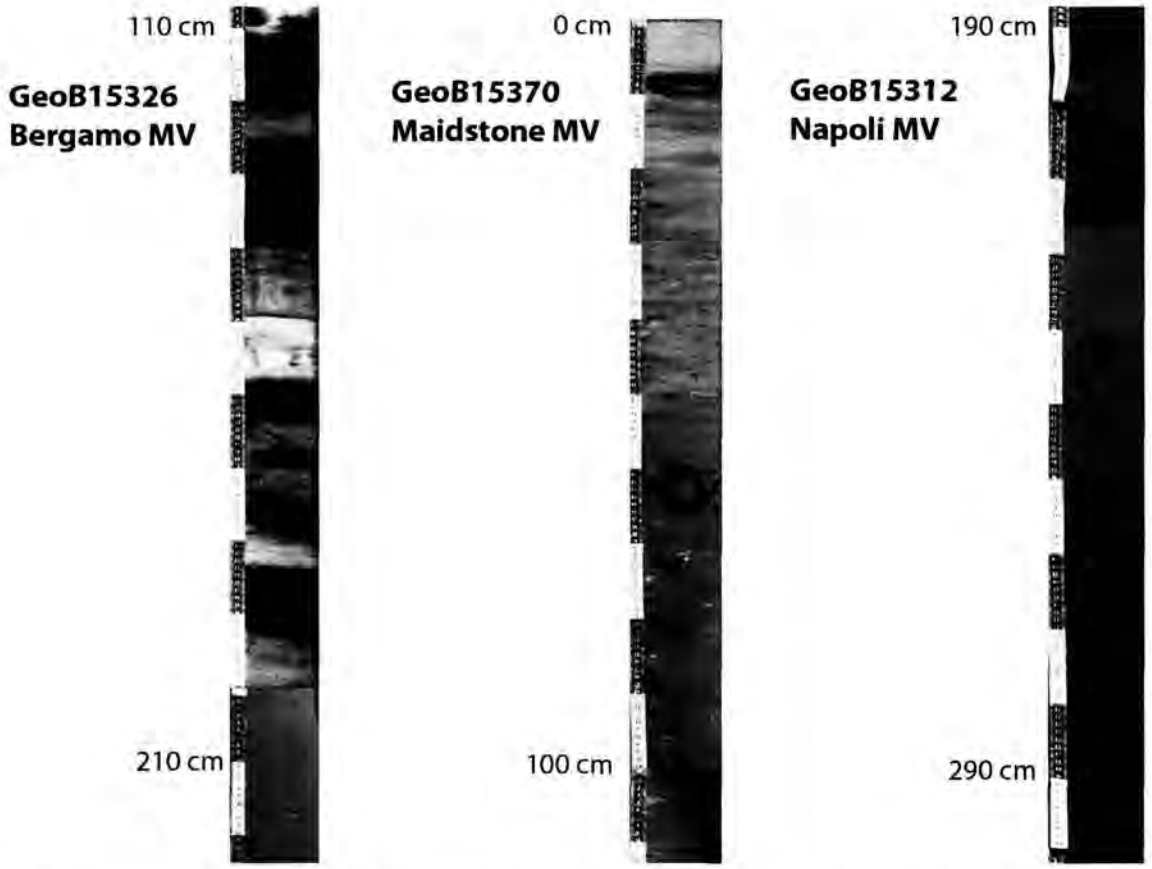

Fig. 35: Selected sections from core photographs of stations GeoB15326 (Bergamo MV with interbedded background sediment and mud breccia), left; GeoB15370 (Maidstone MV with clast-rich mud breccia overlain by hemipelagite), centre; and GeoB15312 (Napoli MV with prominent gas voids).

From the five cores taken at Napoli MV, a fairly comprehensive picture can be gained, in particular with the results from earlier drilling (ODP Site 971; Emeis et al., 1996) and in situ T and pore pressure as well as pore water geochemistry gained during cruise P410. Cores GeoB15311 and -12 correspond to the positions of ODP Holes 971D and 971E, and like the earlier drillings, comprise mud/mud breccia only. Core -12 shows numerous gas voids of several cm (cf. Fig. 35, right), which is somewhat different from the mousse-like texture with small gas pockets at Hole 971E (Emeis et al., 1996). At the top, core -12 consists of light grey mud with an irregular, channelised transition to the darker grey mud breccia underneath (injection channels?, bioturbation?) (see lithologs in Appendix 9.2). Core GeoB15314 is similar to -12, with enigmatic, irregular patterns at around 60 cmbsf and laminated, sometimes horizontally "smeared" mud volcano eruption material. When moving towards the flank and downslope, cores GeoB15320 and -21 show 25 cm and 71 cm of hemipelagic sediment overlying the mud breccia, respectively. Again, this finding is consistent with the results from ODP Leg 160.

The remaining mud volcanic features, namely Lich MV and the mud ridge, show hemipelagic sediment throughout and lack evidence for active fluid flow or sediment mobilisation. Cores GeoB15302 and -03 both contain sapropel S1, with -02 being a much condensed version of -03 (see lithologs in Appendix 9.2). Cores GeoB15329 and -30 seem to mirror -02 and -03, i.e. -30 being the

condensed version of -29 with eiether sequence recovered sporting S1. Interestingly, core -31 somewhat deviates from this pattern since it shows a comprehensive, 165 cm-long succession above S1 (similar to e.g. -03), but then a condensed interlayering of grey, white and yellowish deposits of only ca. 65 cm until S2 is recovered (see lithologs in Appendix 9.2). Core -31 represents the longest hemipelagic record back in time from all mud volcano cores.

Core GeoB15369 taken on the mud ridge in the southern part of the olimpi field region (Fig. 34) is different from any of the cores recoevred in the neighbourhood. It contains grey sediment on top of inclined red material (upper 21 cmbsf), both overlying a beige/yellowish brown mud of homogeneous nature (21-ca. 40 cmbsf). Underneath, the texture becomes mottled and irregular and oftentimes, darker patches of presumed organic-rich material are found (at appx. 140-160 cmbsf; see lithologs in Appendix 9.2). For the ca. 160-170 cm underneath, the sediment is predominantly grey and may be of mud extrusive origin. However, there is abundant evidence for soft sediment deformation so that an accretionary origin cannot be excluded. The structural grain of the crest of the ridge is in favour of such an interpretation.

6.6.2 Inner deformation front

A total of nine gravity cores (Table 3) were taken along the northernmost portion of the Mediterranean Ridge accretionary complex and its contact to the Inner Ridge, its presumed older counterpart (Kopf et al., 2003). The cores recovered can be – very boadly – be split into two groups: Those containing grey indurated mud very similar to that found in some mud volcano cores (see above), and those without such material, but hemipelagic background sediment throughout. Some of that "background sediment", however, is well indurated and may point towards an accretionary origin.

The first group of cores contains stations GeoB15334, -37, and -41. Core -34 at first glance resembles a typical mud volcano core, with predominantly grey mud with angular (rip-up) clasts which is overlain by yellowish and reddish hemipelagite at dip angles of appx. 20° (Fig. 36, left). Core -37 also has a hemipelagic cover, however, terminal depth was only 87 cmbsf and the lowermost decometer was pebbly mud with clasts of white, rounded rock (Fig. 36, centre). White and beige broken-up material is also found in core -41 where it overlies an erosional, truncated surface of reddish hemiplagic clayey ooze (Fig. 36, right). Our tentative interpretation is that some of the hard or even lithified material, and definitively the grey mud, is older accreted material. This is supported by the shear strength data and will possibly be verified by dating post-cruise.

The second group of cores recovered from the Inner deformation front has in common that pockets of fluid are found. These soupy areas are within the hemipelgic oozes, and in one case both fluidised zones and pebbly, beige materials at the base of the core are found (see GeoB15345 litholog description in Appendix 9.2). This core is also characterised by faulting and mottling. The same is

found in core -44 and, to a larger extent, core -43 (faulting, irregular contacts, injection channel, mottling). In contrast, core -35 has just one soupy zone at the base (223-250 cmbsf; see lithologs in Appendix 9.2) whereas cores -39 and -40 show hemipelagics with fauirly hard layers (causing low recovery).

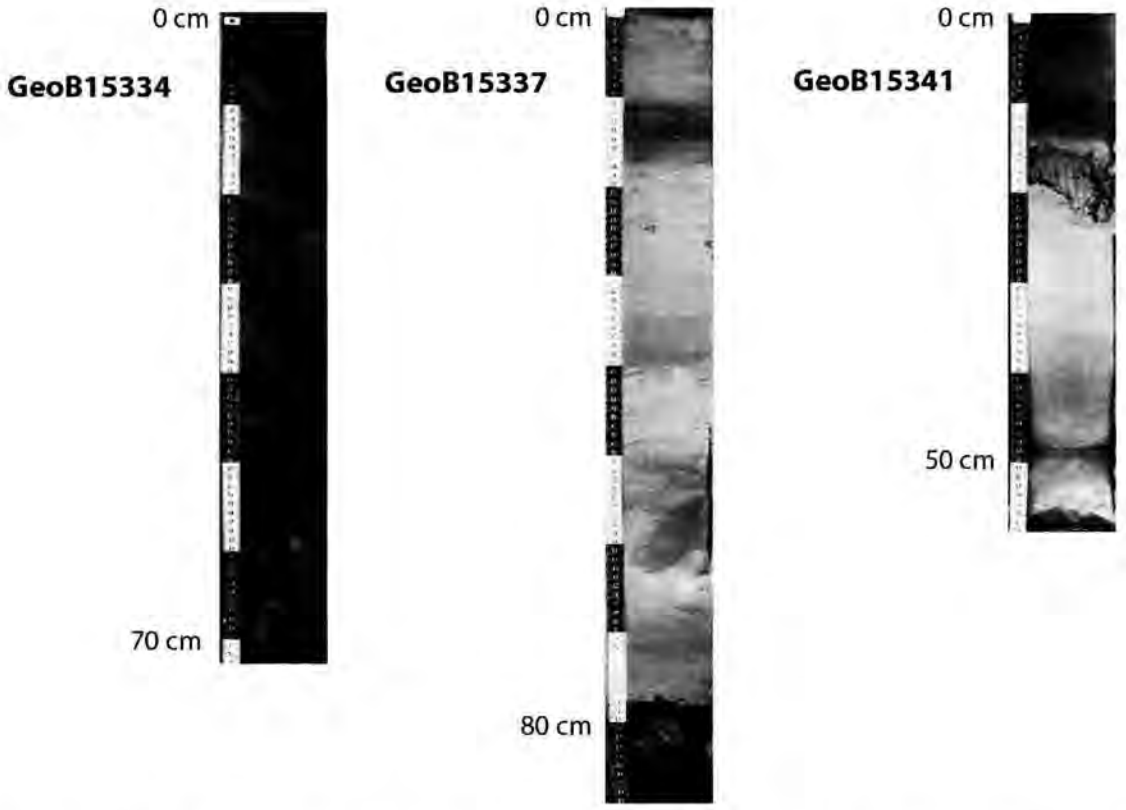

Fig. 36: Selected sections from core photographs of stations GeoB15334, -37 and -41 with some evidence for accreted strata. Note that terminal depth of all cores is very low, indicating a well-compacted nature of the material at the base. Note also the similarity between the mud in -34 and that recovered in MVs (cf. Fig. 35).

6.6.3 Inner Ridge – Cretan Margin

Along the contact between the Inner Ridge ancient accretionary complex and the Cretan Margin, and in fact some kilometers into the Cretan Margin further north, a total of 11 gravity cores were recovered during cruise P410 (Table 3). In general, these cores are not so dissimilar from the ones recovered at the Inner deformation front, both regarding the total length (i.e. shorter than e.g. the MV cores) and the sediment they comprise. Hence we also divide them into two groups.

Group 1 consists of only two cores, GeoB15358-1 and -3. Both cores contain grey mud with dark grey pebbles and lighter grey rip-up clasts. In case of core -1 an inclined surface between hemipelagic cover (5-10 cm) and the grey mud and mudstone is seen (Fig. 37). We assume that this material has been mobilised at larger depth, since recovery is low, shear strength is high, and the colour, texture and mineralogy is similar to materials recovered from mud domes (Fig. 36 and Table 3) as well as on the MedRidge - Inner Ridge transition (Fig. 36).

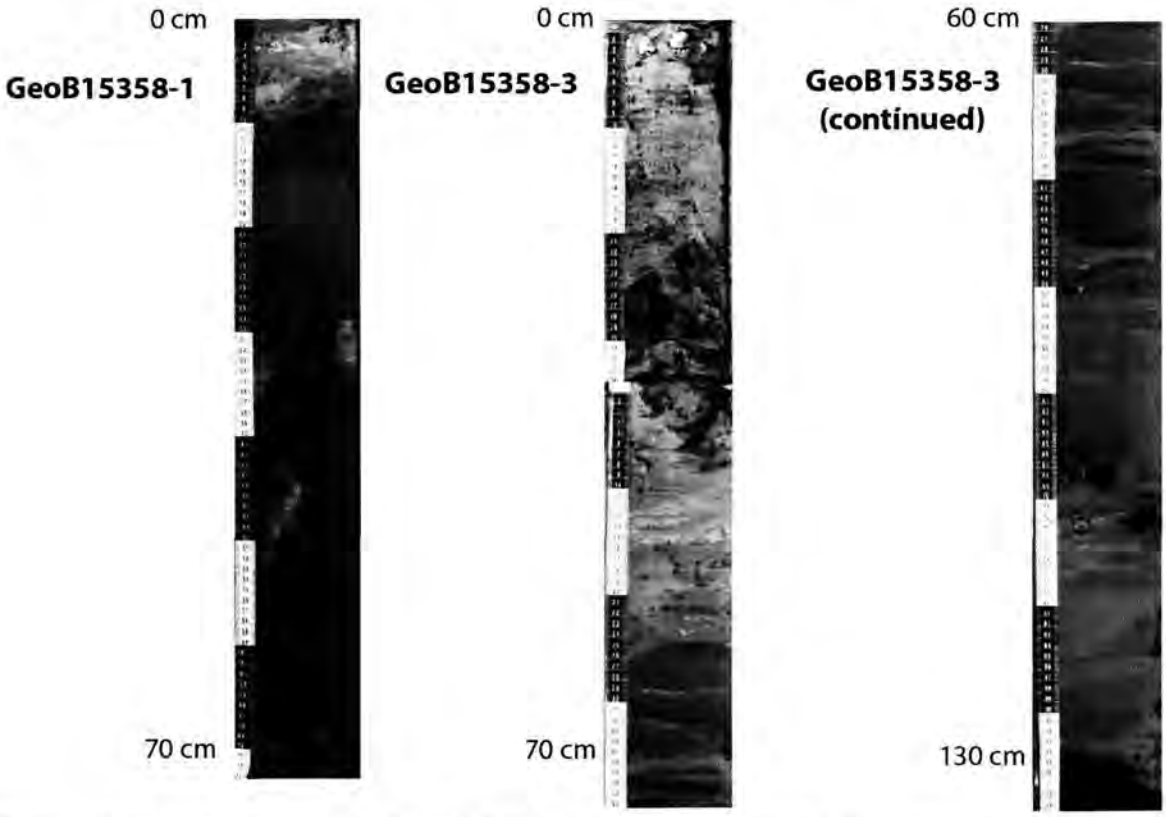

Fig. 37: Core photographs of stations GeoB15358-1 (left) and -3 (centre, right) showing grey mud with pebbles, which is similar to that found occassionally at the Inner deformation front (Fig. 36) and commonly in the majority of the MVs (Fig. 35). See text.

The second group of cores is characterised by hemipelagic sediment with occasional (minor) faults (usually normal faults); they are cores GeoB15351, -52, -53, -54, -56. Three additional cores also comprise small, beige pebbles (cores -47, -49 and -57). For full lithologivcal description and core photographs, refere to Appendices 9.2 and 9.3.

6.7. Physical properties

(G. Wiemer, S. Haas)

All sediments of on board split cores have been analysed for their key physical parameters. Shear strength has been determined on board right after splitting of the cores, using both a fall cone and a vane shear testing device (see section 5.7 above). Those data are presented next to the lithological core logs in Appendix 9.2. Density, porosity, p-wave velocity and magnetic susceptibility have been measured on land using the MSCL logging device at the MARUM (see Appendix 9.3). The two following subchapters focus on the shear strength and MSCL data and relate some of those to the in-situ temperature gradients (see section 6.3 above).

The study area can be divided in three geological sections (see section 6.6 above): (i) the mud volcanoes on the landward portion of the active MedRidge accretionary complex, (ii) the inner deformation front, where the MedRidge is backthrust over the Inner Ridge (comprising old accreted

starta; see Kopf et al., 2003), and (iii) the inner ridge to Cretan margin area. Region I comprises all cores that have been taken in or in proximity of the mud volcanoes (GeoB15307, -09, -10, -11, -12, -14, -17, -20, -21, -23, -25, -26, -29, -30, -31, -32, -62, -63, -66, -67). Region II comprises cores GeoB 15320; -35; -37; -39; -41; -43; -44; -45. Region III comprises GeoB15347, -48, -49, -51, -52, -53, -54, -56, -57, -58-1, -58-3.

6.7.1. Shear strength from fall cone and vane testing

Mud Volcanoes

Napoli, Bergamo and Milano MVs show similar shear strength data: The shear strength of the moussy and muddy sediment matrix originated mostly in the centre or on the edge of the MVs rarely exceeds 10 kPa even in depths of ~3 mbsf. This indicates a general state of underconsolidation. Some outstanding peaks in shear strength (> 130 kPa) can be related to the presence of mud or hard rock clasts such as clay or siltstone. The sediment taken on the flanks show hemipelagic background sediment in the top sequence and reach slightly higher shear strength at depth (~20 kPa). The sediment of Napoli MV (GeoB15314) and Milano MV (GeoB15362) shows outstandingly low shear strength (3- 6 kPa) at central location and at depth > 2.5 mbsf. GeoB15306 (Milano MV) on the other hand contains only hard rock clasts. A general lack of hemipelagic cover can be observed at these locations. These MVs have been interpreted as active or recently active. Temperature gradients at these locations enforce this interpretation. Milano MV shows an outstandingly high gradient of 1224 C°/km indicating hot fluid seepage. Napoli MV shows a gradient of 78C°/km at location GeoB15314. The gradients generally decrease from central to flank positions from high (>50 C°/km) to low (< 25 C°/km) values.

All gravity cores taken on the MVs Monza, Leipzig and Lich show hemipelagic sediment in the upper few decimeters and were interpreted as being inactive. The shear strength increases gradually with depth and stays within the range of normal consolidation. Local high shear strength values can sometimes be related to mud clasts. Leipzig MV shows normal to slightly elevated geothermal gradients ranging from 24-37 C°/km. Lich MV shows a low gradient of only 16 C°/km.

The Inner deformation front

The sediment of the inner deformation front indicates normal to slight overconsolidation. The shear strength increases gradually with depth up to values of 30-40 kPa. Generally speaking the sediment shows relatively high deformation such as slump structures and fractures. The overconsolidation can be related to the accommodation of the sediment to the convergence of the African and Eurasian plates. Individual outstanding peaks of the fall cone penetrometer data are interpreted as impacts on

mud calsts or slump, carbonate clasts or concretions. The temperature gradients in this area range from 11-50 C°/km.

The Inner Ridge to Cretan margin area

The cores that are closer to the Cretan margin show very similar sediment, deformation structures and shear strength data to the sediment around Lich MV and the inner deformation front. The shear strength increases gradually and reaches values up to 30-40 kPa. The highest values can reach more than 100 kPa.

Stations GeoB15348 and -58 are located close to the thrust of the inner ridge and show high geothermal gradients (59 C°/km and 123 C°/km, respectively; see section 6.3 above). The gradients decrease toward the Cretan margin and range from 3 C°/km to 25 C°/km.

6.7.2 MSCL

This subchapter regards the bulk density and magnetic susceptibility of the MSCL dataset. See Appendix 9.3 for all other parameters and plots of the data on a core-by-core basis.

Mud Volcanoes

The MVs Napoli, Bergamo and Milano show average bulk densities of 1.75 ± 0.05 g/cm³ at central positions. Average bulk density rises towards the edges and flanks of these MVs up to 1.8 ± 0.05 g/cm³. The cores taken at central locations show slightly decreasing bulk density with depth. The decrease of average bulk density towards the centre of these MV and the decrease of the bulk density with depth at central positions can be related to the rising amount of gas in the sediments pore space. In the central portion (crest region) of Monza, Leipzig and Lich MVs average bulk densities in the order of 1.8 ± 0.05 g/cm³ are found, which is similar to values obtained at the flanks of the other MVs. Regarding the evolution of the bulk density with depth, the data shows a slight gradual increase. This fact underpins the distinction in active and dormant MVs formerly based on the shear strength data alone (see section 6.7.1 above).

The average magnetic susceptibility of the sediment coming from active MVs (Napoli, Bergamo and Milano) is slightly lower (10 ± 3) than the average magnetic susceptibility of cores from inactive MVs Monza and Leipzig (12 ± 1). No clear pattern can be observed regarding cores from central to peripheral positions of a given mud volcano. Cores from Lich MV show average magnetic susceptibilities of 25 ±5 SI, being indicative of hemipelagic sediment cover and inactivity.

The inner deformation front

The sediment from the inner deformation front shows average bulk density values of 1.87 ± 0.03 g/cm³ in all cores. Generally, bulk density increases slightly with depth. The magnetic susceptibility lies at 15 ± 5 SI in average.

The Inner Ridge to Cretan margin area

For cores from this area, the bulk density generally shows values of 1.85 ± 0.03 g/cm³. Exceptions are cores GeoB15356 and -57. Their average bulk density is significantly lower (1.72 ± 0.01 g/cm³), however, it is not linked to admixture of (i.e. liquefaction by) freshened fluids. The average magnetic susceptibility of the sediment coming from this area ranges from 14 SI to 38 SI. Exceptions are cores GeoB15358-1 and 15358-3 whose average magnetic susceptibility ranges around 6 SI, which is similar to the sediment's magnetic susceptibility found at Napoli MV (i.e. the most active of the mud domes investigated). However, GeoB15358-1 and GeoB15358-3 contain mostly hemipelagic background sediment and lack the evidence of free gas or freshened pore water (see section 6.8 below).

6.8. Pore water geochemistry

(M. Zabel, K. Kirsch)

During this cruise, pore water geochemistry was conducted mainly to find indications for the upward transport of deep-seated subduction zone fluids. In this context salinity, mainly expressed by the concentrations of chloride, sodium, sulfate, magnesium, calcium and potassium, is of utmost importsnce. In addition, especially sulfate, iron and manganese should be used to characterise both, the geochemical environments and the intensities of microbial activity. For these purposes 460 samples of interstitial waters were extracted from 42 sediment cores (GeoB15302, -03, -06, -07, -10--12, -14, -17, -18, -20, -21, -23, -25, -26, -29—32, -34, -35, -37, -39—41, -43—45, -47—49, -51—53, -56—58, -62, -63, -69, and -70; cf. Fig. 34).

Based on the geochemistry of the pore waters, at least three different environments can be distinguished. Two groups show clear indications for an advective, upward flow component. Both show typical concave up profile shapes. In the first case, very high saline waters migrate upward, as indicated by increasing chloride concentration up to appx. 9 times higher salinity than normal sea water (Fig. 35). Noticeable is the parallel decrease of manganese, potassium and lithium (the latter two not shown here). However, these features, found in cores from the Napoli mud volcano, may be caused by the influence of deep brine fluids, which have been suggested to be associated with the Messinian evaporites, widely distributed in the deep basins of the Mediterranean Sea (see ODP Leg 160 results; Emeis et al., 1996; De Lange & Brumsack, 1998).

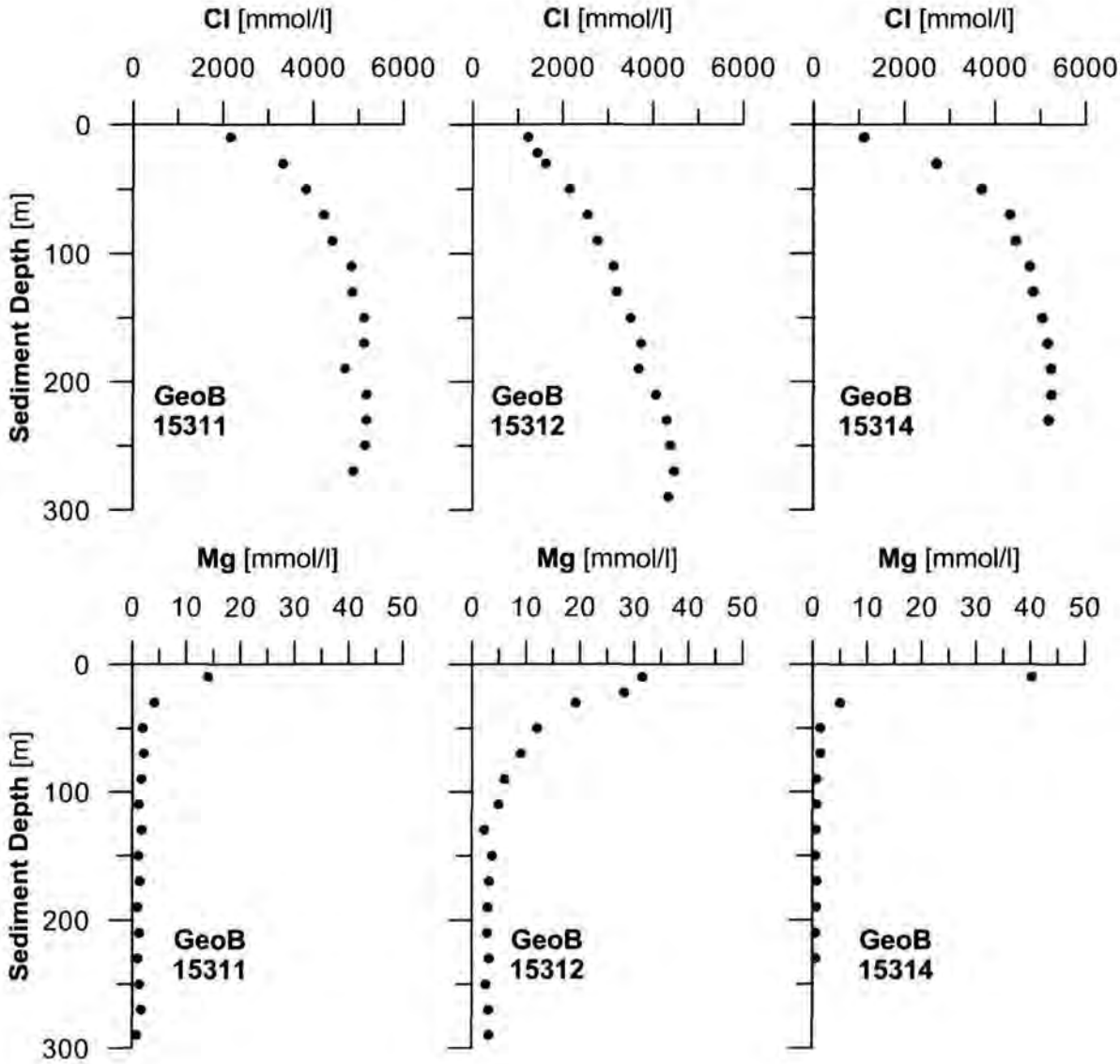

Fig. 35: Pore water concentration profiles of chloride and mangnesium from sediment cores retrieved from Napoli MV.

The second group shows just the opposite characteristics, at least for chloride and sodium (Fig. 36). In cores from Milano and Bergamo MVs the salinity decreases rapidly with increasing sediment depth. This freshening, down to less than a tenth of the chloride content in normal sea water, could in principle be caused by two processes that result in a release of fresh water into the sediment matrix: the destabilisation of gas hydrates and mineral transformation under elevated pressure conditions, which is associated with dewatering of the deposits (and there, mostly clay minerals). There are no indications for the existence of gas hydrates in this area and so the first reason can be excluded. Therefore we assume that, together with the mud, crystalline waters are transported from very deep sections to the sediment surface.

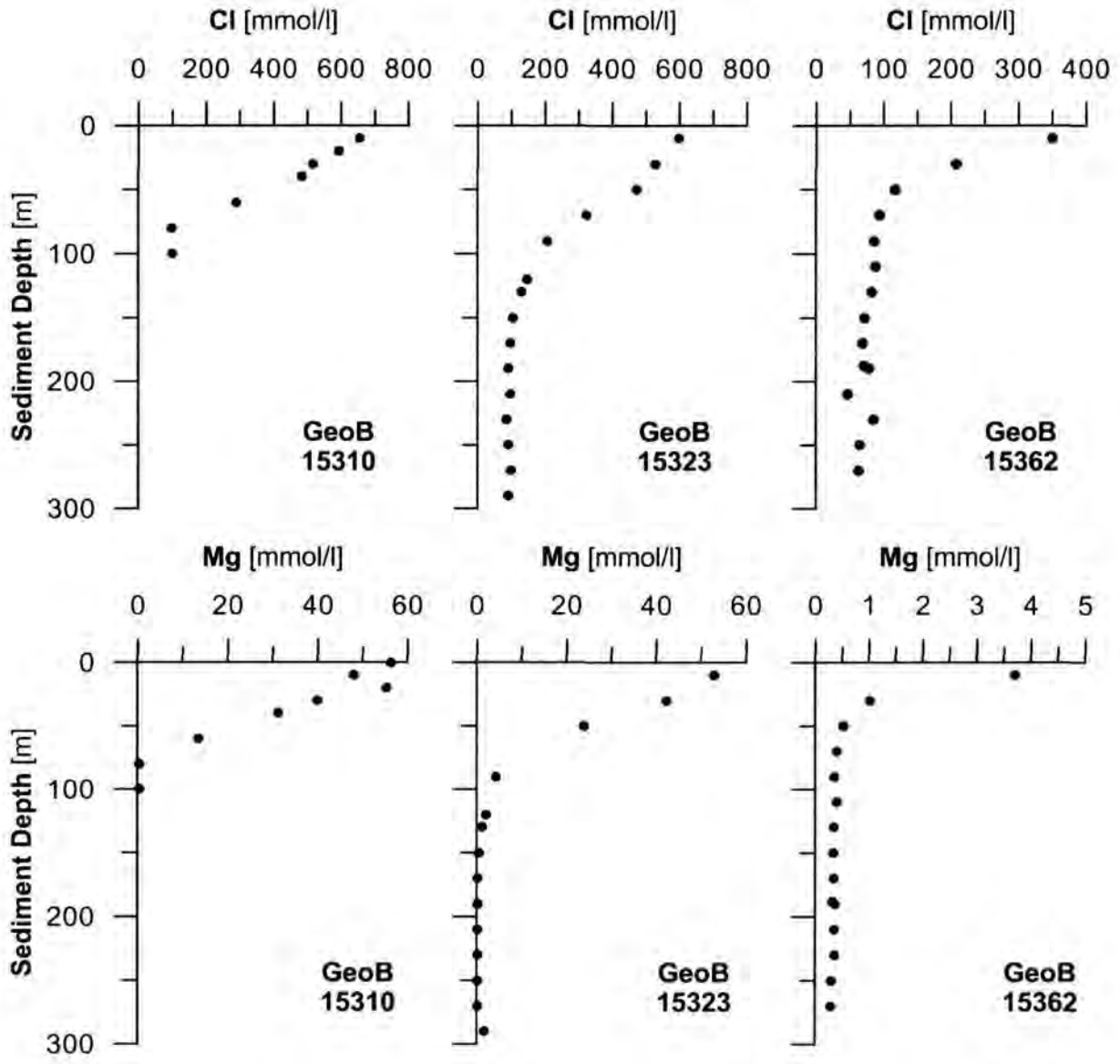

Fig. 36: Pore water concentration profiles of chloride and mangnesium from sediment cores retrieved from the Milano (GeoB 15310 and GeoB 15362) and the Bergamo (GeoB 15323) mud volcanoes.

Very interesting sulfate profiles are found in cores from Napoli mud volcano. They all show a clear minimum within the upper 50 cm, where sulfate is nearly depleted (Fig. 37). Below, concentrations increase again up to more or less constant values, which vary between 10 and about 50 mmol/l. Especially in context with indications made for the distribution of chloride, these features are hard to explain sufficiently. As a first attempt, we assume that sulfate sinks are products of anaerobic sulfate reduction. Futher analysis on methane concentrations could be used to validate this hypothesis. Because of the rather oligotrophic situation, we tend to neglect an importance of microbial sulfate consumption in context with organic carbon degradation. If the pore water sulfate distribution in the core from Bergamo MV (GeoB15323) can be explained with the freshening of the fluids mentioned above, this may become more clear by transport-reaction modeling.

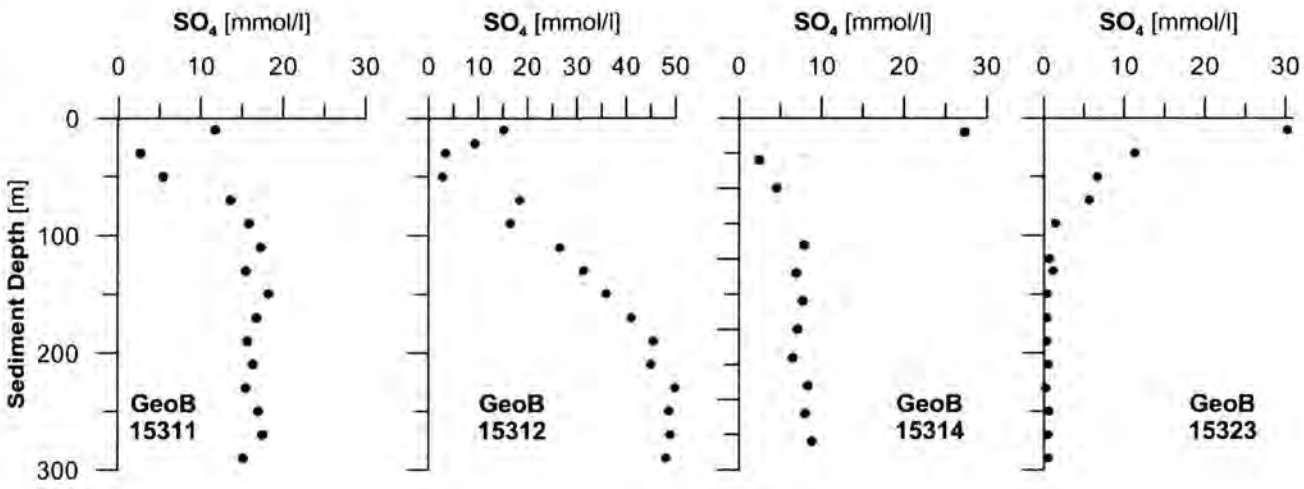

Fig. 37: Pore water concentration profiles of sulfate from sediment cores retrieved from Napoli (GeoB 15311, GeoB15312 and GeoB15314) and Bergamo (GeoB 15323) mud volcanoes.

The relatively low primary production in this region of the Mediterranean Sea, which causes a low input of organic matter into the sediments, is also indicated by the broadened expansion of the classic redox sequence. As examples for the third category of sediments, we have chosen one example each from the three prime categories, ie.e. the mud volcano province (example: Lich MV, core GeoB15303), the inner deformation front (example: core GeoB15335) and the Inner Ridge-Cretan margin transition (example: core GeoB15345). Figure 38 shows pore water concentration profiles from those stations, indicating iron and manganese reduction zones in depths between 50 and 400 cm. Obviously, the microbial activity in these sediments is rather low.

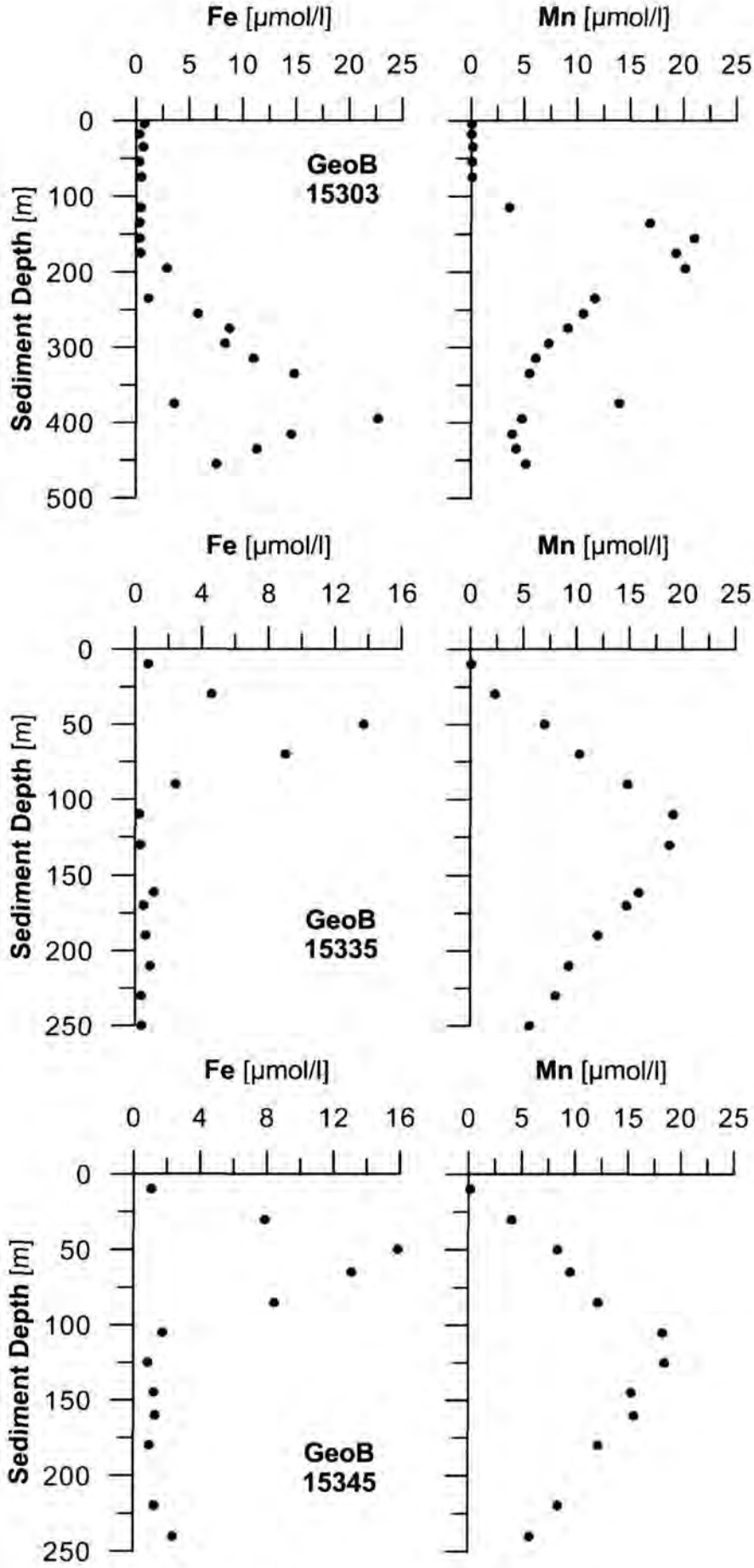

Fig. 38: Pore water concentration profiles of iron and manganese from sediment cores retrieved from the Lich mud volcano (GeoB15303) and the inner deformation front (GeoB15335 and GeoB15345).

6.9. ARGO floats

(A. Kopf)

In accordance with the naval authorities in charge of the ARGO programme, we deployed three of the devices. The positions are given in Figure 39 (see also station list, Appendix 9.1)

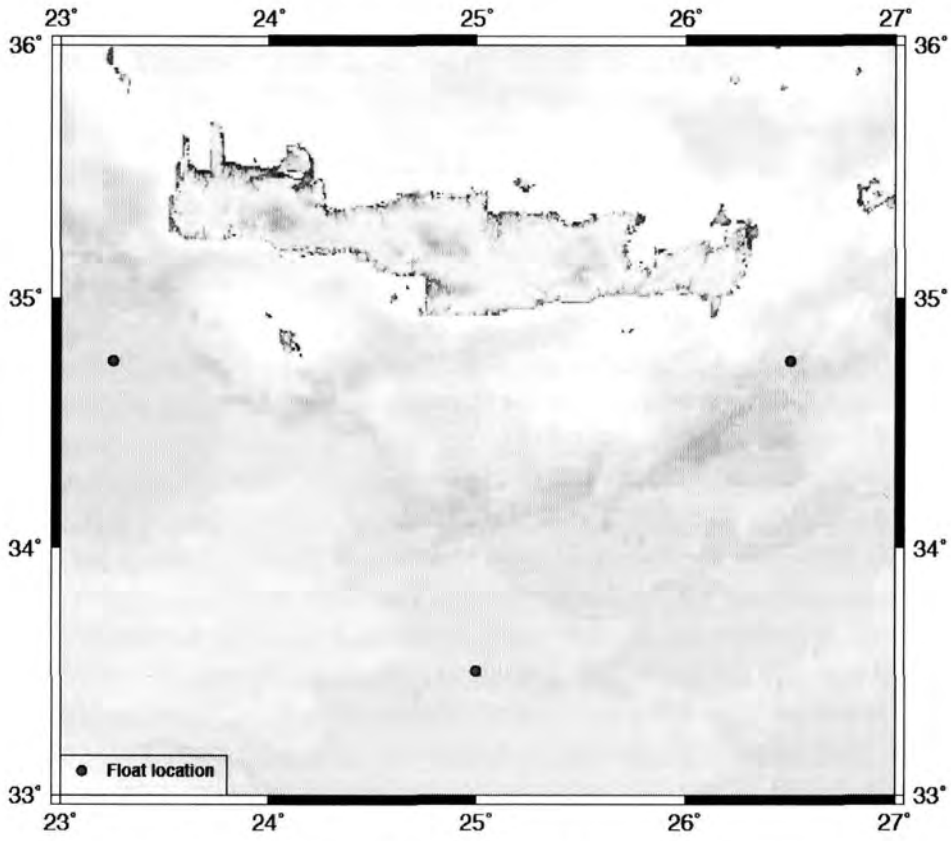

Fig. 39: Map showing the locations of the ARGO float deployments.

7. References

Bebout, G.E., Ryan, J.G., Leeman, W.P., Bebout, A.E., 1999. Fractionation of trace elements by subduction zone metamorphism - effect on convergent margin thermal evolution. Earth Planet. Sci. Letts., 171: 63-81

Behrmann JH, Lewis SD, Musgrave RJ, and Shipboard Scientific Party Leg 141 (1992) Proc. ODP, Init. Repts., 141, College Station, TX (Ocean Drilling Program): 709pp

Bekins, B. A., A. McCaffrey, S.J. Dreiss, 1995, Episodic and constant flow models for the origin of low-chloride waters in a modern accretionary complex, *Water Resour. Res., 31*, 3205-3215.

Bekins, B.A., Screaton, E.J., 2007. Pore Pressure and Fluid Flow in the Northern Barbados Accretionary Complex: A Synthesis, *in*: The Seismogenic Zone of Subduction Thrust Faults, edited by T. Dixon et al., Columbia University Press: 148-170

Bennett, R.H., et al., 1985. In-Situ Undrained Shear Strengths and Permeabilities Derrived from Piezometer Measurements. In: Strength testing of Marine Sediments: Laboratory and In-Situ-Measurements. American Society for Testing and Materials ASTM STP 883, Philadelphia, 1985

Bjorlykke, K., Hoeg, K., 1997. Effects of burial diagenesis on stresses, compaction and fluid flow in sedimentary basins. *Mar. Petr. Geol.*, 14/3: 267-276

Brenan, J.M., Shaw, H.F., Ryerson, F.J., Phinney, D.L., 1995. Mineral-aqueous fluid partitioning of trace elements at 900°C and 2 GPa: constraints on the trace element geochemistry of mantle and deep crustal fluids. *Geochim. Cosmochim. Acta*, 59: 3331-3350

Brix, M.R., Thomson, S.N., Stöckhert B., 2008. SHALLOW SUBDUCTION EROSION AT A RETREATING CONVERGENT MARGIN – THE THERMOCHRONOMETRIC RECORD OF THE "UPPERMOST UNIT" ON CRETE, GREECE . In: Garver, J.I., and Montario, M.J. (eds.), Proc. 11th International Conference on Thermochronometry, Anchorage Alaska, Sept. 2008, p. 42

Brown, K.M., Tryon, M.D., DeShon, H., Dorman, L.M., Schwartz, S.Y., 2005, Correlated transient fluid pulsing and seismic tremor in the Costa Rica subduction zone, *Earth Planet. Sci. Lett.*, 238, 189-203.

Byerlee, J.D., 1978. Friction of rocks. *Pure and Applied Geophys.* 116, 615-626.

Chapple, W.M., 1978. Mechanics of thin-skinned fold-and-thrust belts. GSA Bull., 89: 1189-1198

Chaumillon, E., Mascle, J., 1997. From foreland to forearc domains: new multichannel seismic reflection survey of th e Mediterranean Ridge accretionary complex (Eastern Mediterranean). Mar. Geology, 138: 237-259

Chronis, G., Lykousis, V., Anagnostus, C., Karageorgis, A., Stavrakakis, S., Poulus, S., 2000. Sedimentological processes in the southern margin of the Crete Sea (NE Mediterranean). Progress in Oceanography 46, 143-160

Dählmann, A., de Lange, G.J., 2003. Fluid-sediment interactions at Eastern Mediterranean mud volcanoes : a stable isotope study from ODP Leg 160. *Earth Planet. Sci. Letts.*, 212: 377-391.

Davis, D.M., Dahlen, A., Suppe, J., 1983. Mechanics of fold-and-thrust belts and accretionary wedges, *J Geophys Res.*, 88: 1153-1172.

Davis, E.E., et al., 2001. An episode of seafloor spreading and associated plate deformation inferred from crustal fluid pressure transients, *J. Geophys Res.*, 106, 21953-21963.

Davis, E.E., et al., 2004, Hydrological response to a seafloor spreading episode on the Juan de Fuca ridge, *Nature*, 430: 335-338.

Davis, E.E., et al., 2006, A discrete episode of seismic and aseismic deformation of the Nankai Trough subduction zone accretionary prism and incoming Philippine Sea plate, *Earth Planet. Sci. Lett.*, 242, 73-84.

Dayal U., Allen J.H. 1975. The effect of penetration rate on the strength of remolded clay and sand samples. *Can. Geotech. J.* 12:336–348

Davis, E.E., Villinger, H., 2006. Transient formation fluid pressures and temperatures in the Costa Rica forearc prism and subducting oceanic basement: CORK monitoring at ODP Sites 1253 and 1255; *Earth Planet. Sci. Letters*, 245: 232–244.

De Lange, G.J., Brumsack, H.J., 1998. Pore-water indications for the occurrence of gas hydrates in Eastern Mediterranean mud dome structures, in: A.H.F. Robertson, K.-C. Emeis, C. Richter, A. Camerlenghi (Eds.),

Proc. ODP Sci. Res.: 160, 569-574.

Dewhurst, D.N., Yang, Y., Aplin, A., 1999. Permeability and fluid flow in natural mudstones. *Geol. Soc. London, Spec. Publ.* 158: 23-43

Deyhle, A., Kopf, A., 2001. Deep fluids and ancient pore waters at the backstop: Stable isotope systematics (C, B, O) of mud volcano deposits on the Mediterranean Ridge accretionary wedge. *Geology*, 29/11: 1031-1034.

Deyhle, A., Kopf, A., 2002. Strong B enrichment and anomalous $d^{11}B$ in pore fluids from the Japan Trench forearc. *Marine Geology* 183: 1-15.

Deyhle, A., Kopf, A., Aloisi, G., 2003. Boron and boron isotopes as a tracer for diagenetic reactions and depth of mobilization, using muds and authigenic carbonates from eastern Mediterranean mud volcanoes. In: Maltman, A.J., Van Rensbergen, P. & Hillis, R. (eds.) Subsurface sediment mobilisation. *Geol. Soc. London, Spec. Publications* 216, 493-505.

Deyhle, A., Kopf, A.J., 2005. The use and usefulness of boron isotopes in natural silicate-water systems. *Physics and Chemistry of the Earth*,30: 1038-1046.

Dia, A.N., Castrec-Rouelle, M., Boulègue, J., and Boudou, J.P., 1995. Major and trace elements and Sr isotope constraints on fluid circulations in the Barbados accretionary complex. Part 1: Fluid origin. *Earth Planet. Sci. Letts.*, 134: 69-85.

Elliot, T., Plank, T., Zindler, A., White, W., Bourdon, B.,1997. Element transport from slab to volcanic front at the Mariana arc. *J Geophys Res* 102: 14,991-15,019.

Emeis, K.-C., Robertson, A.H.F., Richter, C., Shipboard Scientific Party, 1996. Proc. ODP, Init. Repts., 160, College Station, TX (Ocean Drilling Program), 972pp.

Expedition 308 Scientists, 2005, Overpressure and fluid flow processes in the deepwater Gulf of Mexico: slope stability, seeps, and shallow-water flow, *IODP Prel. Rept.*, 308, doi:10:2204/iodp.pr.308.2005

Fassoulas, C, Kilias, A, Mountrakis, D., 1994. Postnappe stacking extension and exhumation of high-pressure/low-temperature rocks in the island of Crete; Greece. *Tectonics*, 13/1: 127-138

Ge S., E.J. Screaton, 2005, Modeling seismically induced deformation and fluid flow in the Nankai subduction zone, *Geophys. Res. Lett.*, 32, doi:10.1029/2005GL023473.

Gennerich, H.H., Grevemeyer, I., Heesemann, B., Heesemann, M., Kaul., N., Müller, M., Schneider, J., Wallmann, K. & Villinger, H., 2002. First measurements with a new 6m long violin-bow marine heat probe off Costa Rica. *EOS Trans. AGU*, 83/47, F1333-1334

Gerya , T.V., Stöckhert , B., Perchuk, A.L., 2002. Exhumation of high-pressure metamorphic rocks in a subduction channel—a numerical simulation. Tectonics, 21, 1056, doi:10.1029/2002TC001406

Giresse, P., Buscail, R., Charriere, B., 2003. Late Holocene multisource material input into the Aegean Sea: depositional and post-depositional processes. Oceanologica Acta 26, 657-672

Grevemeyer, I., Kopf, A.J., Fekete, N., Kaul, N., Villinger, H.W., Heesemann, M., Wallmann, K., Spiess, V., Gennerich, H.-H., Müller M., and Weinrebe, W., 2004. Fluid flow through active mud dome Mound Culebra offshore Nicoya Peninsula, Costa Rica: evidence from heat flow surveying. *Marine Geology*, 207:145-157

Grevemeyer, I., Kaul, N., Kopf, A., 2009. Heat flow anomalies in the Gulf of Cadiz and off Cape San Vincente, Portugal. *Marine Petroleum Geology, in press*

Guangzhi, T., 1996. *Low-Temperature Geochemistry*. Bejing, China (Science Press), 216pp.

Gutscher, M.-A., Kukowski N., Malavieille J., Lallemand S.E., 1998. Material transfer in accretionary wedges from analysis of a systematic series of analog experiments. *J. Struct. Geol.*, 20/4: 407-416

Harms, U., Koeberl, C., Zoback, M.D. (eds.), 2007. *Continental Scientific Drilling*, Springer Berlin, 364pp.

Hedberg, H., 1974. Relation of methane generation to undercompacted shales, shale diapirs and mud volcanoes. *AAPG Bull.*, 58: 661-673

Henry, P., Le Pichon, X., Lallemant, S., Lance, S., Martin, J. B., Foucher, J.-P., Fiala-Médioni, A., Rostek, F., Guilhaumou, N., Pranal, V., and Castrec, M., 1996. Fluid flow in and around a mud volcano field seaward of the Barbados accretionary wedge: Results from Manon cruise. Journal of Geophysical Research 101(B9), 20297-20323

Heesemann, M., Villinger, H., Jannasch, H.W., Kastner, M. & 301T scientists, 2006. Long-term temperature

measurements in holes 1253A and 1255A off Costa Rica, ODP Leg 205. In: Morris, Villinger, H.W., Klaus, A., et al., *Proc. ODP, Sci. Res.*, 205: College Station, TX (Ocean Drilling Program).

Higgins, G.E., Saunders, J.B., 1974. Mud volcanoes – Their nature and origin. *Verhandlungen der Naturforschenden Gesellschaft Basel*, 84: 101–152

Hüpers, A., A. Kopf, 2009. The thermal influence on the consolidation state of underthrust sediments from the Nankai margin and its implications for excess pore pressure, *Earth Planet. Sci. Letts.* 286: 324-332.

Hüpers, A., S. Kreiter, A. Kopf, The role of temperature on pre-consolidation stress determination for the projected sedimentary underthrust sequence at the Nankai margin *Marine Petroleum Geology* 27 (7), 1565-1571, doi:10.1016/j.marpetgeo.2010.03.014.

Hüpers, A., Bach, W., Zabel, M., A. Kopf, in press. Effects of experimental hydrothermal consolidation on pore water chemistry: implications for the alteration of underthrust sediments. *Geochimica Cosmochimica Acta*

Hubbert, M., Rubey, W.W., 1959. Role of fluid pressure in mechanisms of overthrust faulting: I. Mechanics of fluid-filled porous solids and its application overthrust faulting. *GSA Bull.*, 70: 115-160

IODP, 2001. Earth, oceans and life, Integrated Ocean Drilling Program Initial Science Plan: IWG, Washington, 110 p.

Johnson, M.C., Plank, T., 1999. Dehydration and melting experiments constrain the fate of subducted sediments. *Geochemistry, Geophysics, Geosystems - G* ^{3} 1:paper1999GC000014

Kamber, B.S., Collerson, K.D., 2000. Role of "hidden" deeply subducted slabs in mantle depletion. *Chem Geol* 166: 241—254.

Kastens K., 1991. Rate of outward growth of the Mediterranean Ridge accretionary complex. *Tectonophysics*199: 25-50

Kastner, M., et al., 2005, Continuous Chemical and Fluid Flux Monitoring in Two Distinct Fluid Flow Systems at the Costa Rica Subduction Zone, *Eos Trans. AGU, 86*(52), Fall Meet. Suppl.

Kawamura, K., Ogawa, Y., 2004. Progressive change in pelagic clay microstructure during burial process: examples from piston cores and ODP cores. *Marine Geol.* 207: 131-144

Kogiso T., Tatsumi Y., Nakano S., 1997. Trace element transport during dehydration processes in the subducted oceanic crust: 1. Experiments and implications for the origin of oceanic island basalts. *Earth Planet Sci Lett* 148: 193-205

Kopf, A., Robertson, A.H.F., Clennell, M.B., Flecker, R., 1998a.. Mechanisms of mud extrusion on the Mediterranean Ridge Accretionary Prism. Geo-Marine Letters, 18: 97-114.

Kopf, A., Clennell, M.B., Camerlenghi, A., 1998b. Variations in sediment physical properties and permeability of mud volcano deposits from Napoli dome and adjacent mud volcano. In: Robertson, A.H.F., Emeis, K.-C., Richter, C., et al., 1998. Proc. ODP, Sci. Results., 160, College Station, TX (Ocean Drilling Program), 625-644.

Kopf, A., Robertson, A.H.F., Screaton, E.J., Mascle, J., Parkes, R.J., Foucher, J.P., DeLange, G.J., Stöckhert, B., Sakellariou, D., 1999. Backstop hydrogeology of a wide accretionary complex south of Crete, Eastern Mediterranean Sea. Full drilling proposal (#555) for the Ocean Drilling Program, 25pp

Kopf, A., Behrmann, J.H., 2000. Extrusion dynamics of mud volcanoes on the Mediterranean Ridge accretionary complex. In: Vendeville, B., Mart, Y. & Vigneresse, J.-L. (eds.), From the Arctic to the Mediterranean: Salt, shale, and igneous diapirs in and around Europe. Geol. Soc. London, Spec. Publ., 174: 169-204

Kopf, A., Deyhle, A., Zuleger, E., 2000. Evidence for deep fluid circulation and gas hydrate dissociation using boron and boron isotopes in forearc sediments from Costa Rica (ODP Leg 170). Marine Geology, 167: 1-28

Kopf, A., Klaeschen, D., Mascle, J., 2001. Extreme efficiency of mud volcanism in dewatering accretionary prisms. *Earth Planet. Sci. Letters*, 189/3-4: 295-313

Kopf, A., 2002. Significance of mud volcanism. *Reviews of Geophysics*, 40/2, 52pp. [DOI 10.1029/2000RG000093]

Kopf, A.J., Deyhle, A., 2002. Back to the roots: Source depths of mud volcanoes and diapirs using boron and B isotopes. *Chem. Geology*, 192: 195-210.

Kopf, A., P.R. Castillo, A. Deyhle, 2002. Water-Rock Interaction in the Upper Seismogenic Zone in the Nankai Trough Subduction Factory. *EOS, Trans. AGU (Supplement),* 83/47, F1294.

Kopf, A., Mascle, J., Klaeschen, D., 2003a. The Mediterranean Ridge: A mass balance across the fastest growing accretionary complex on Earth. *J. Geophys. Research* 108, 2372-2403, doi:10.1029/2001JB000473.

Kopf, A., Deyhle, A., Behrmann, J.H., Roller, S., Erlenkheuser, H., 2003b. Stable isotopic evidence (B, C, O) of deep fluid processes in fault rocks from the active Woodlark Basin detachment zone. *Earth Planet. Sci. Letters* 208: 51-68

Kopf, A., Clennell, M.B., Brown, K.M., 2005. Physical properties of extruded muds and their relationship to episodic extrusion and seismogenesis. Martinelli, G., Panahi, B. (Eds.), Mud volcanoes, geodynamics and seismicity. *NATO Sci. Ser. IV*: 263-283

Kopf, A., Alves, T., Heesemann, B., Kaul., N.E., Kock, I., Krastel, S., Reichelt, M., Schäfer, R., Stegmann, S., Strasser, M., Thölen, M., 2006. REPORT & PRELIMINARY RESULTS OF POSEIDON CRUISE P336: CRESTS - Cretan Sea Tectonics and Sedimentation. *Berichte aus dem Fachbereich Geowissenschaften, Univ. Bremen,* No. 253: 140pp.

Kopf, A., Stegmann, S., Krastel, S., Förster, A., Strasser, M, Irving, M., 2007. Marine deep-water Free-fall CPT measurements for landslide characterisation off Crete, Greece (Eastern Mediterranean Sea) --- PART 2: Initial data from the western Cretan Sea. In: Lykousis, V., Sakellariou, D., Locat, J. (eds.), Submarine Mass movements and their consequences. *Advances in Natural and Technological Hazards Series*, Springer, 199-208.

Kopf, A., Bohnhoff, M., 2007. Fault zone drilling in the backstop to the Mediterranean ridge accretionary complex off Crete, Greece. *Scientific Drilling*, Spec. issue 1: 45-46

Kopf, A., 2009 (in press). Effective strength of incoming sediments and its implications for plate boundary propagation and mass balances: The Costa Rica and Nankai margins. *Geochemistry, Geophysics, and Geosystems (G3).*

Kopf, A., Stegmann, S., Delisle, G., Panahi, B., Aliyev, C.S., Guliyev, I., 2009. *In situ* CPTU experiments at active Dashgil mud volcano, Azerbaijan: Evidence for excess fluid pressure, updoming, and possible future violent eruption. *Mar. Petrol. Geology*

Kukowski N., von Huene R., Malavieille J., Lallemand S.E., 1994. Sediment accretion against a buttress beneath the Peruvian continental margin at 12°S as simulated with sandbox modeling. *Geol. Rundschau,* 83/4: 822-831

Lallemand S.E., Schnurle P., Malavieille J., 1994. Coulomb theory applied to accretinary and non-accretionarywedges - possible causes for tectonic erosion and/or frontal accretion. *J. Geophys. Res.*, 99: 12033-12055

Lavrushin, V.U., Polyak, B.G., Prasolov, R.M., Kamenskii, I.L., 1996. Sources of material in mud volcano products (based on isotopic, hydrochemical, and geological data). *Lithology Min. Resources,* 31/6: 557-578

Lunne T., Robertson P.K., Powell J.J.M., 1997. Cone penetration testing in geotechnical practice. Spon Press, London

Lunne T., 2010. The CPT in offshore soil investigations – a historic perspective. In: Mitchell et al (eds) CPT'10, Huntington Beach, California

Malavieille J. 1984. Modélisation experimentale des chevauchements imbriqués: application aux chaines de montagnes. Bull. Soc. Géol. Fr., 7: 129-138

Mascle, J., Huguen, C., Benkhelil, J., Chamot-Rooke, N. Chaumillon, E., Foucher, J.-P., Griboulard, R., Kopf, A., Lamarche, G., Volkonskaia, A., Woodside, J., and Zitter, T., 1999. Images may show start of European-African Plate collision. *EOS Trans. AGU,* 80/37: 421-428

Meier, T., Becker D., Endrun, B., Rische, M., Bohnhoff, M., Stöckhert, B. & Harjes, H.-P., 2007. A model fort he Hellenic subduction zone in the area of Crete based on seismological investigations. In: Taymaz, T., Yilmaz, Y. & Dilek, Y. (eds.), Geodynamics of the Aegean and Anatolia, *Geol. Soc. London, Spec. Publ.*, 291: 183-199.

Mitchell J.K. 1976. Fundamentals of Soil Behavior. Wiley New York

Moore, J.C., Saffer, D., 2001. Updip limit of the seismogenic zone beneath the accretionary prism of southwest

Japan: An effect of diagenetic to low-grade metamorphic processes and increasing effective stress. *Geology*, 29: 183-186

Moore, G.F., A. Taira, A. Klaus, et al., 2001. New insights into deformation and fluid flow processes in the Nankai Trough accretionary prism: Results of Ocean Drilling Program Leg 190, *Geochem., Geophys., Geosyst., 2:* 10.129/2001GC000166.

Morgan, J. K., Boettcher, M. S., 1999. Numerical simulations of granular shear zones using the distinct element method 1. Shear zone kinematics and the micromechanics of localisation. *J. Geophys. Res.*, 104: 2703-2719

Morris J.D., Leeman W.P., Tera F.,1990. The subducted component in island arc lavas: Constraints from Be isotopes and B-Be systematics. Nature 344: 31-36.

Neuzil, C.E., 1994, How permeable are clays and shales? *Water Res. Res., 30*, 145-150.

Nygard, R., Gutierrez, M., Gautam, R., Hoeg, K., 2004. Comnpaction behaviour of argillaceous sediments as a function of diagenesis. *Mar. Petr. Geol.*, 21: 349-362.

Parkes, R. J. B.A. Cragg, S.J. Bale, J.M. Getliff, K. Goodman, P.A. Rochelle, J.C. Fry, A.J. Weightman & S. M. Harvey, 1994. Deep bacterial biosphere in Pacific Ocean sediments. *Nature*, 371: 410-413

Peacock, S.A., 1990. Fluid processes in subduction zones. Science, 248: 329-337.

Pfender, M., H.W. Villinger, 2002. Miniaturized data logger for deep sea sediment temperature measurements, Mar. Geol. 186: 557-570

Plank, T., Langmuir, C.H., 1998. The chemical composition of subducting sediment and its consequences for the crust and mantle. *Chem. Geol.* 145: 325-394.

Platt, J.P.,1990. Thrust mechanics in highly overpressured accretionary wedges. J. Geophys. Res., 95, 9025-9034

Rice, J. R., 1992, Fault stress states, pore pressure distributions, and the weakness of the San Andreas fault, *in* Fault Mechanics and Transport Properties of Rocks, B. Evans, T. F. Wong (eds.), pp. 475-503, Academic, San Diego, CA.

Robertson, A.H.F., Kopf, A., 1998. Origin of clasts and matrix within Milano and Napoli mud volcanoes, Mediterranean Ridge accretionary complex. In: Robertson, A.H.F., Emeis, K.-C., Richter, C., et al., 1998. Proc. ODP, Sci. Results., 160, College Station, TX (Ocean Drilling Program), 575-596

Robertson P.K. 2009. Interpretation of cone penetration tests - a unified approach. Can Geotech J 46: 1337-1355

Ryan W.B.F., Hsü K.C., et al. 1973. Hellenic Trench Sites 127 and 128. *Proc. DSDP, Init. Results*, 13 (US Govt. Printing Office, Washington), Pt. 2: 243-322

Saffer, D.M., Bekins, B.A., 1998. Episodic fluid flow in the Nankai accretionary complex: Timescale, geochemistry, flow rates, and fluid budget: *J. Geophys. Res.*, 103, 30351- 30371.

Saffer, D.M., E.A. Silver, A.T. Fisher, H. Tobin, K. Moran, 2000. Inferred pore pressures at the Costa Rica subduction zone: Implications for dewatering processes, *Earth Planet. Sci. Lett., 177*, 193-207.

Saffer, D.M., and Bekins, B.A., 2002, Hydrologic controls on the mechanics and morphology of accretionary wedges and thrust belts, *Geology, 30*, 271-274.

Saffer, D. M., 2003, Pore pressure development and progressive dewatering in underthrust sediments at the Costa Rican subduction margin: Comparison with Northern Barbados and Nankai, *J. Geophys. Res.*, 108, doi:10.1029/2002JB001787.

Saffer, D.M., McKiernan, A.W., 2005, Permeability of underthrust sediments at the Costa Rican margin: Scale dependence and implications for dewatering, *Geophys. Res. Lett., 32,* doi:10.1029/2004GL021388.

Saffer, D.M., Kopf, A., 2006. Quantifying the source regions of observed pore water B and $d^{11}B$ signatures at shallow depths in forearcs. *Eos Trans. AGU, 87*(51), Fall Meet. Suppl.

Saffer, D.M., Kopf, A., 2007. Modelling pore water B and $d^{11}B$ signatures in the shallow subduction zone forearc: Examples from the Barbados, Costa Rica and Northern Japan margins. *Proc. Goldschmidt Conference*, 19.-24.08.07, Cologne, 1p.

Scholl, D.W., et al., 1994. SCIENCE OPPORTUNITIES IN OCEAN DRILLING TO INVESTIGATE RECYCLING PROCESSES AND MATERIAL FLUXES AT SUBDUCTION ZONES Proc. JOI/USSAC Workshop, Avalon, California, 84pp.

Schultheiss, P.J., 1990. Pore pressures in marine sediments: An overview of measurement techniques and some geological and engineering applications. *Mar. Geophys. Res.*, 12: 153-168

Screaton, E.J., D.R. Wuthritch, S.J. Dreiss, 1990, Permeabilities, fluid pressures, and flowrates in the Barbados ridge complex, *J. Geophys. Res., 95*, 8997-9007.

Screaton, E.J., et al., 1997, Barbados ridge hydrogeologic tests: Implications for fluid migrationalong an active décollement, *Geology*, 25, 239-242.

Screaton, E.J., D.M. Saffer, P. Henry, S. Hunze, Leg 190 Shipboard Scientific Party, 2002. Porosity loss within underthrust sediments of the Nankai accretionary complex: Implicationsfor overpressures, *Geology*, 30, p. 19-22.

Screaton, E.J., et al., 2005, Numerical Modeling of Steady State Pore Pressures and CoseismicPressure Changes at the Nankai Margin off the Kii Peninsula, Japan, *Eos Trans. AGU, 86*(52), Fall Meet. Suppl., 1pp

Seeberg-Elverfeldt, J., Schlüter, M., Feseker, T., Kölling, M. (2005) Rhizon sampling of porewaters near the sediment-water interface of aquatic systems. Limnol. Oceanogr. Methods, 3: 361-371.

Shipboard Scientific Party, 2002. Leg 195 summary. *In* Salisbury, M.H., Shinohara, M., Richter, C., et al., *Proc. ODP, Init. Repts.*, 195: College Station, TX (Ocean Drilling Program), 1–63. doi:10.2973/odp.proc.ir.195.101.2002

Song, C.R., Voyiadjis, G.Z., Tumay, M.T., 1999. Determination of permeability of soil using the multiple piezo-element penetrometer. *International Journal for Numerical and Analytical Methods in Geomechanics*, 23, 1609-1629.

Spivack, A. J., Palmer, M.R., Edmond, J. M., 1987. The sedimentary cycle of the boron isotopes. *Geochim. Cosmo. Acta* 51, 1939-1949

Stegmann, S., Moerz, T., Kopf, A., 2006. Initial Results of a new Free Fall-Cone Penetrometer (FF-CPT) for geotechnical *in situ* characterisation of soft marine sediments. *Norwegian Journal of Geology*, 86/3: 199-208.

Stegmann, S., Strasser, M., Anselmetti, F.S., Kopf, A., 2007. Geotechnical *in situ* characterisation of subaquatic slopes: The role of pore pressure transients versus frictional strength in landslide initiation. *Geophysical Research Letts.*, 34/7, doi:10.1029/2006GL029122.

Steiner A., L'Heureux J.S., Kopf A., Vanneste M., Longva O., Lange M., Haflidason H., 2012. An in-situ free-fall piezocone penetrometer for characterizing soft and sensitive clays at Finneidfjord, northern Norway. In: Yamada Y et al (eds) Submarine mass movements and their consequences, vol. 31, Advances in natural and technological hazards research. Springer, Dordrecht, 99–109.

Strayer, L.M., Hudleston, P.J., Lorig, L.J., 2001. A numerical model of deformation and fluid-flow in an evolving thrust wedge. *Tectonophysics*, 335: 121-145

Tera, F., Brown, L., Morris, J., Sacks, I.S., Klein, J., Middleton, R., 1986. Sediment incorporation in island arc magmas: inferences from ^{10}Be, *Geochim. Cosmochim. Acta*, 50: 636-660

Thomson, S.N., Stöckhert, B., Brix, M.R., 1998. Thermochronology of the high-pressure metamorphic rocks of Crete, Greece: Implications for the speed of tectonic processes. *Geology*, 26/3: 259-262

Tobin, H., Kinoshita, M., 2007. The IODP Nankai Trough Seismogenic Zone Experiment. *Scientific Drilling*, Spec. issue 1: 39-41

Tryon, M.D., Brown, K.M., Dorman, L., Sauter, A., 2001. A new benthic aqueous flux meter for very low to moderate discharge rates. *Deep Sea Research* Pt. I, 48: 2121-2146

Tryon, M.D., K.M. Brown, M. Torres (002. Fluid and chemical flux in and out of sediments hosting methane hydrate deposits on Hydrate Ridge, OR, II: Hydrological processes, *Earth Planet. Sci. Lett.*, 201(3-4), 541-557.

Tryon, M.D. 2009. Monitoring aseismic tectonic processes via hydrologic responses: An analysis of log-periodic fluid flow events at the Costa Rica outer rise, *Geology*, 37(2), 163-166.

Tryon, M.D., Wheat, C.G., Hilton, D.R., 2010. Fluid sources and pathways of the Costa Rica erosional convergent margin. *Geology, Geophysics, and Geosystems (G-Cubed)*, doi:10.1029/2009GC002818

Underwood, M.B. (ed.), 1993. Thermal Evolution of the Tertiary Shimanto Belt, Southwest Japan: An Example of Ridge-Trench Interaction. GSA Special Paper, 273: 172 pp.

Villinger, H., Gennerich, H.H., Grevemeyer, I., Kaul, N., 2002. INGGAS-Flux: New tools for energy and fluid flux, pore pressure and thermal gradient. *GEOTECHNOLOGIEN Science Rept.*, 1: 139-141

von Huene, R., Klaeschen, D., Gutscher, M.A., Fruehn, J., 1998. Mass and fluid flux during accretion at the Alaskan margin. GSA Bull., 110/4: 468-482

Wang, K, Hu, Y., 2006, Accretionary Prisms in Subduction Earthquake Cycles: The Theory of Dynamic Coulomb Wedge, *J. Geophys. Res., 111:* doi:10.1029/2005JB004094

You, C.-F., Spivack, A.J., Smith, J.H., Gieskes, J.M., 1993. Mobilization of boron at convergent magins: Implications for boron geochemical cycle. *Geology*, 21: 207-210

You, C.-F., Castillo, P.R., Gieskes, J.M., Chan, L.H., Spivack, A.J., 1996. Trace element behavior in hydrothermal experiments: Implications for fluid processes at shallow depths in subduction zones. *Earth Planet. Sci. Letts.*, 140, 41-52

8. Acknowledgements

We thank Master Matthias Günther and his officers on the bridge for his expert manoeuvring in the study area, his cooperation, and outstanding support during complex operations, in particular at night. Special thanks go also to the entire crew of R/V *Poseidon* for their friendly support and efficient technical assistance with the various devices used.

Our colleagues at HCMR, namely Vasilis Lykousis, are acknowledged for their helpful discussion of scientific targets.

AWI, and Mechita Schmidt-Aursch in particular, is thanked for having provided the releaser deck unit for the CAT meters. Matthias Hort and Ali Deghani (Univ. Hamburg, Germany) are acknowledged for providing their underwater video equipment to help with surveys and CAT meter deployments.

Partners at MARUM Bremen (Goetz Ruhland, Volker Diekamp) as well as at IfM-GEOMAR (Klas Lackschewitz) have also provided crucial help with expedition planning, logistical decisions, and post-cruise demobilisation. Additionally, Klaus Bohn is thanked for his repeated professional logistical assistance.

Thanks go also to the German Science Foundation (DFG) for providing the funds to realise the *P410* cruise within the frame of MARUM research area SD5 as well as a project termed MUDDY WATERS.

Appendices

9.1. Station list

9.2. Lithologs and shear strength data

9.3. MSCL data logs and core photographs (electronic version only)

9.1 Station list

GeoB153-	Date	Time	PositionLat	PositionLon	Depth [m]	Device
01	14.03.11	00:57	34° 45,00' N	26° 30,00' E	97,4	Float
02	14.03.11	12:42	33° 51,60' N	24° 34,41' E	1910,9	Gravity corer w/ MTL
03	14.03.11	13:49	33° 51,60' N	24° 34,39' E	1916	Gravity corer w/ MTL
04	14.03.11	17:15	33° 51,82' N	24° 34,24' E	1931,4	Cone penetration testing
05	15.03.11	06:12	33° 51,81' N	24° 34,28' E	1915,1	Television multicorer
06	15.03.11	12:28	33° 44,04' N	24° 46,60' E	1925,4	Gravity corer w/ MTL
07	15.03.11	13:55	33° 44,14' N	24° 47,44' E	2003,2	Gravity corer w/ MTL
08	15.03.11	16:47	33° 44,20' N	24° 48,15' E	2043	Television multicorer
09	16.03.11	06:06	33° 44,10' N	24° 46,40' E	1956,6	Gravity corer w/ MTL
10	16.03.11	08:08	33° 44,18' N	24° 46,56' E	1939,6	Gravity corer
11	16.03.11	10:01	33° 43,44' N	24° 41,25' E	1902,9	Gravity corer w/ MTL
12	16.03.11	11:38	33° 43,62' N	24° 40,84' E	1909,4	Gravity corer w/ MTL
13	16.03.11					Multibeam
14	17.03.11	08:12	33° 43,52' N	24° 41,03' E	1905,9	Gravity corer w/ MTL
15	17.03.11	10:22	33° 43,50' N	24° 41,01' E	1907,8	Cone penetration testing
16	17.03.11	12:04	33° 42,50' N	24° 40,40' E	1973,3	Television multicorer
17	17.03.11	15:20	33° 44,07' N	24° 43,46' E	1901,7	Gravity corer w/ MTL
18	17.03.11	16:32	33° 44,08' N	24° 43,47' E	1897,1	Gravity corer w/ MTL
19	17.03.11					Multibeam
20	18.03.11	07:33	33° 43,16' N	24° 41,24' E	1913,8	Gravity corer w/ MTL
21	18.03.11	09:11	33° 44,25' N	24° 41,55' E	1985,4	Gravity corer w/ MTL
22	18.03.11	10:56	33° 43,62' N	24° 40,85' E	1909,8	Cone penetration testing
23	18.03.11	13:37	33° 44,27' N	24° 45,02' E	1911,9	Gravity corer w/ MTL
24	18.03.11					Multibeam
25	19.03.11	06:53	33° 44,43' N	24° 44,95' E	1913,7	Gravity corer w/ MTL
26	19.03.11	08:40	33° 44,12' N	24° 44,87' E	1925,7	Gravity corer
27	19.03.11	10:52	33° 47,25' N	24° 45,01' E	2016	Cone penetration testing
28-1	19.03.11					Multibeam
28-2	19.03.11	14:48	33° 30,02' N	25° 0,01' E	2207,3	Float
29	20.03.11	08:06	33° 51,56' N	24° 33,78' E	1909,7	Gravity corer w/ MTL
30	20.03.11	10:02	33° 51,42' N	24° 34,09' E	1937,3	Gravity corer w/ MTL
31	20.03.11	11:38	33° 51,46' N	24° 35,07' E	1898,7	Gravity corer w/ MTL
32	20.03.11	13:48	33° 47,02' N	24° 39,15' E	1893,7	Gravity corer w/ MTL
33	20.03.11					Multibeam
34	21.03.11	08:20	34° 6,16' N	24° 21,04' E	2062,7	Gravity corer w/ MTL
35	21.03.11	10:52	34° 12,75' N	24° 13,27' E	1377,4	Gravity corer w/ MTL
36-1	21.03.11	12:07	34° 12,60' N	24° 13,61' E	1472,4	Gravity corer w/ MTL
36-3	21.03.11	13:09	34° 12,59' N	24° 13,62' E	1456,8	Gravity corer
37	21.03.11	14:19	34° 12,79' N	24° 13,75' E	1648,5	Gravity corer
38	21.03.11					Multibeam
39	22.03.11	07:21	34° 7,94' N	24° 22,91' E	0	Gravity corer
40	22.03.11	09:41	34° 11,72' N	24° 20,18' E	2092,7	Gravity corer
41	22.03.11	12:38	34° 17,38' N	24° 16,47' E	0	Gravity corer
42	22.03.11					Multibeam
43	23.03.11	07:41	34° 18,20' N	24° 14,30' E	2212,1	Gravity corer w/ MTL
44	23.03.11	09:24	34° 17,40' N	24° 16,47' E	0	Gravity corer w/ MTL
45	23.03.11	11:53	34° 16,30' N	24° 17,50' E	0	Gravity corer w/ MTL
46	23.03.11					Multibeam
47	24.03.11	06:52	34° 17,09' N	24° 31,91' E	0	Gravity corer w/ MTL
48	24.03.11	09:02	34° 20,16' N	24° 32,95' E	2699,7	Gravity corer w/ MTL
49	24.03.11	11:39	34° 19,16' N	24° 33,18' E	2637,2	Gravity corer
50	24.03.11					Multibeam

51	25.03.11	08:04	34° 16,95' N	24° 38,35' E	2819,3	Gravity corer
52	25.03.11	10:19	34° 8,87' N	24° 46,59' E	3082,6	Gravity corer w/ MTL
53	25.03.11	12:34	34° 6,88' N	24° 47,01' E	2946,3	Gravity corer w/ MTL
54	25.03.11	15:26	34° 14,57' N	24° 49,33' E	2218,5	Gravity corer w/ MTL
55	25.03.11					Multibeam
56	26.03.11	04:54	34° 18,61' N	24° 54,30' E	2765,2	Gravity corer w/ MTL
57	26.03.11	06:32	34° 16,61' N	24° 58,41' E	2793,3	Gravity corer w/ MTL
58-1	26.03.11	11:25	34° 5,67' N	24° 58,45' E	3159	Gravity corer w/ MTL
58-3	26.03.11	13:37	34° 5,67' N	24° 58,45' E	3237,3	Gravity corer
59-1	26.03.11	15:56	34° 5,68' N	24° 58,69' E	3280,4	Gravity corer
59-2	26.03.11	16:45	34° 5,67' N	24° 58,69' E	3131,9	Gravity corer
60	26.03.11	18:10	34° 5,66' N	24° 58,46' E	3165,7	CAT Meter
61	26.03.11					Multibeam
62	27.03.11	06:05	33° 44,07' N	24° 46,58' E	1923,7	Gravity corer w/ MTL
63	27.03.11	07:46	33° 44,12' N	24° 44,85' E	1939,4	Gravity corer w/ MTL
64	27.03.11	10:15	33° 44,12' N	24° 44,87' E	1927,2	Cone penetration testing
65	27.03.11	12:15	33° 47,02' N	24° 39,14' E	1886	Cone penetration testing
66	27.03.11	13:36	33° 47,02' N	24° 39,15' E	1891,4	Gravity corer w/ MTL
67	27.03.11	16:12	33° 37,10' N	24° 40,31' E	1936,3	Gravity corer w/ MTL
68	27.03.11					Multibeam
69	28.03.11	07:14	33° 40,00' N	24° 32,85' E	1785,1	Gravity corer w/ MTL
70	28.03.11	08:53	33° 37,26' N	24° 40,31' E	1913,7	Gravity corer w/ MTL
71	28.03.11	10:24	33° 37,23' N	24° 40,32' E	1915,7	Cone penetration testing
72	28.03.11	12:26	33° 43,53' N	24° 41,01' E	1906,2	Cone penetration testing
73	28.03.11	13:45	33° 43,45' N	24° 41,15' E	1912	CAT Meter
74	28.03.11	15:25	33° 44,02' N	24° 46,57' E	1942,3	CAT Meter
75	28.03.11					Multibeam
76	29.03.11	18:52	34° 45,08' N	23° 15,12' E	2751,8	Float

9.2 Lithologs and shear strength data

GeoB 15302

Date : 14.03.2011 12:42
Water Depth : 1914 m
Study Area : BUTT3

Position : 33° 51.598' N
24° 34.405' E
Core Length : 140 cm

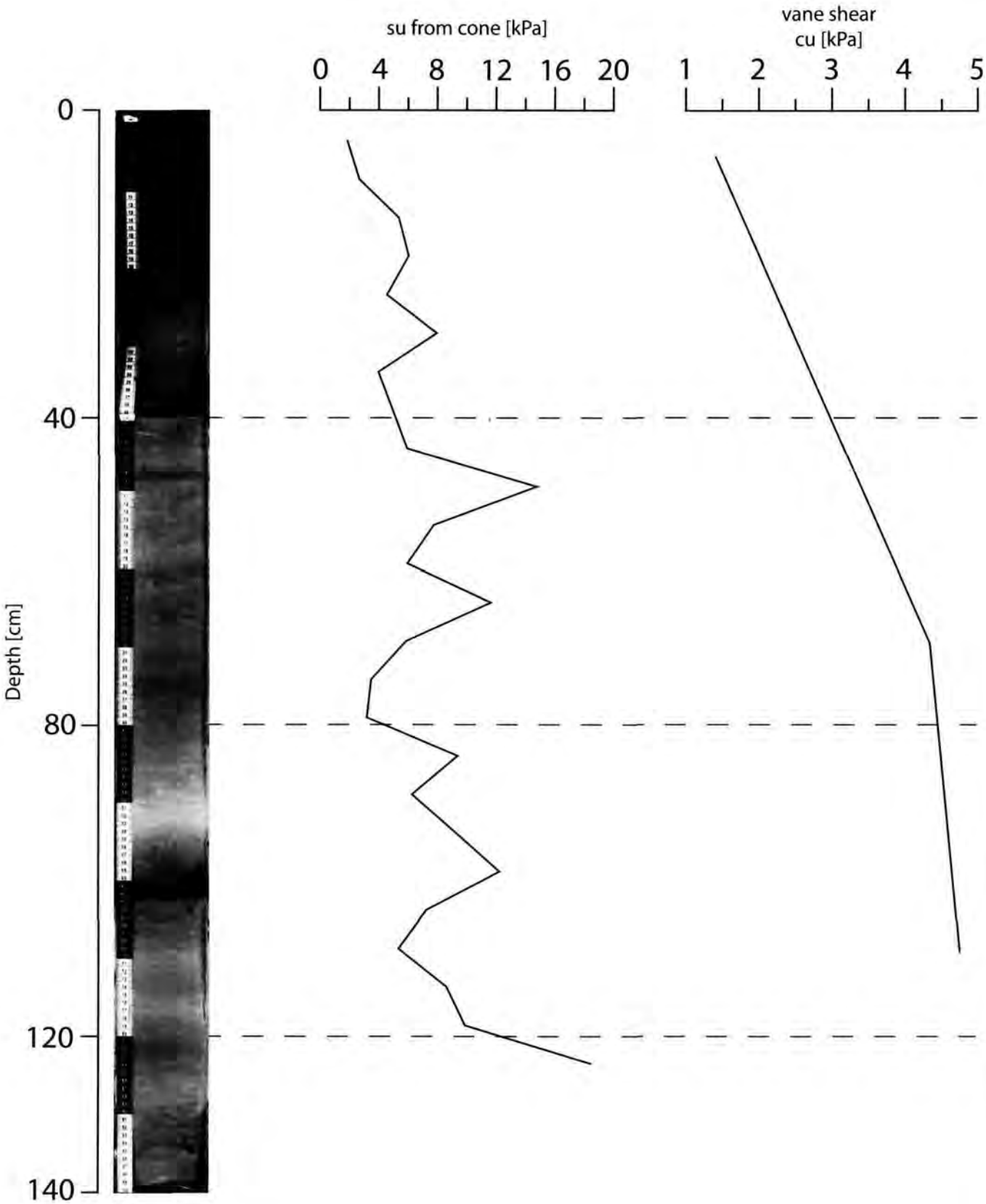

GeoB 15303

Date : 14.03.2011 14:39
Water Depth : 1972 m
Study Area : BUTT3 crest

Position : 33° 51.307' N
24° 34.103' E
Core Length : 465 cm

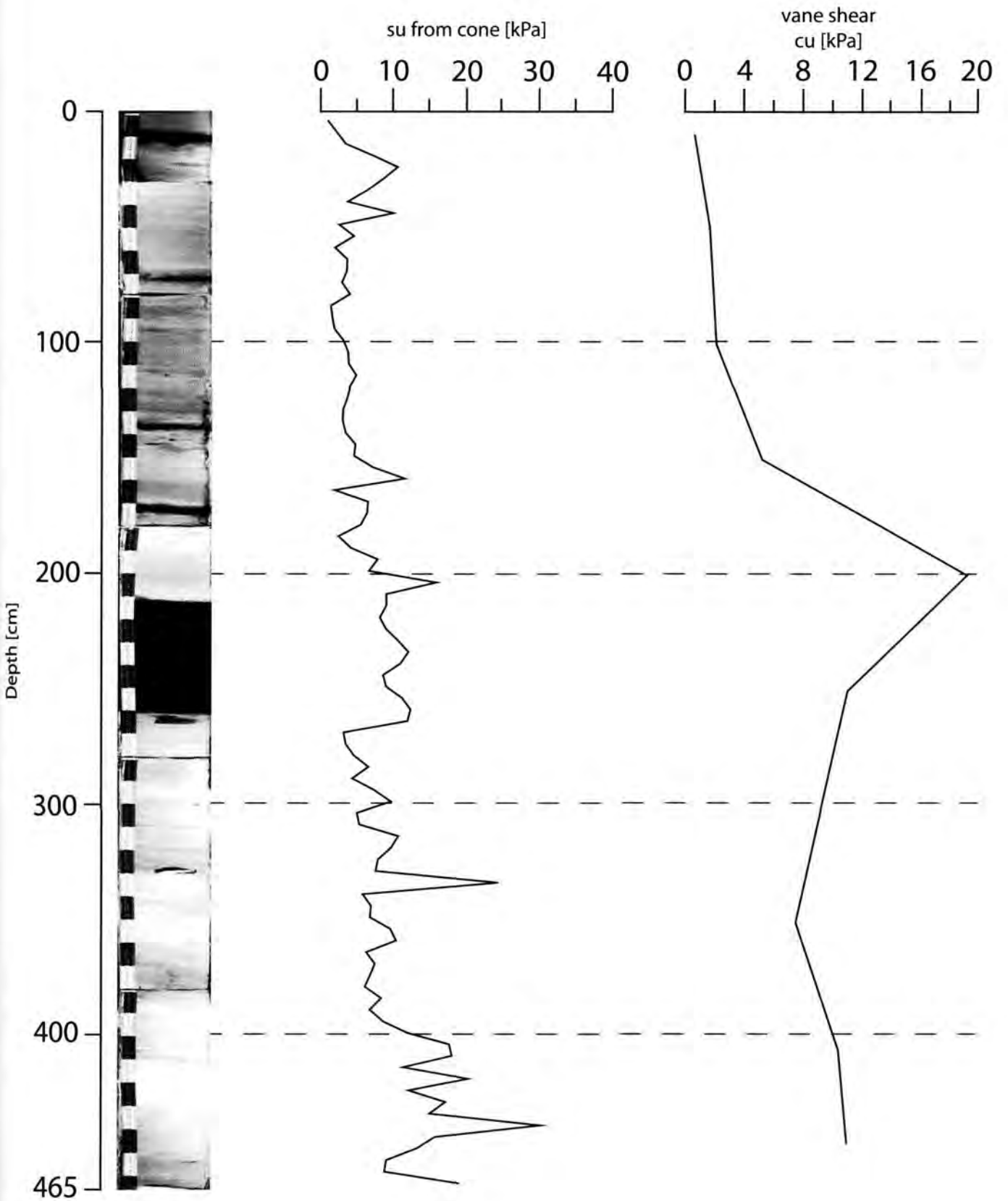

GeoB 15307

Date : 15.03.2011 13:54
Water Depth : 2000 m
Study Area : Milano 970

Position : 33° 44.13' N
24° 47.44' E
Core Length : 200 cm

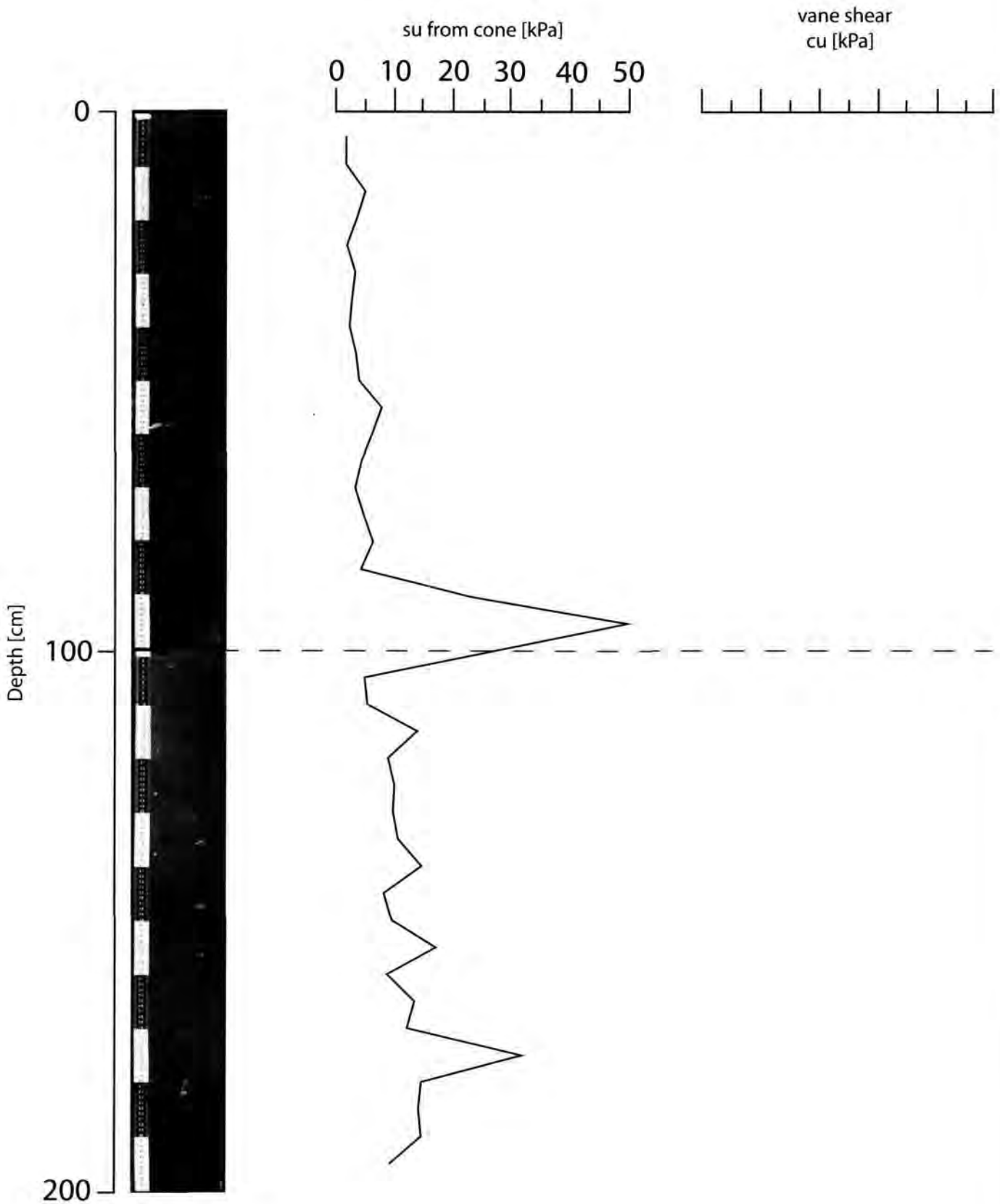

GeoB 15309

Date : 16.03.2011 06:05
Water Depth : 1931 m
Study Area : Milano

Position : 33° 44.099' N
24° 46.399' E
Core Length : 40 cm

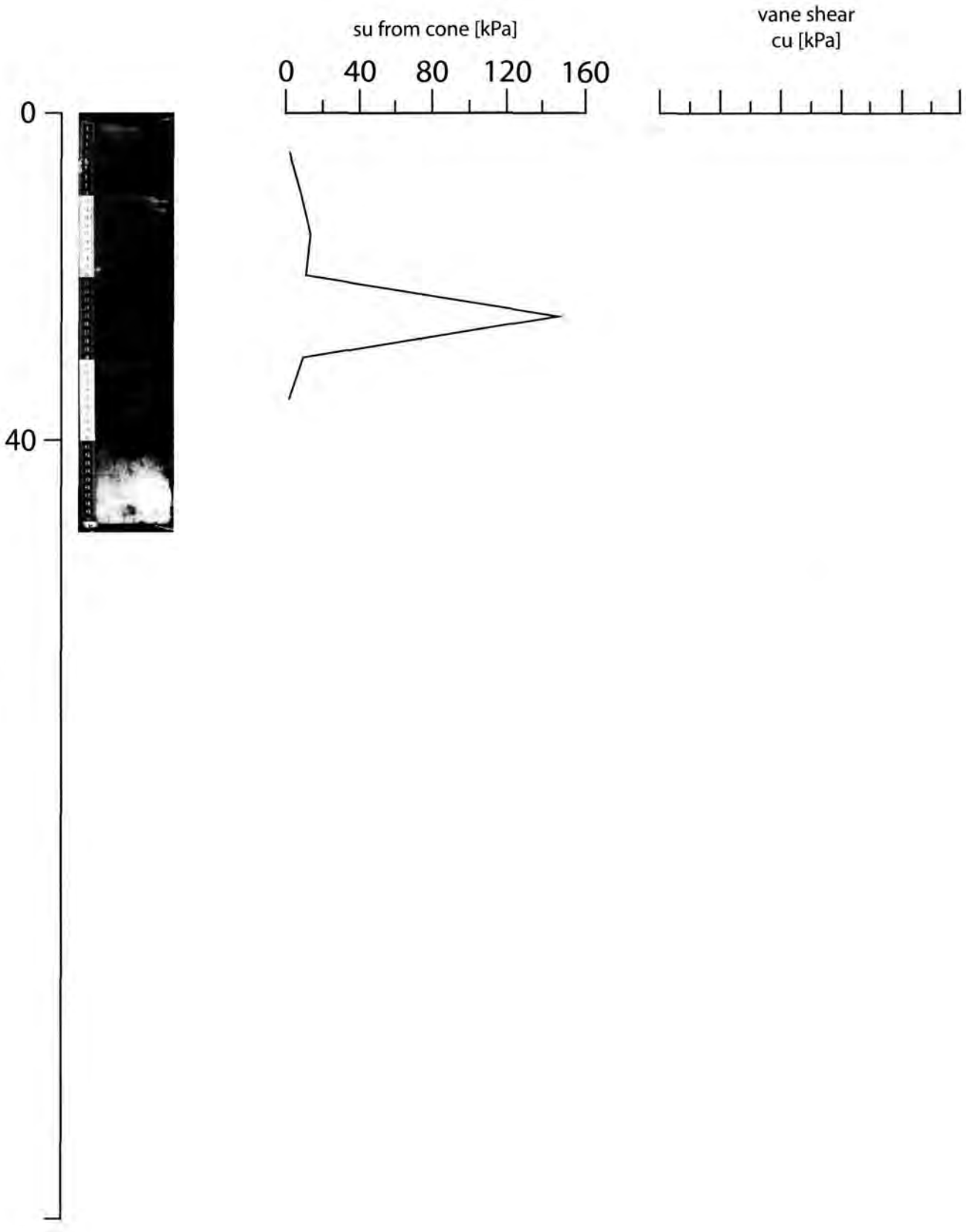

GeoB 15310

Date : 16.03.2011 08:34
Water Depth : 1935 m
Study Area : Milano

Position : 33° 44.187' N
24° 46.566' E
Core Length : 90 cm

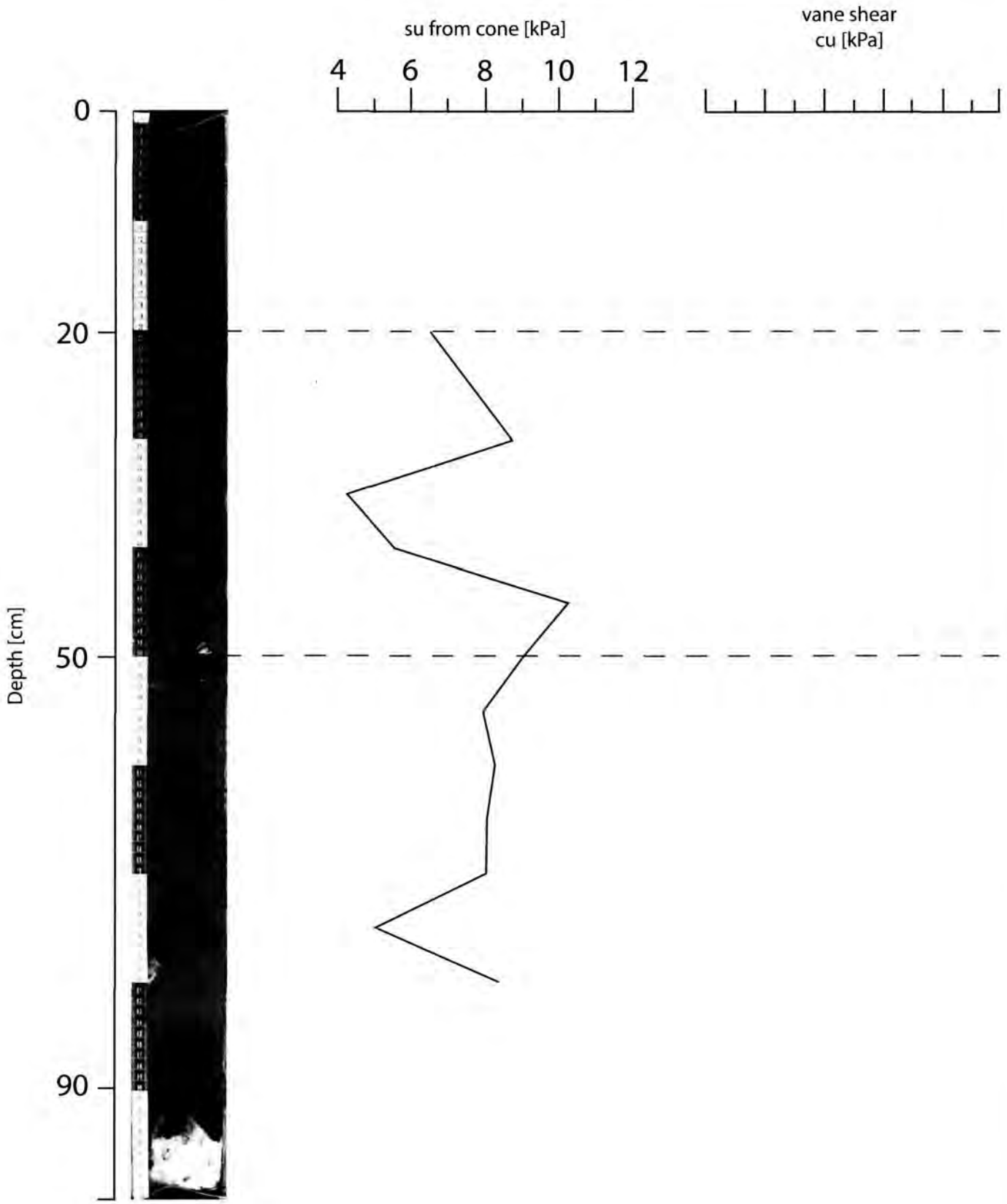

GeoB 15311

Date : 16.03.2011 09:59 Position : 33° 43.44' N
Water Depth : 1901 m 24° 41.25' E
Study Area : Napoli 971D Core Length : 300cm

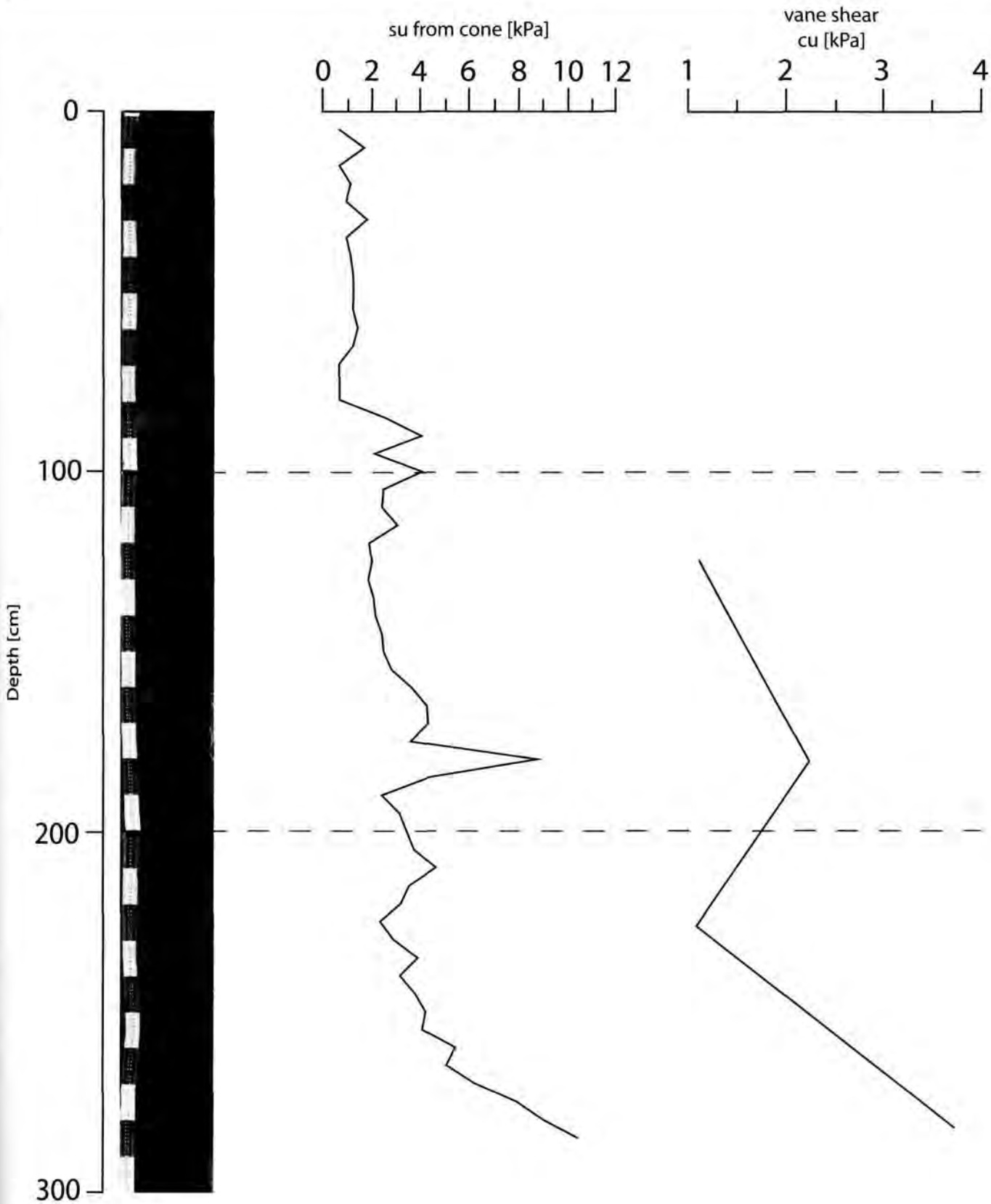

GeoB 15312

Date : 16.03.2011 11:35
Water Depth : 1908 m
Study Area : Napoli

Position : 33° 43.62' N
24° 40.84' E
Core Length : 300cm

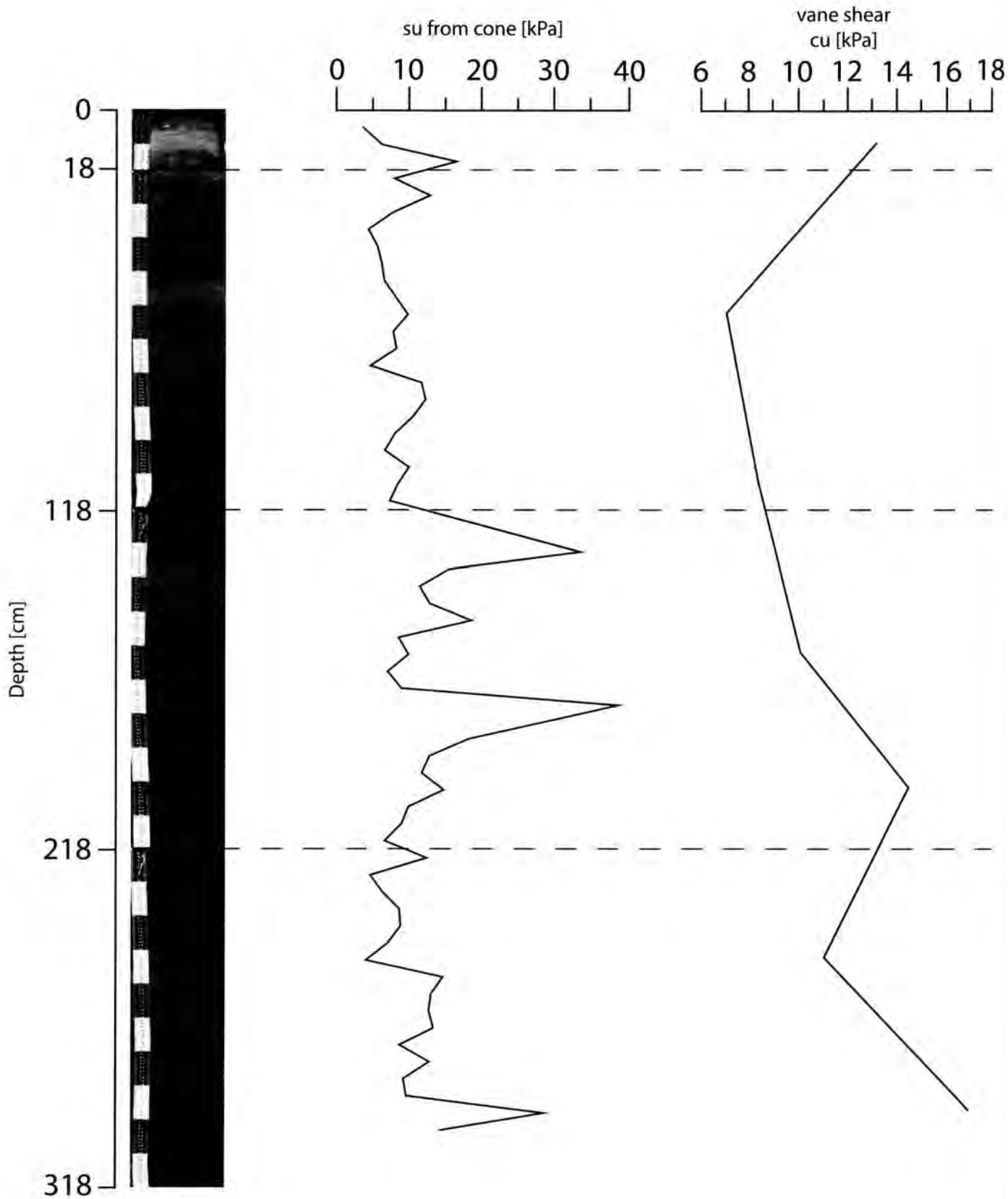

GeoB 15314

Date : 17.03.2011 08:07
Water Depth : 1909 m
Study Area : Napoli plateau

Position : 33° 43.509' N
24° 41.023' E
Core Length : 260 cm

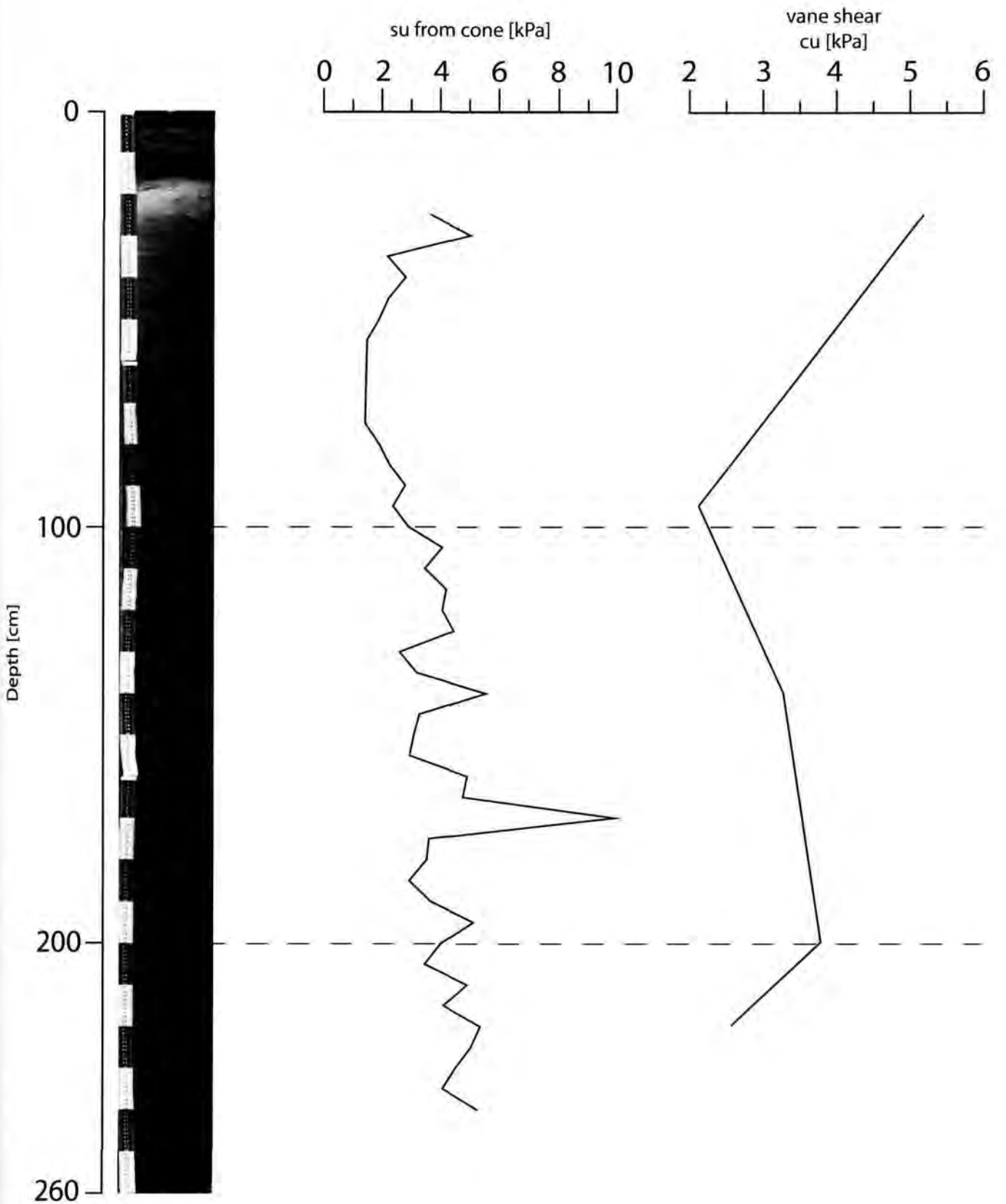

GeoB 15317

Date : 17.03.2011 15:20
Water Depth : 1903 m
Study Area : Bergamo

Position : 33° 44.08' N
24° 43.47' E
Core Length : 60 cm

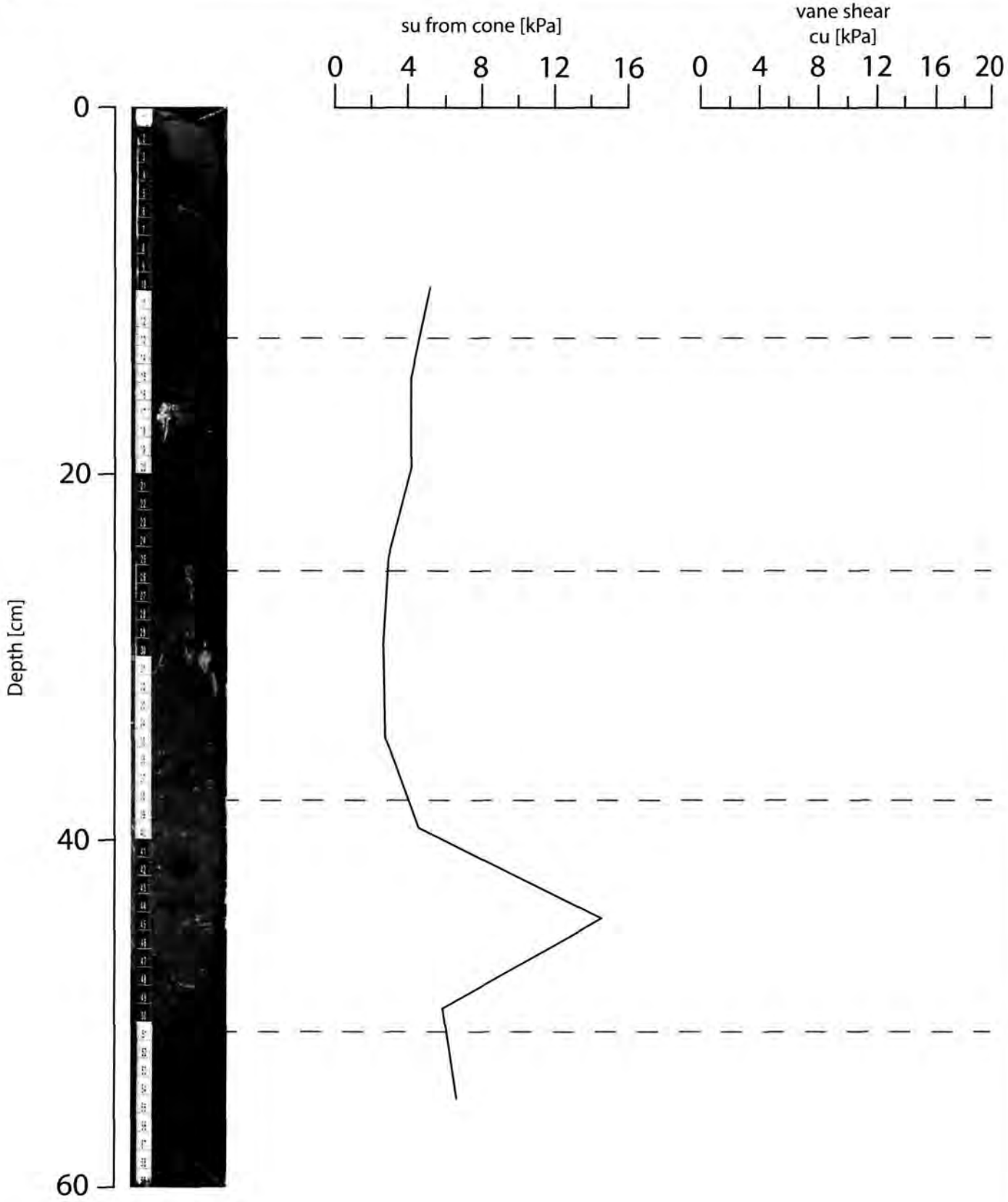

GeoB 15320

Date : 18.03.2011 07:30
Water Depth : 1908 m
Study Area : Napoli

Position : 33° 43.16' N
24° 41.24' E
Core Length : 47 cm

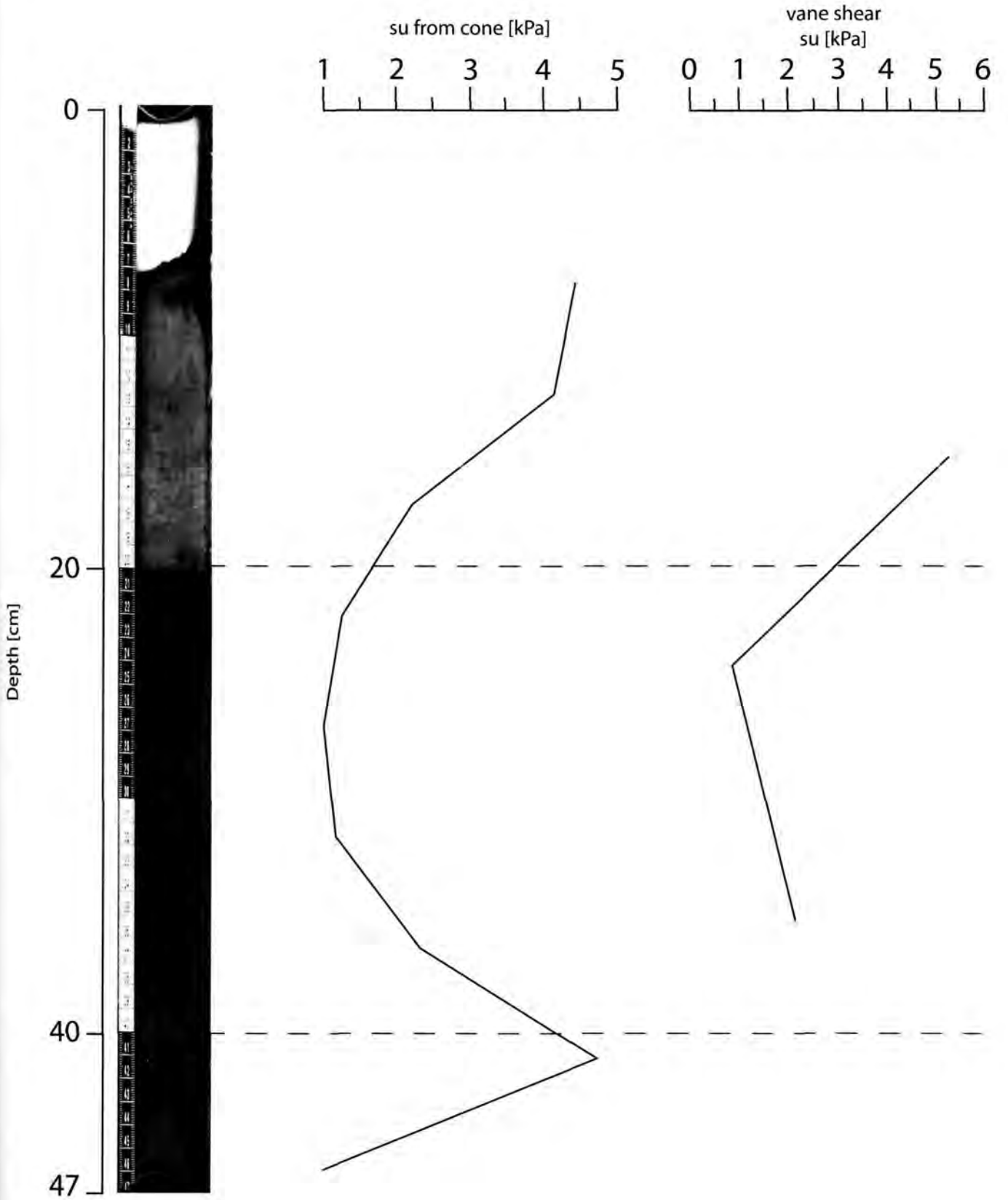

GeoB 15321

Date : 18.03.2011 09:13
Water Depth : 1986 m
Study Area : Napoli NE-Flanke

Position : 33° 44.24' N
24° 41.53' E
Core Length : 262 cm

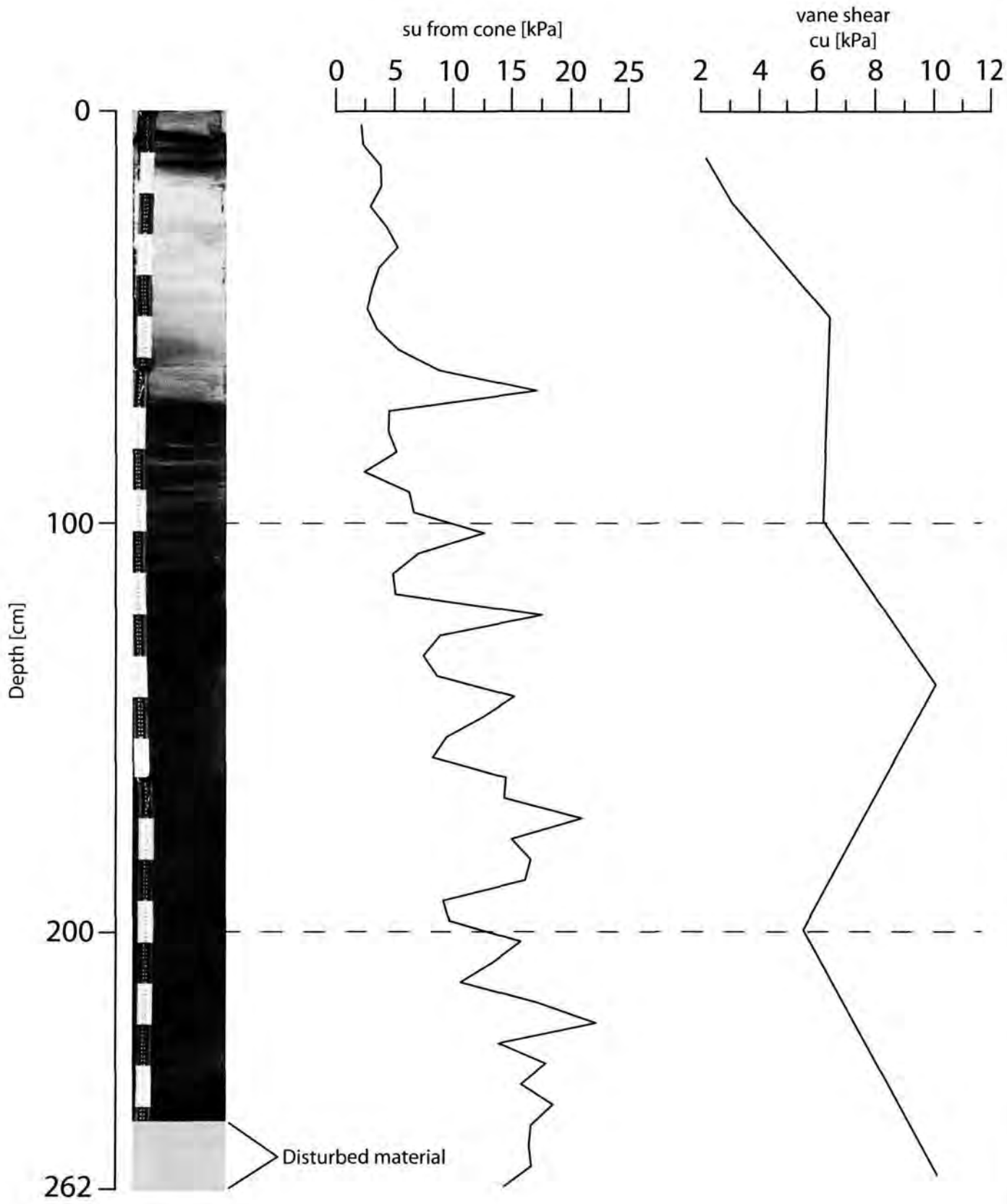

GeoB 15323

Date : 18.03.2011 13:37
Water Depth : 1912,2 m
Study Area : Bergamo

Position : 33° 44.266' N
24° 45.022' E
Core Length : 301 cm

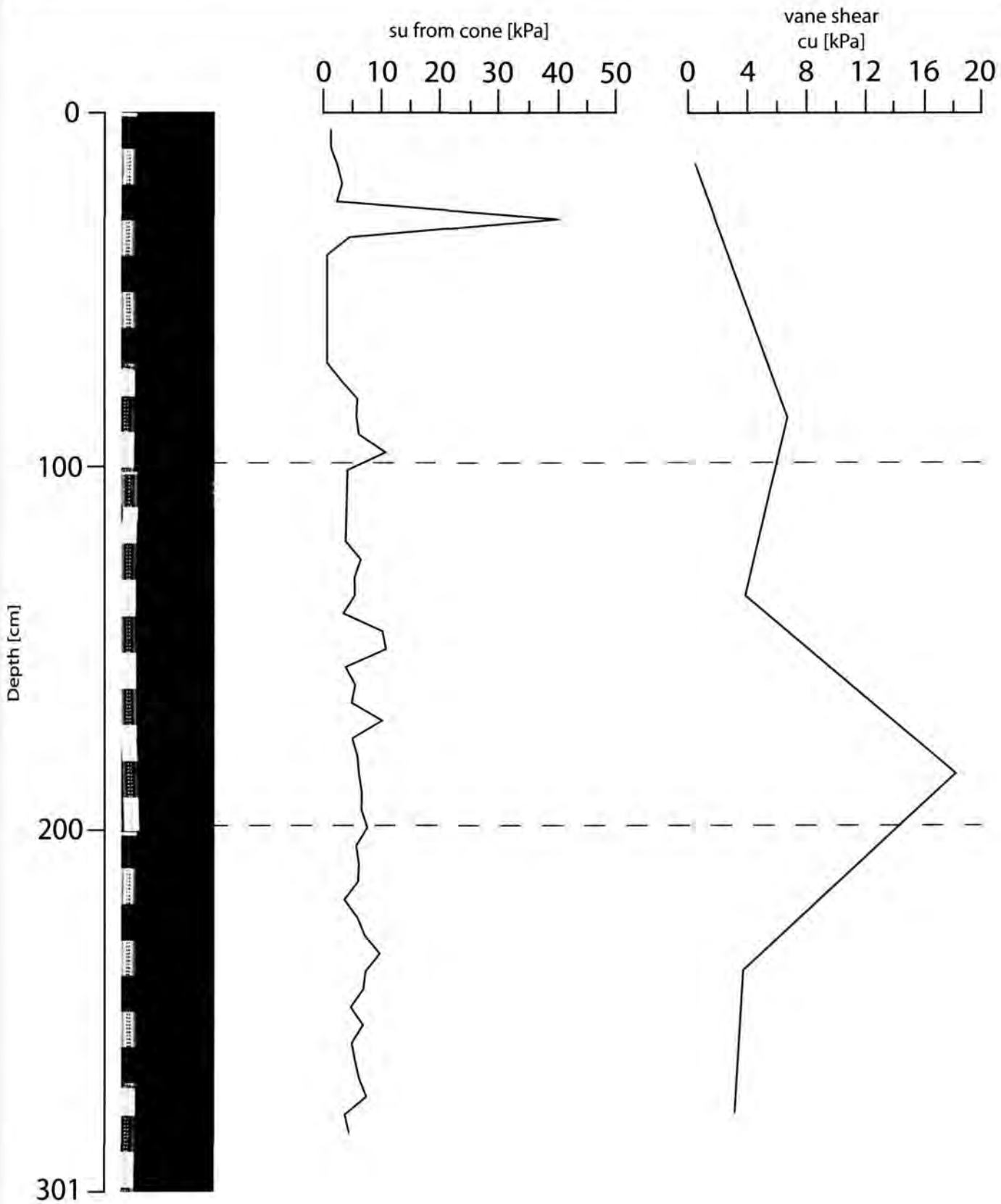

GeoB 15325

Date : 19.03.2011 06:53
Water Depth : 1935 m
Study Area : Bergamo

Position : 33° 44.430' N
24° 44.946' E
Core Length : 100 cm

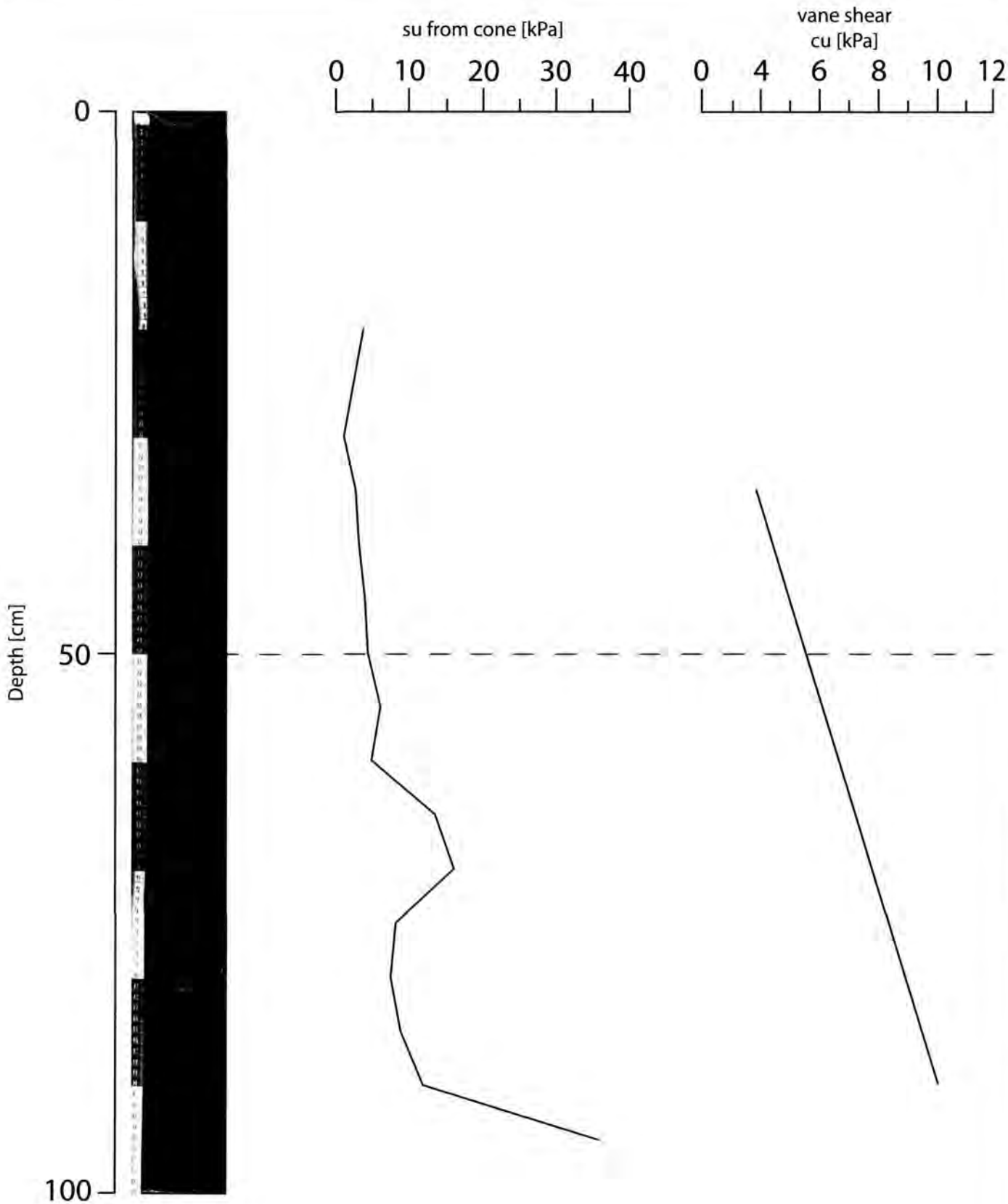

GeoB 15326

Date : 19.03.2011 08:40
Water Depth : 1927,9 m
Study Area : Bergamo

Position : 33° 44.118' N
24° 44.865' E
Core Length : 300 cm

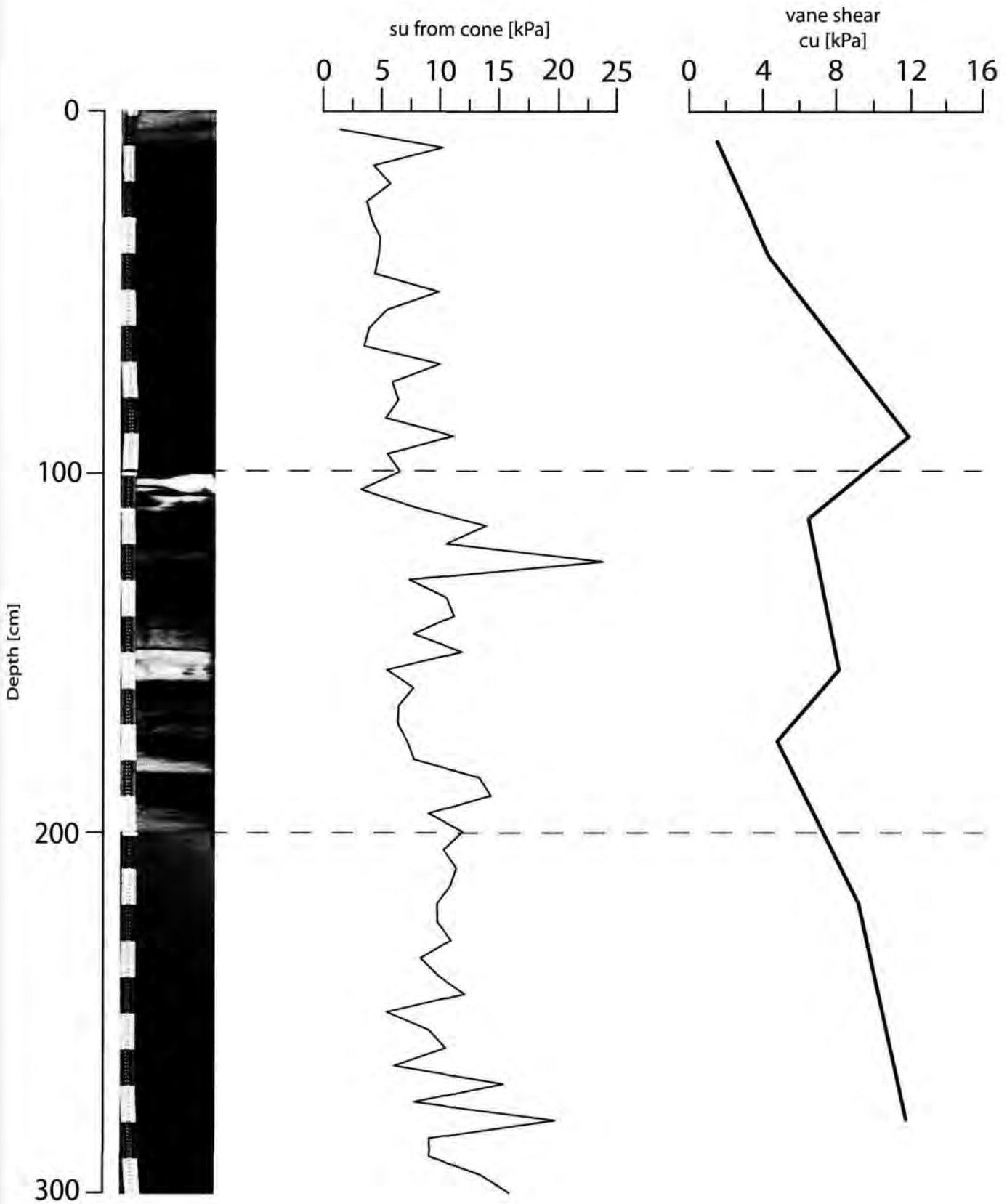

GeoB 15329

Date : 20.03.2011 08:05
Water Depth : 1911 m
Study Area : M. V. Lich

Position : 33° 51.56' N
24° 33.79' E
Core Length : 280 cm

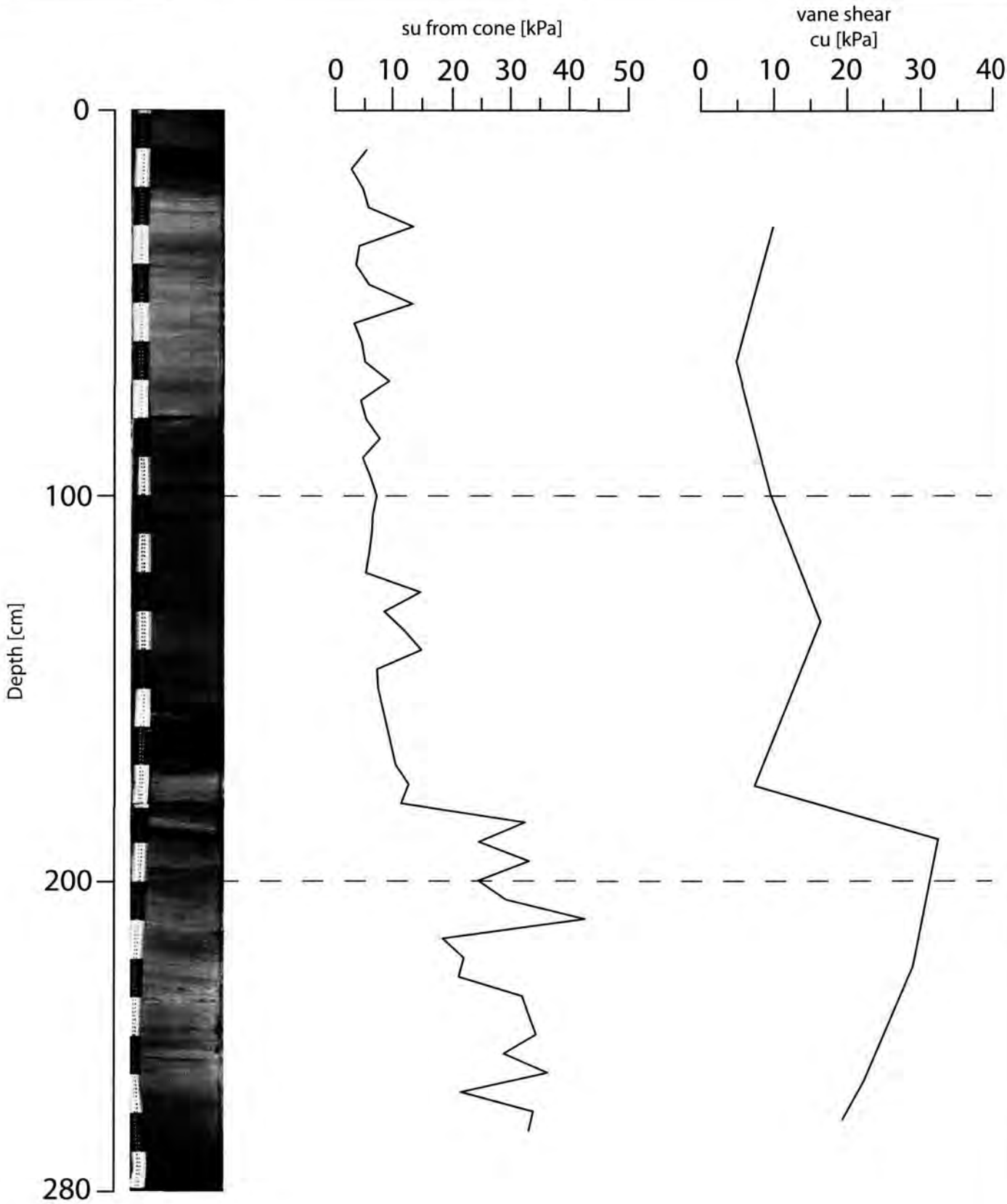

GeoB 15330

Date : 20.03.2011 14:39
Water Depth : 1939 m
Study Area : M. V. Lich

Position : 33° 51.423' N
24° 34.088' E
Core Length : 146 cm

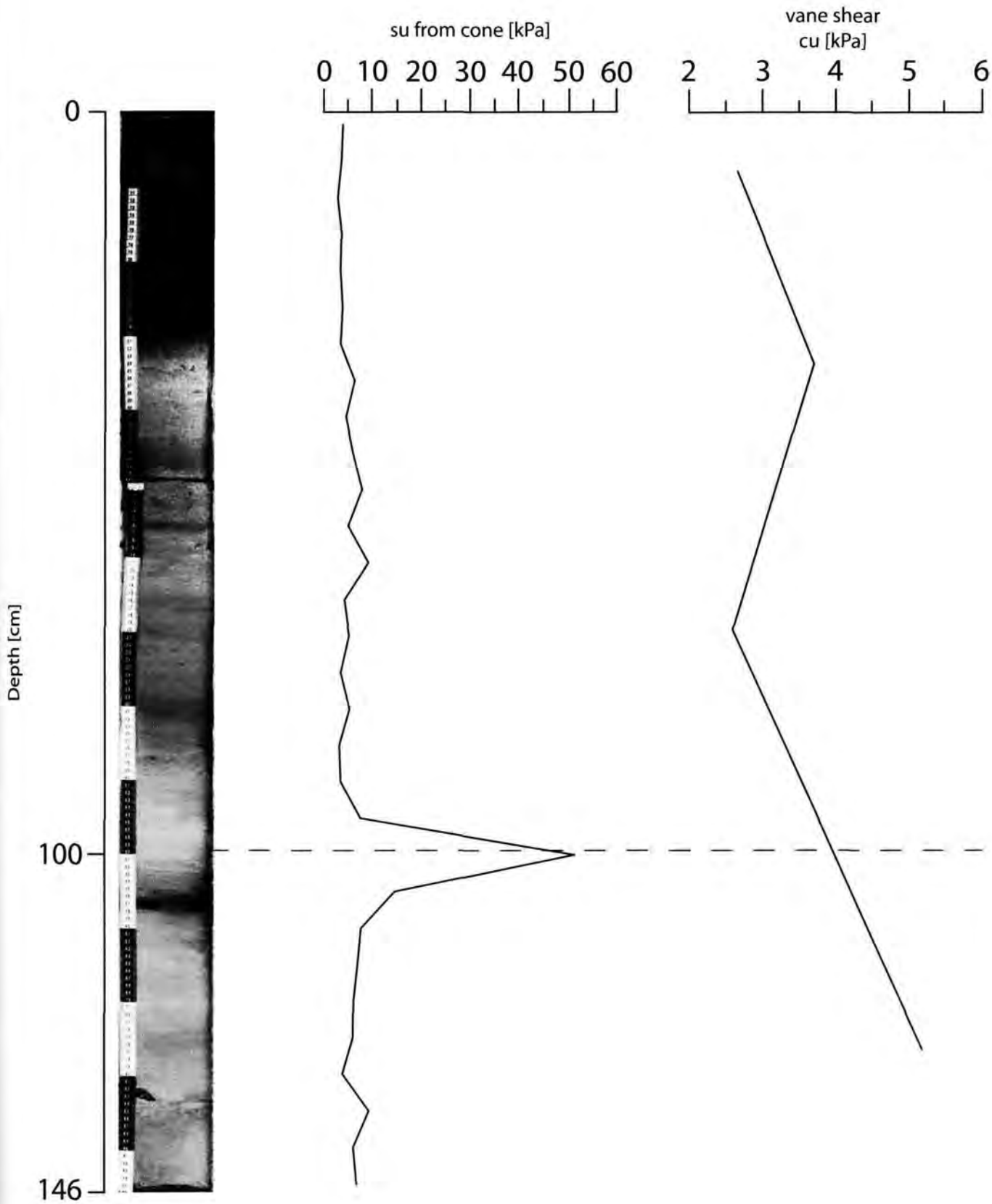

GeoB 15331

Date : 20.03.2011 11:38
Water Depth : 1884,8 m
Study Area :

Position : 33° 51.462' N
24° 35.086' E
Core Length : 289 cm

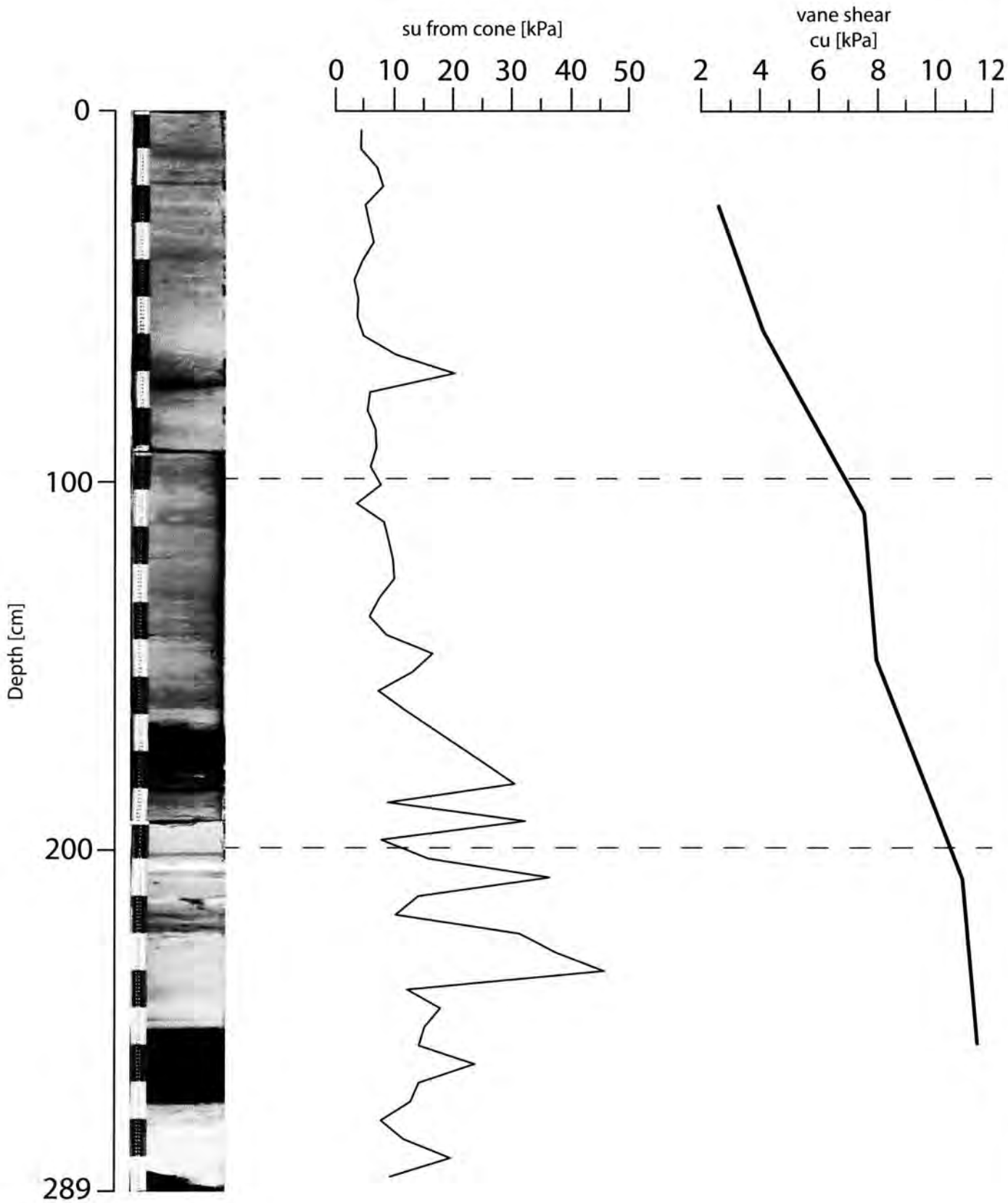

GeoB 15332

Date : 20.03.2011 19:48
Water Depth : 1891m
Study Area : M. V. Lich

Position : 33° 47.02' N
24° 39.15' E
Core Length : 188 cm

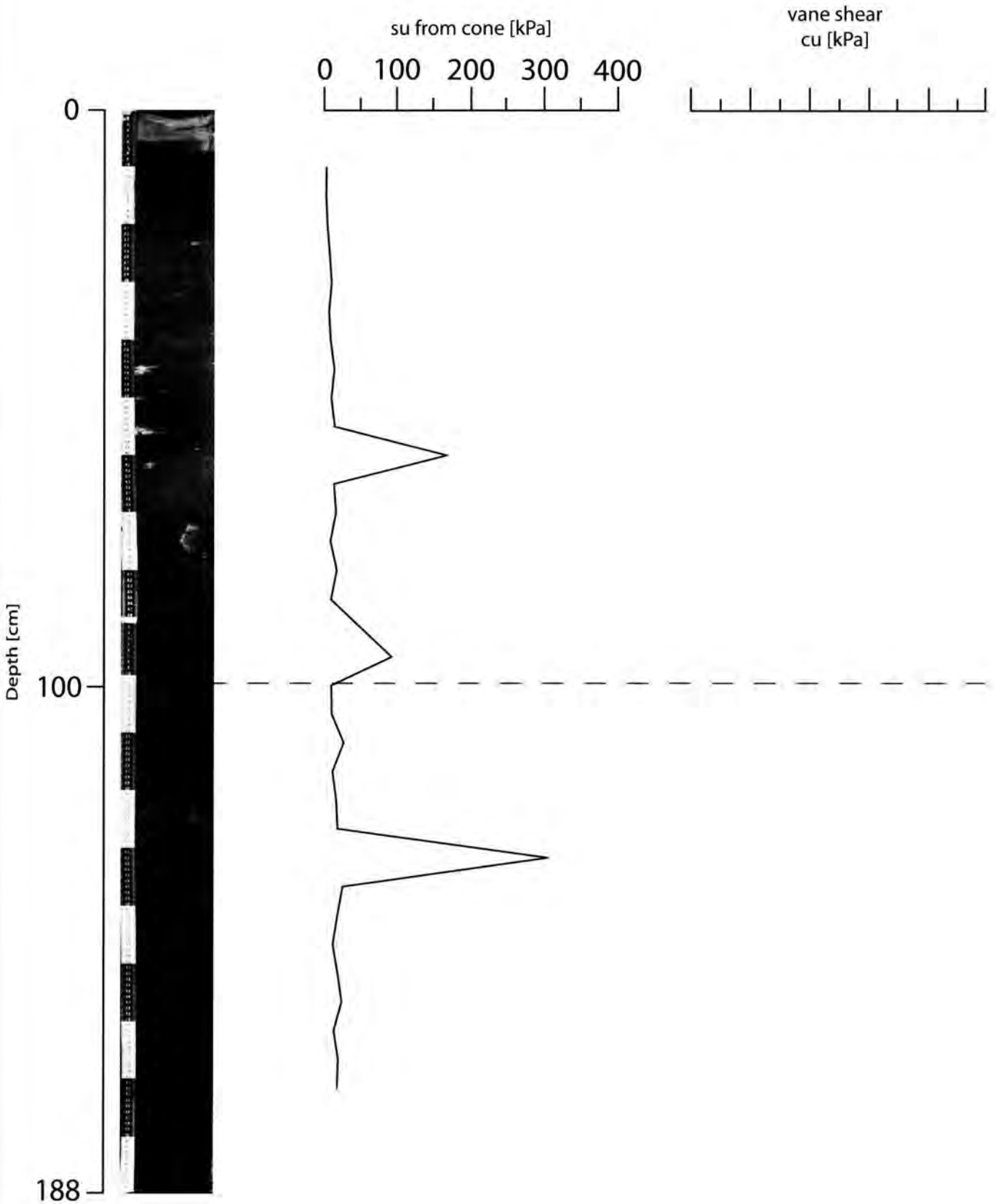

GeoB 15334

Date : 21.03.2011 08:18
Water Depth : 2054 m
Study Area :

Position : 34° 06.15' N
24° 21.05' E
Core Length : 73 cm

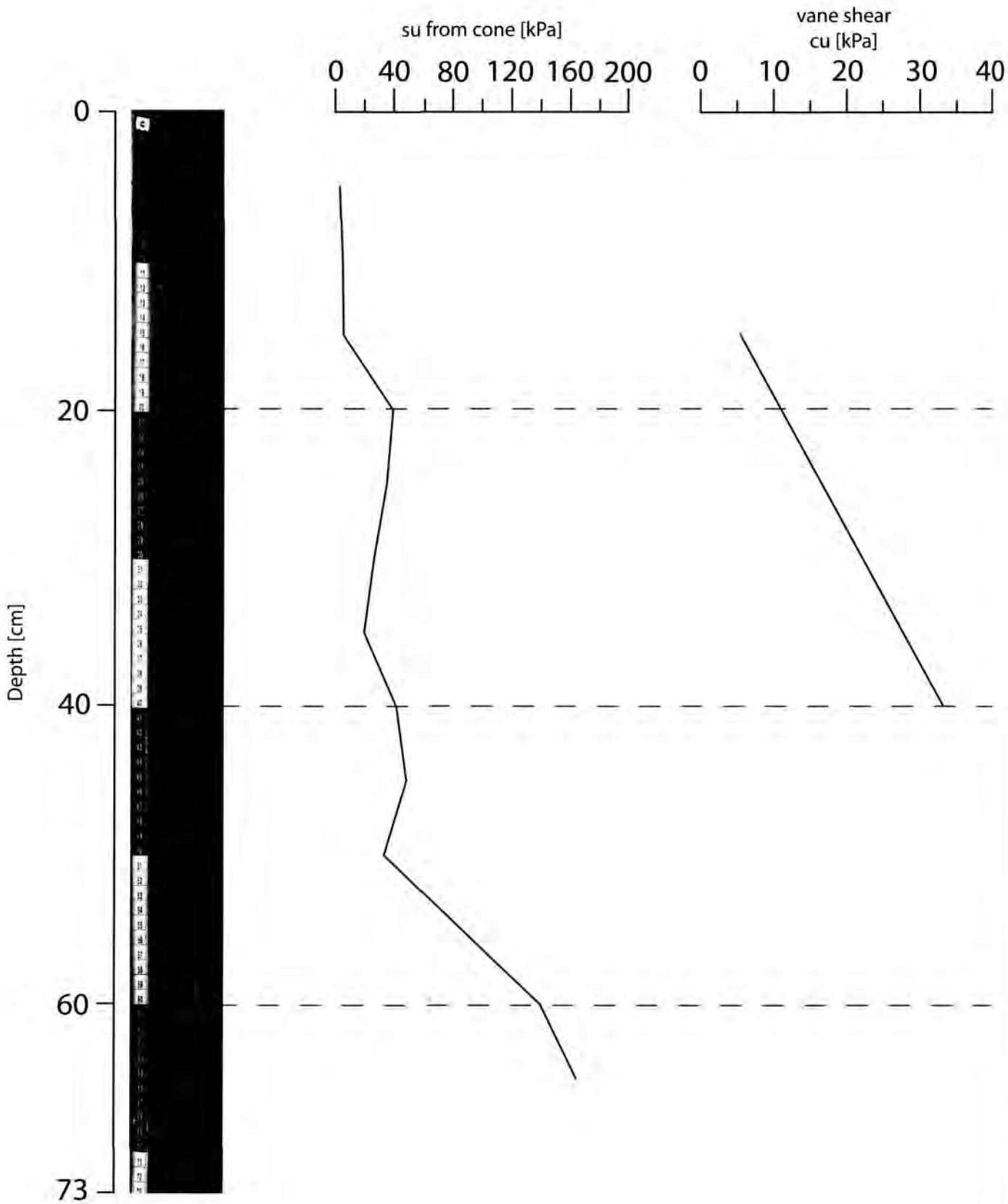

GeoB 15335

Date : 21.03.2011 10:50
Water Depth : 1377 m
Study Area :

Position : 34° 12.752' N
24° 13.272' E
Core Length : 239 cm

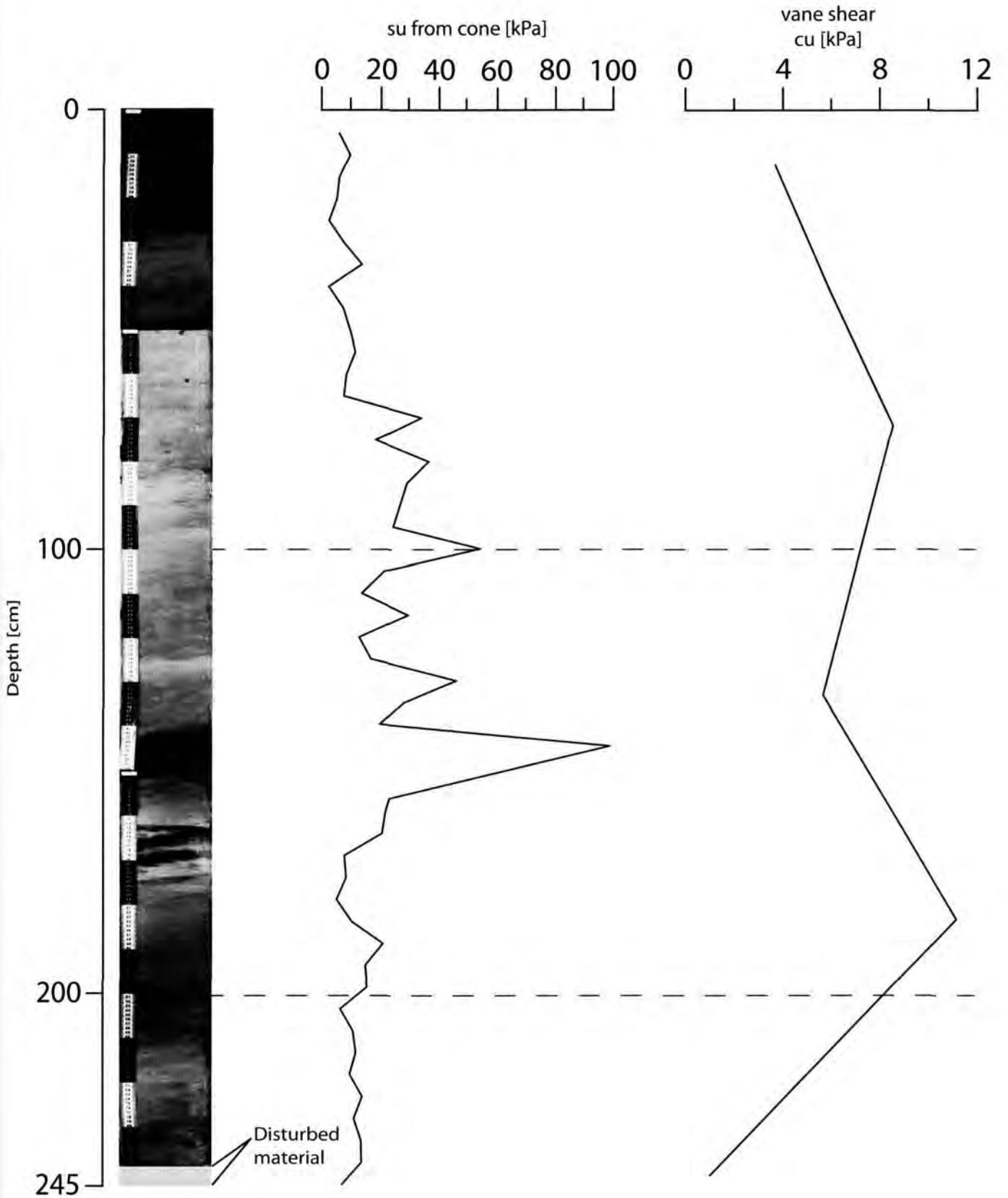

GeoB 15337

Date : 21.03.2011 14:16
Water Depth : 1649 m
Study Area :

Position : 34° 12.785' N
24° 13.749' E
Core Length : 89 cm

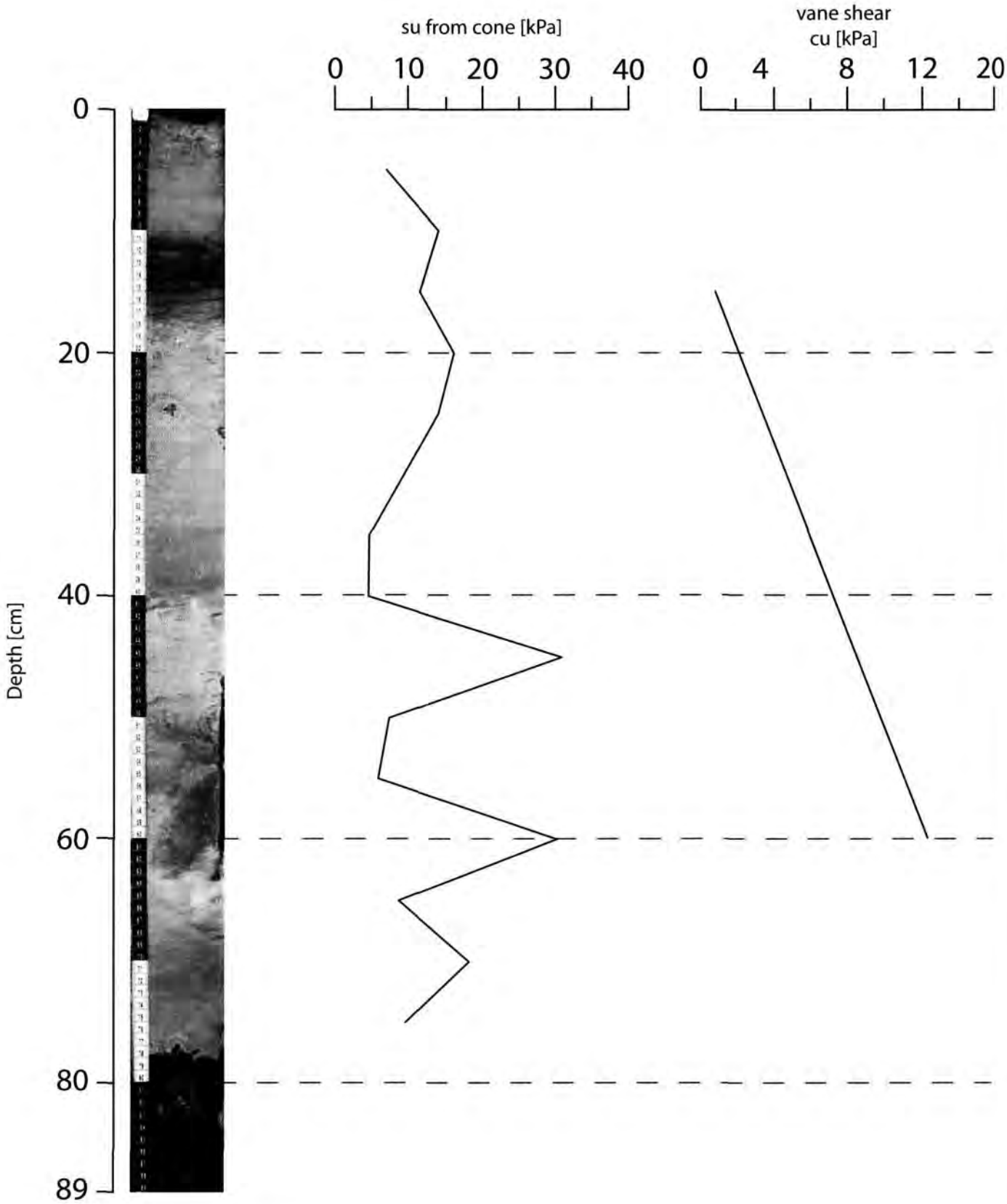

GeoB 15339

Date : 22.03.2011 07:20
Water Depth : 2255.5 m
Study Area :

Position : 34° 07.936' N
24° 22.91' E
Core Length : 325 cm

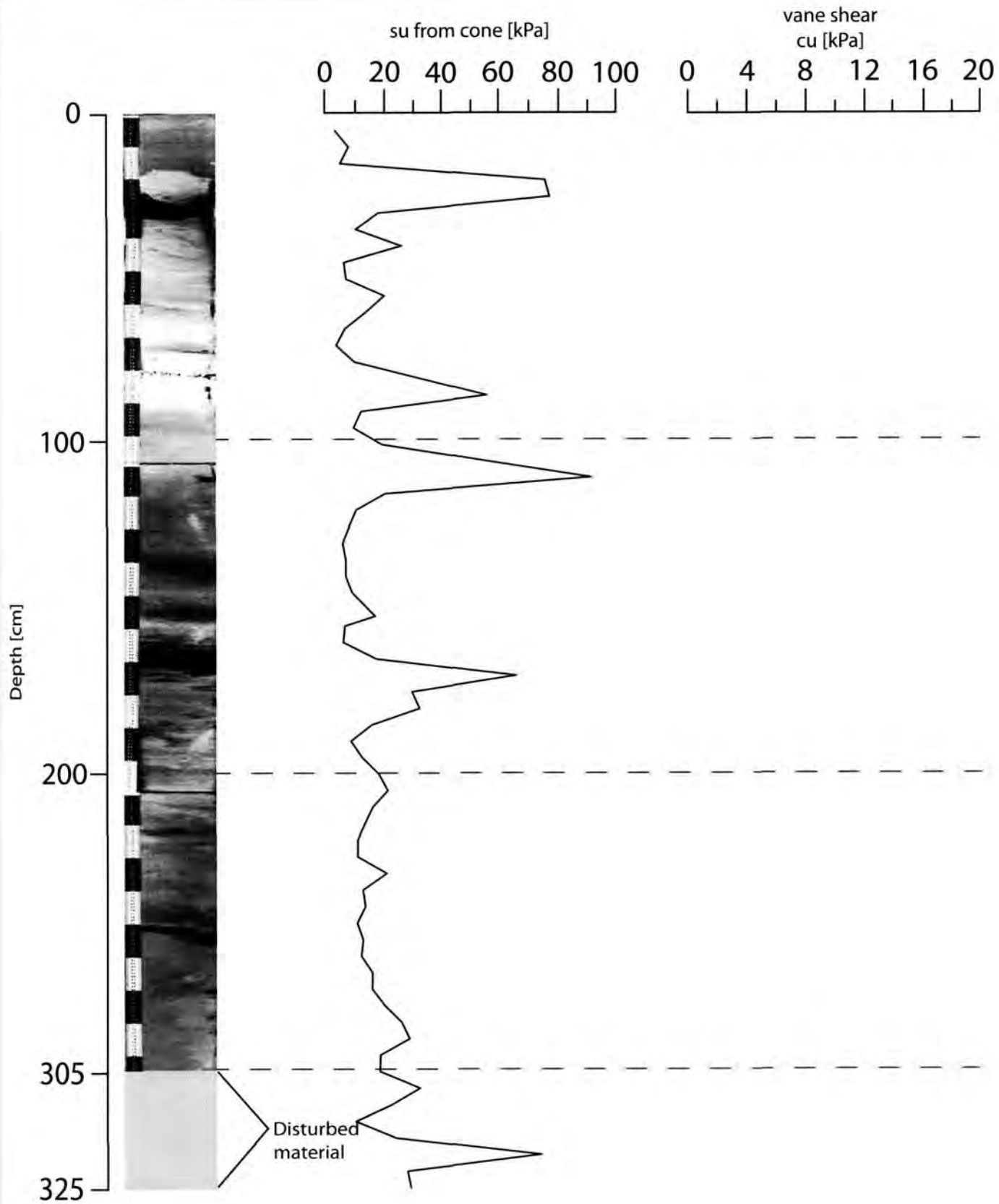

GeoB 15340

Date : 22.03.2011 09:41
Water Depth : 2092.7 m
Study Area :

Position : 34° 11.714' N
24° 20.176' E
Core Length : 79 cm

su from cone [kPa]

vane shear
cu [kPa]

Depth [cm]

0

50

79

GeoB 15341

Date : 22.03.2011 12:35
Water Depth : 2117 m
Study Area :

Position : 34° 17.371' N
24° 16.478' E
Core Length : 58 cm

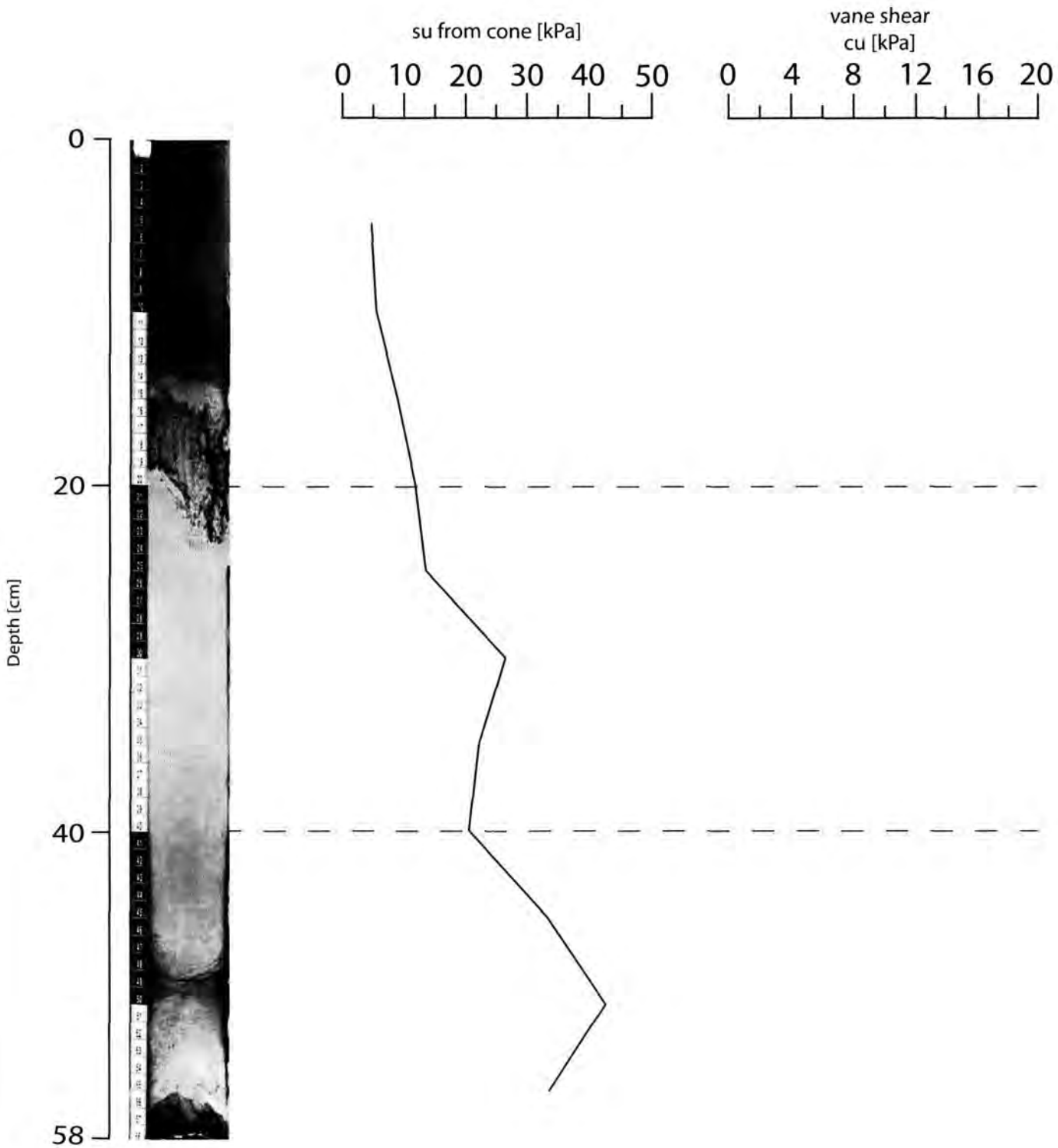

GeoB 15343

Date : 23.03.2011 09:05
Water Depth : 2212 m
Study Area : Outer to inner ridge border

Position : 34° 18.285' N
24° 14.28' E
Core Length : 540 cm

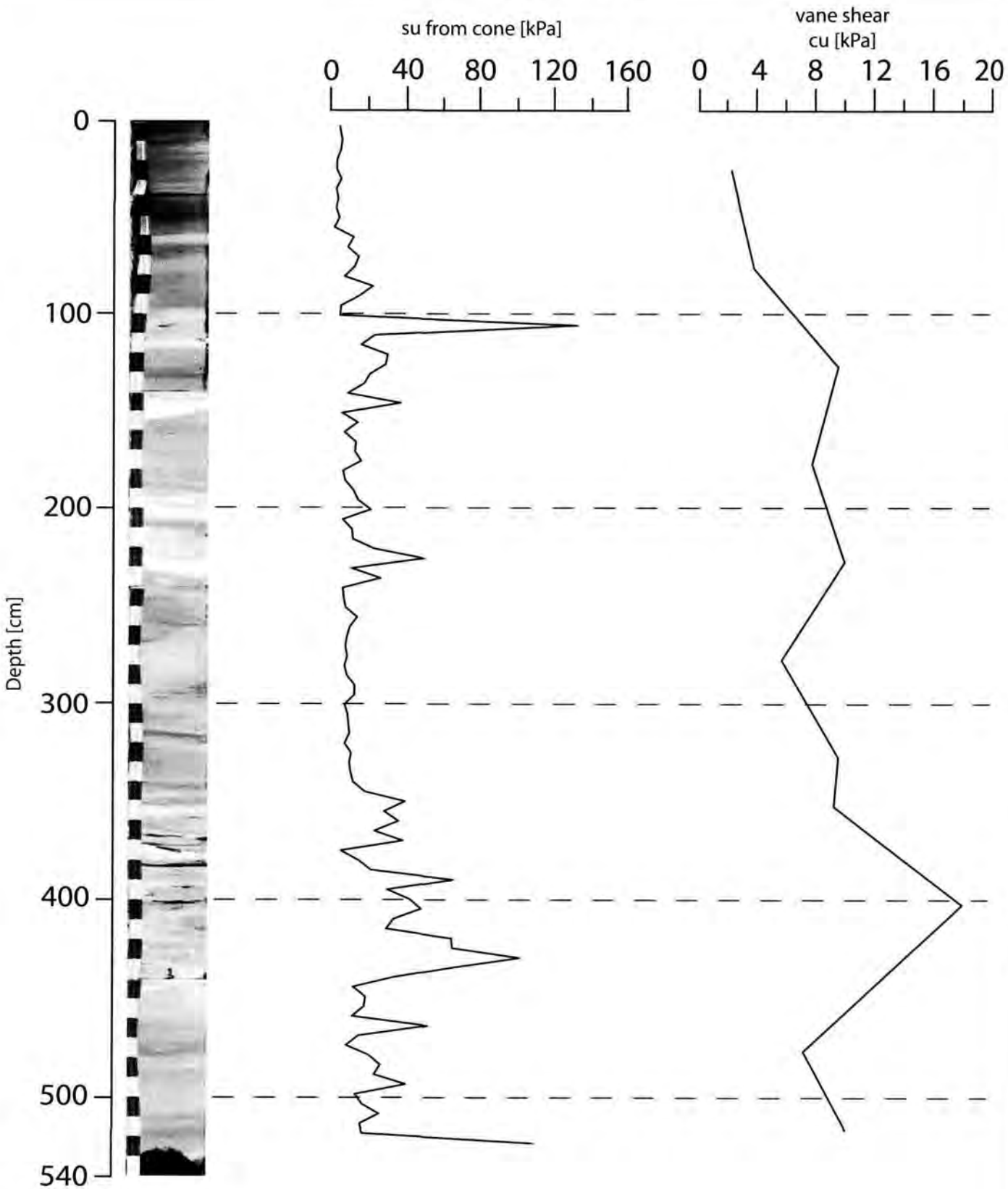

GeoB 15344

Date : 23.03.2011 11:25
Water Depth : 2098 m
Study Area : Outer to inner ridge border

Position : 34° 17.40' N
24° 16.47' E
Core Length : 200 cm

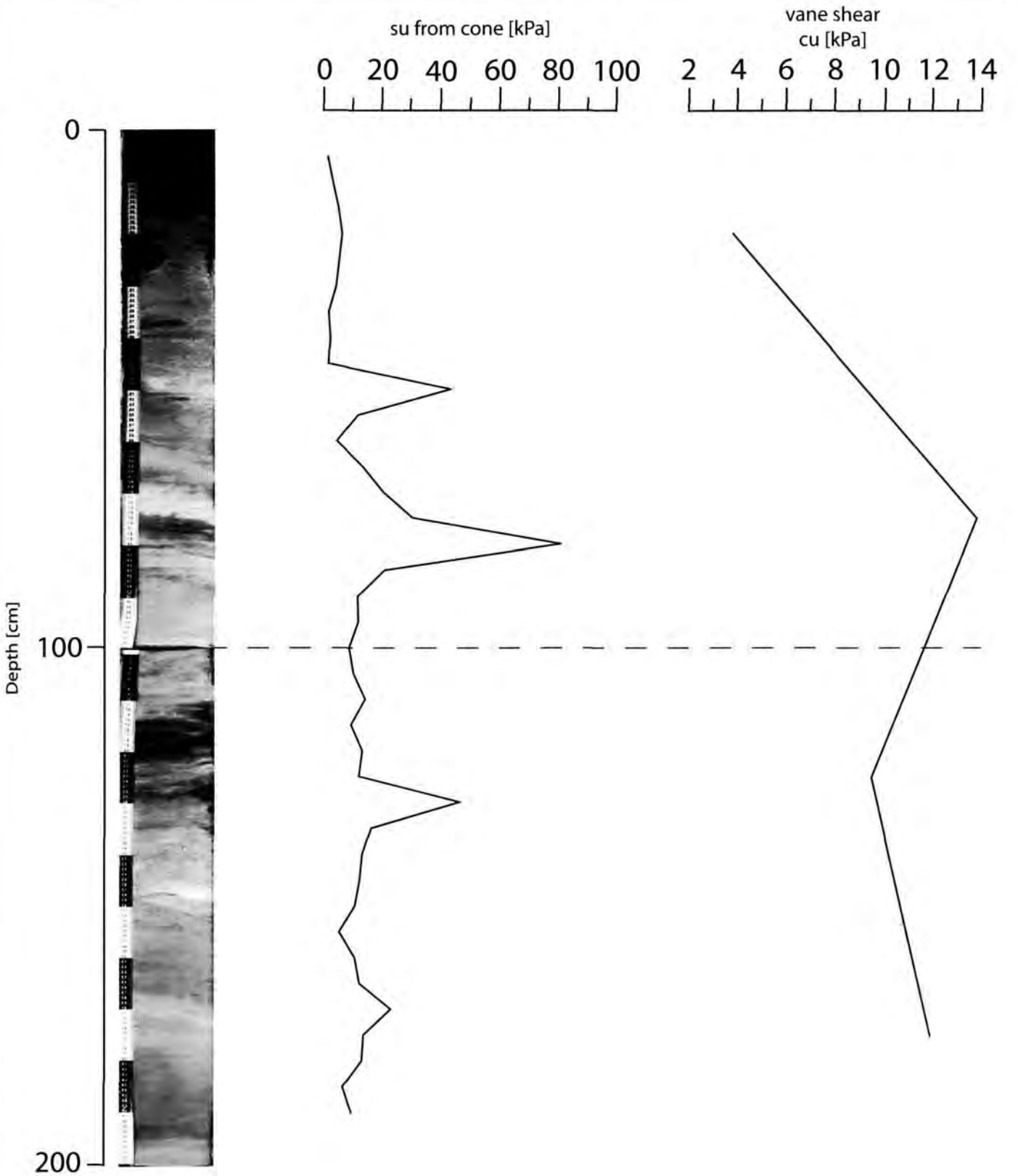

GeoB 15345

Date : 23.03.2011 11:53
Water Depth : 2110 m
Study Area : Outer to inner ridge border

Position : 34° 16.30' N
24° 17.50' E
Core Length : 254 cm

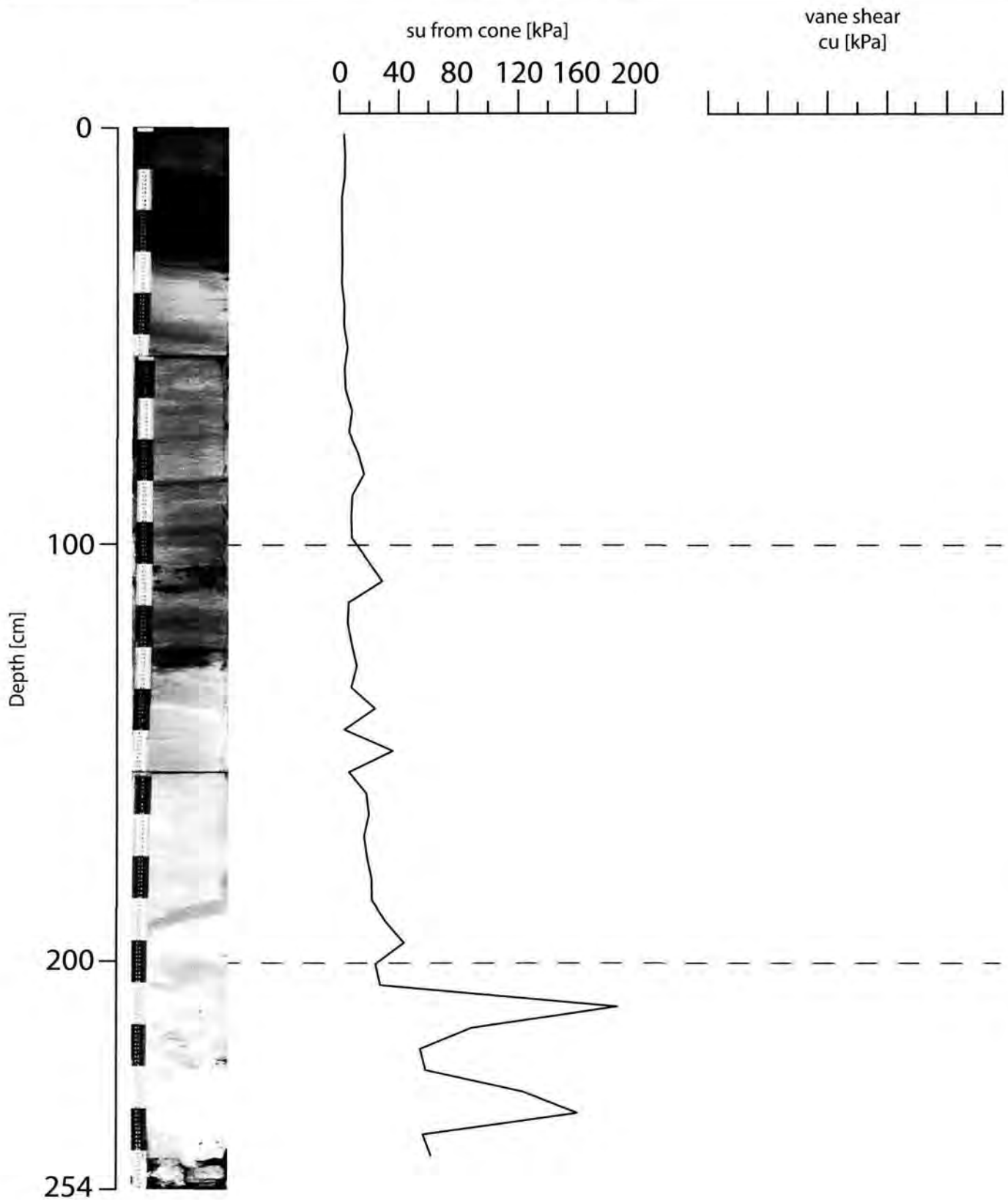

GeoB 15347

Date : 24.03.2011 06:07
Water Depth : 1972 m
Study Area : Inner ridge
Creta Margin

Position : 34° 17.117' N
24° 31.907' E
Core Length : 179 cm

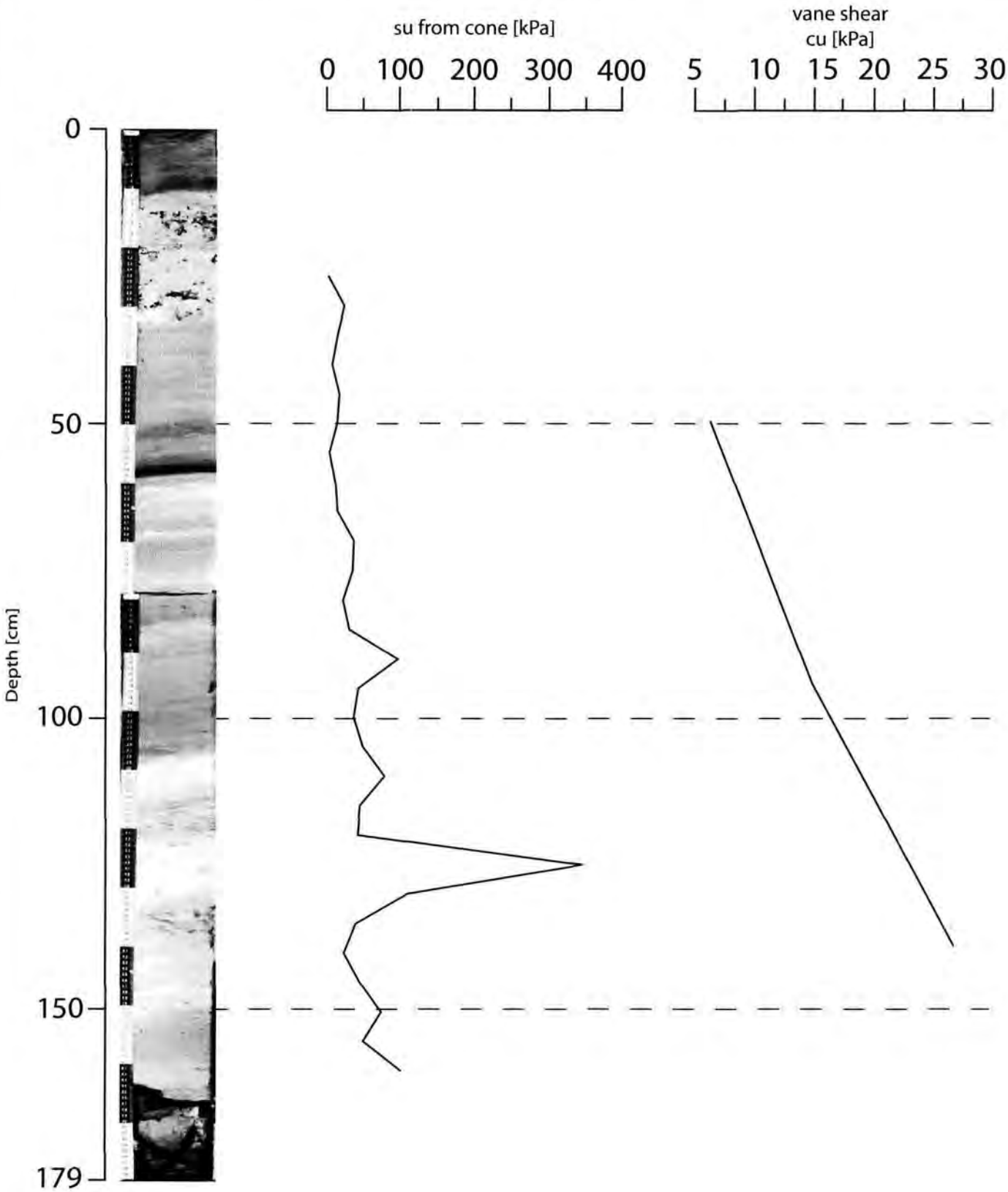

GeoB 15348

Date : 24.03.2011 09:03
Water Depth : 2699 m
Study Area : Inner ridge
Creta Margin

Position : 34° 20.157' N
24° 32.953' E
Core Length : 48 cm

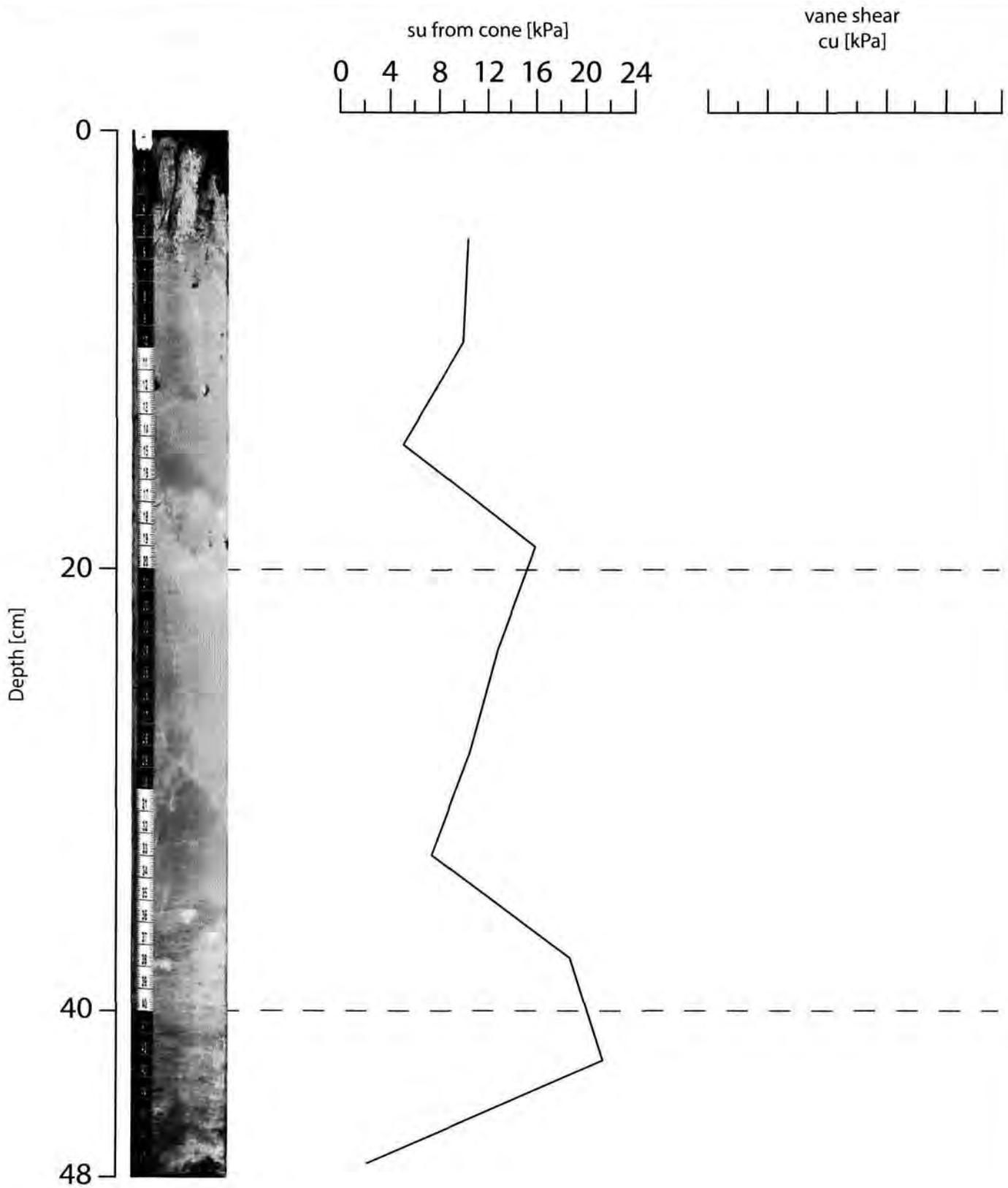

GeoB 15349

Date : 24.03.2011 11:37
Water Depth : 2600 m
Study Area :

Position : 34° 19.161' N
24° 33.173' E
Core Length : 275 cm

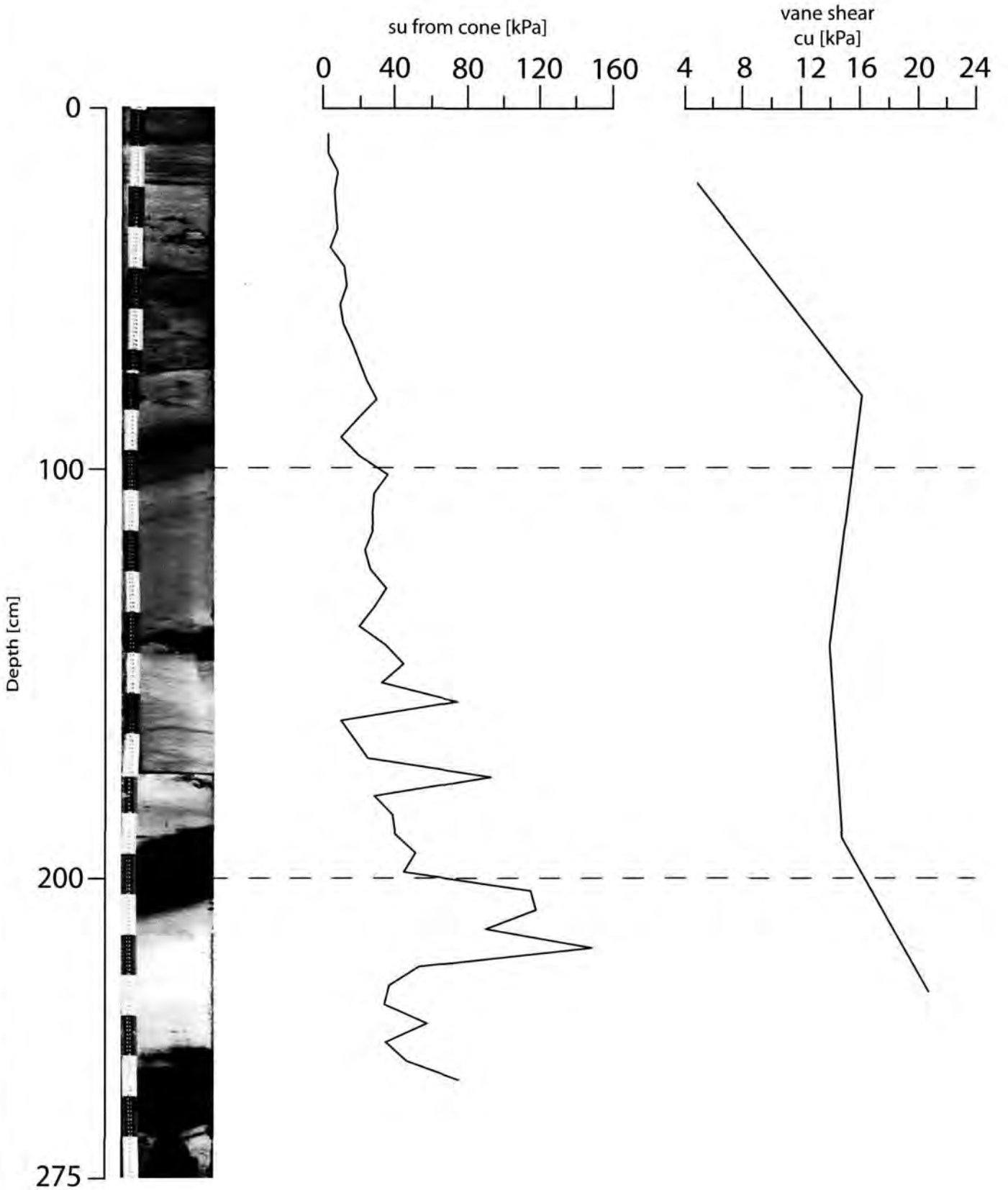

GeoB 15351

Date : 25.03.2011 14:39
Water Depth : 2834 m
Study Area :

Position : 34° 16.95' N
24° 38.25' E
Core Length : 149 cm

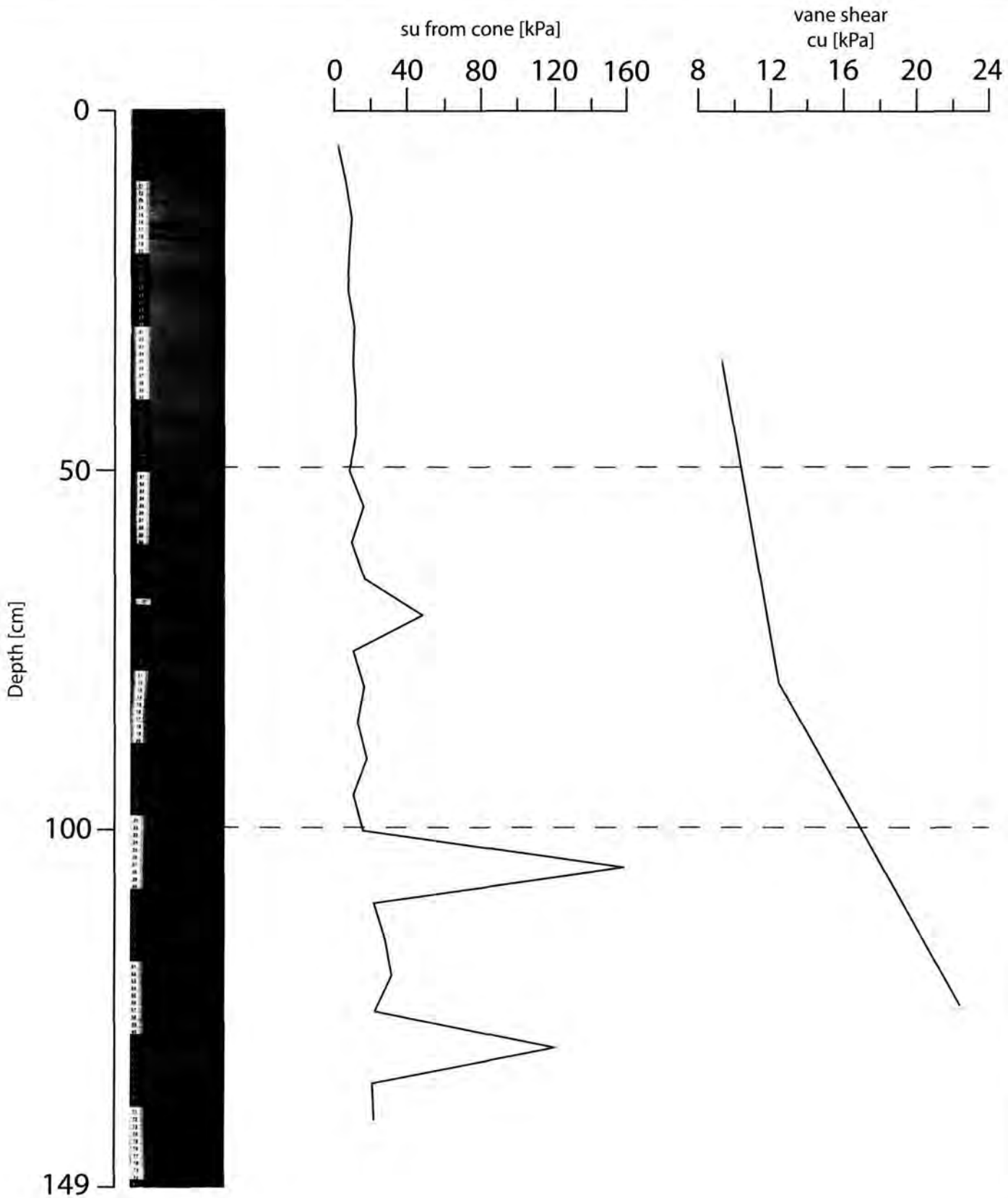

GeoB 15352

Date : 25.03.2011 10:18
Water Depth : 3066 m
Study Area : Inner ridge
Creta Margin

Position : 34° 08.874' N
24° 46.582' E
Core Length : 463 cm

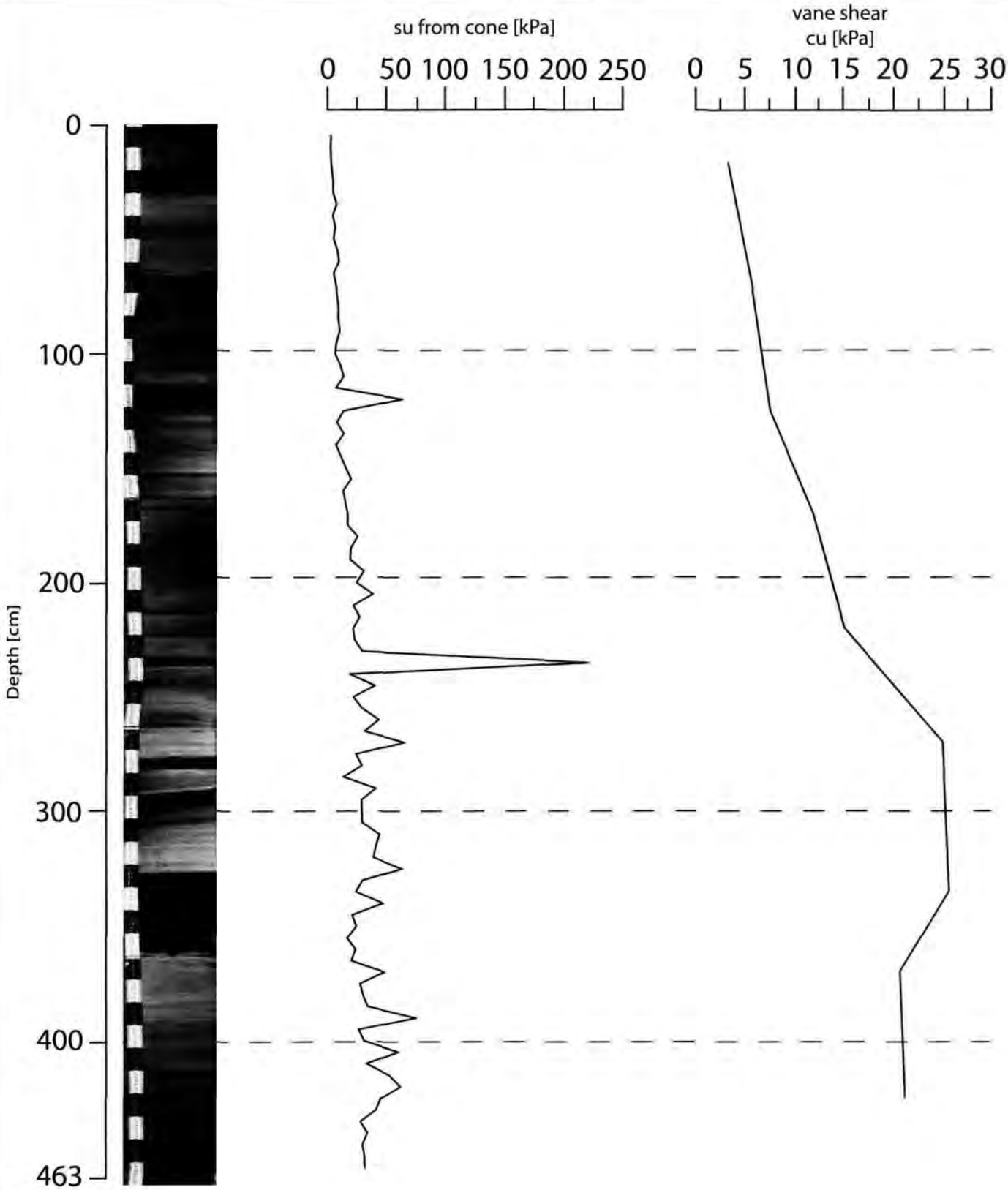

GeoB 15353

Date : 25.03.2011 12:34
Water Depth : 2960 m
Study Area : Inner ridge
Creta Margin

Position : 34° 06.88' N
24° 47.01' E
Core Length : 366 cm

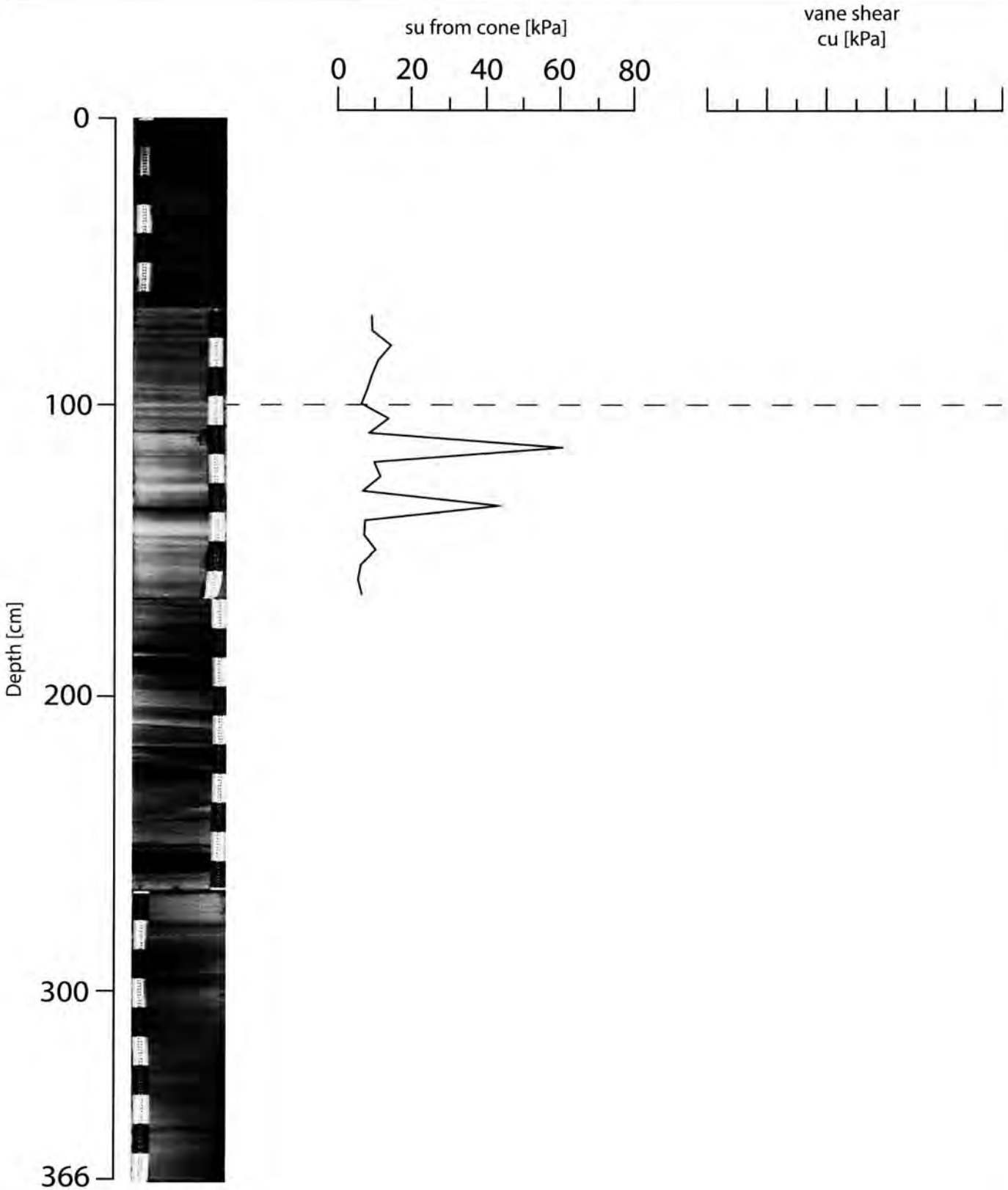

GeoB 15354

Date : 25.03.2011 15:25
Water Depth : 2220 m
Study Area : Creta Margin

Position : 34° 14.573' N
24° 49.334' E
Core Length : 440cm

su from cone [kPa]

vane shear
cu [kPa]

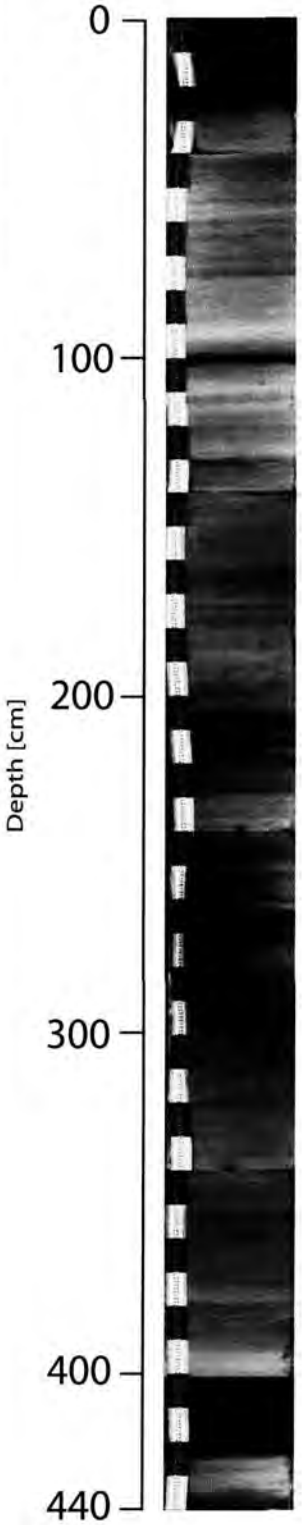

GeoB 15356

Date : 26.03.2011 04:10
Water Depth : 2770 m
Study Area : Cretan Margin

Position : 34° 18.65' N
24° 54.327' E
Core Length : 299 cm

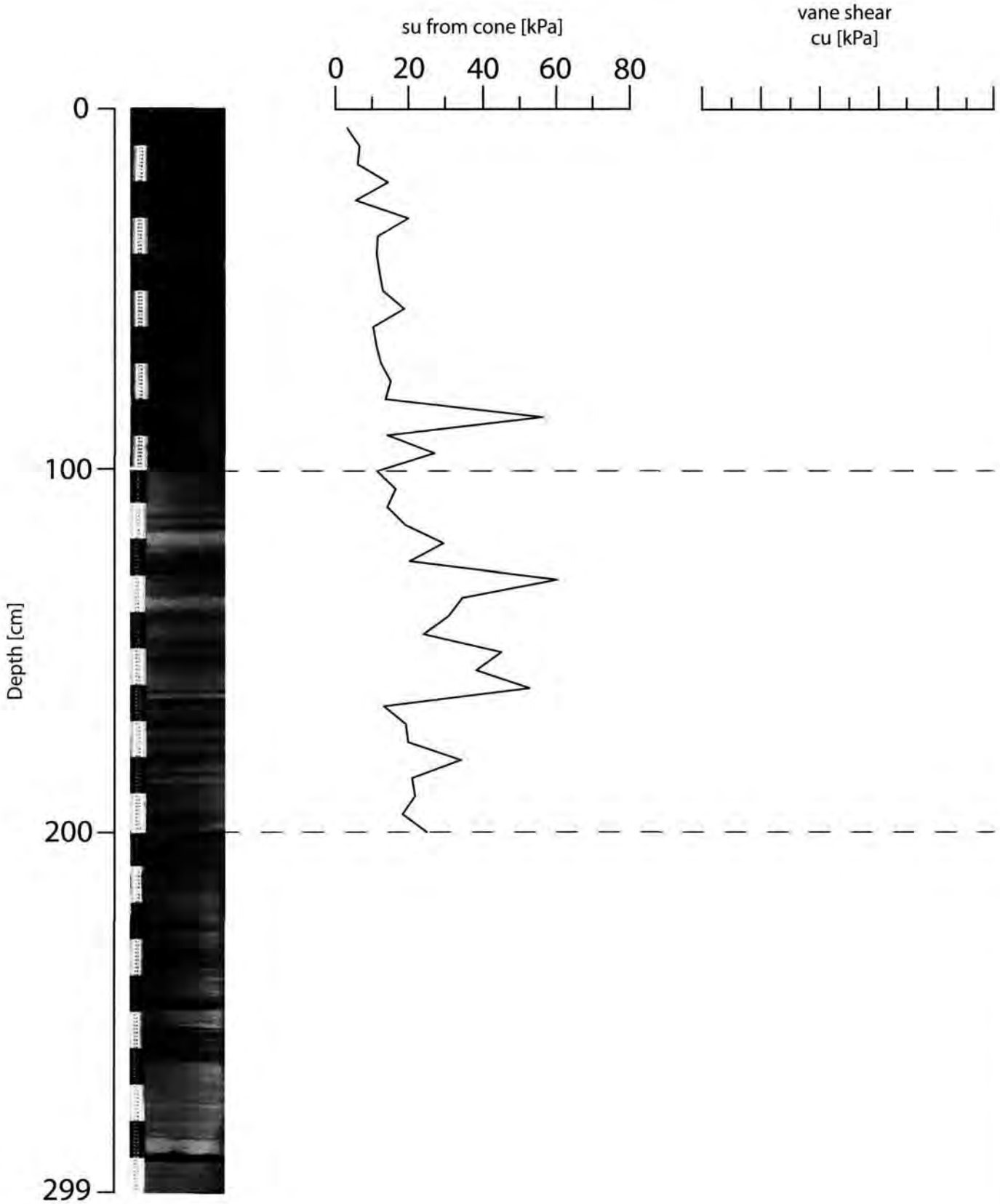

GeoB 15357

Date : 26.03.2011 06:33
Water Depth : 2820m
Study Area : Cretan Margin

Position : 34° 16.617' N
24° 58.395' E
Core Length : 200 cm

su from cone [kPa]

vane shear
cu [kPa]

Depth [cm]

0

100

200

GeoB 15358

Date : 26.03.2011 11:24
Water Depth : 3119 m
Study Area : Inner ridge
Cretan Margin

Position : 34° 5.67' N
24° 58.45' E
Core Length : 73 cm

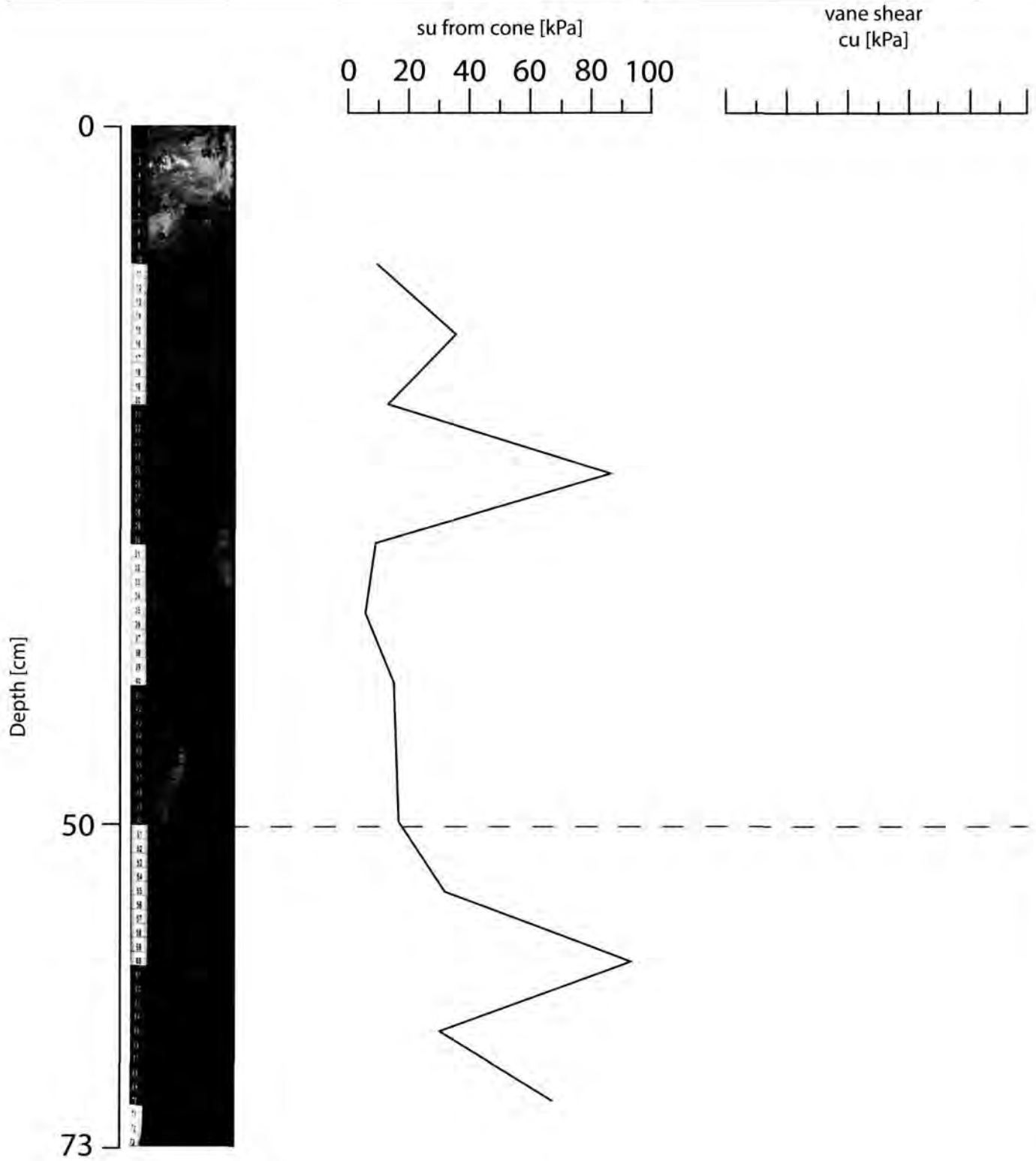

GeoB 15358-3

Date : 26.03.2011 13:37
Water Depth : 3133 m
Study Area : Inner ridge
Cretan Margin

Position : 34° 5.67' N
24° 58.45' E
Core Length : 134 cm

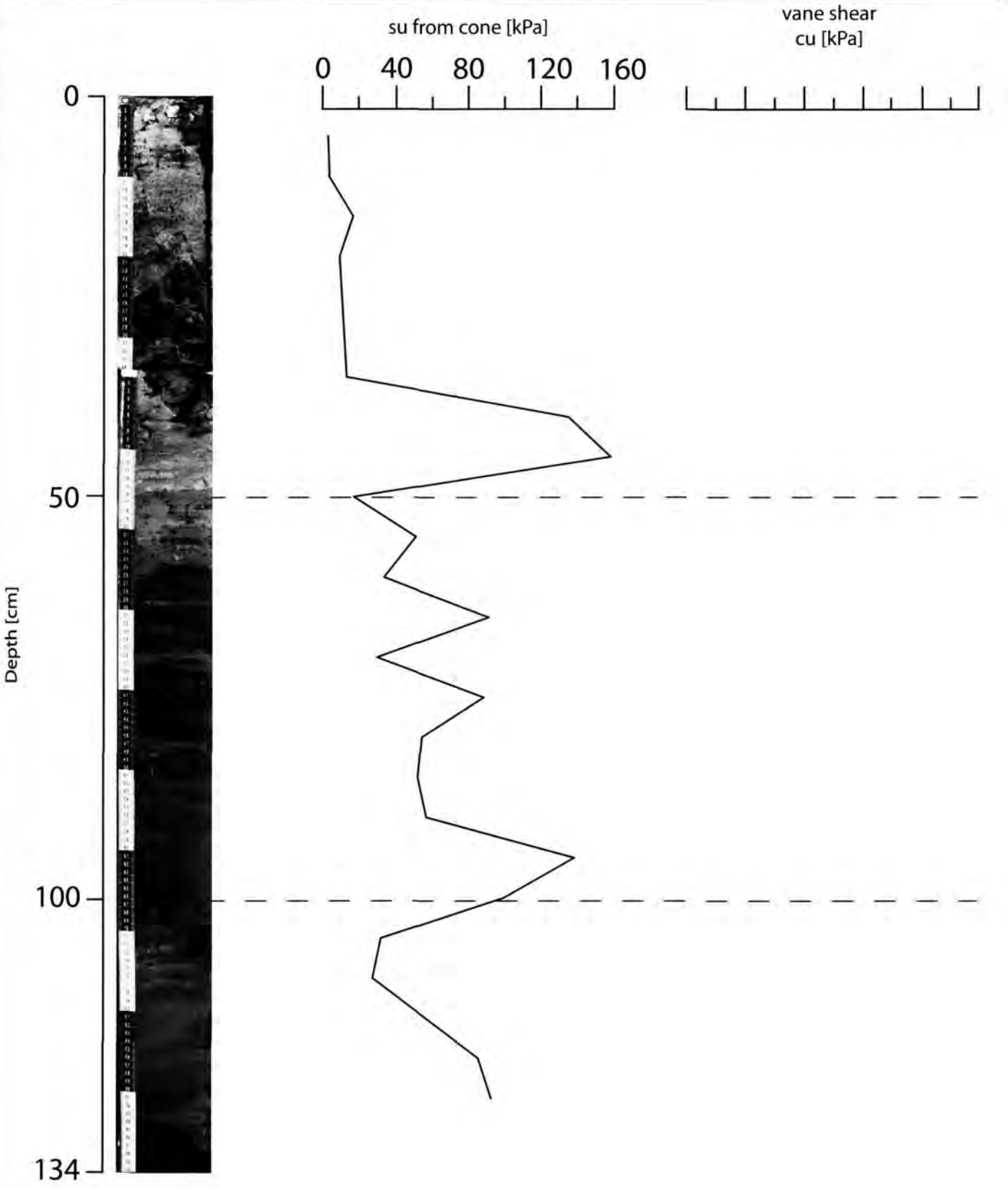

GeoB 15362

Date : 27.03.2011 06:03
Water Depth : 1928 m
Study Area : M.V. Milano

Position : 33° 44.06' N
24° 46.57' E
Core Length : 300 cm

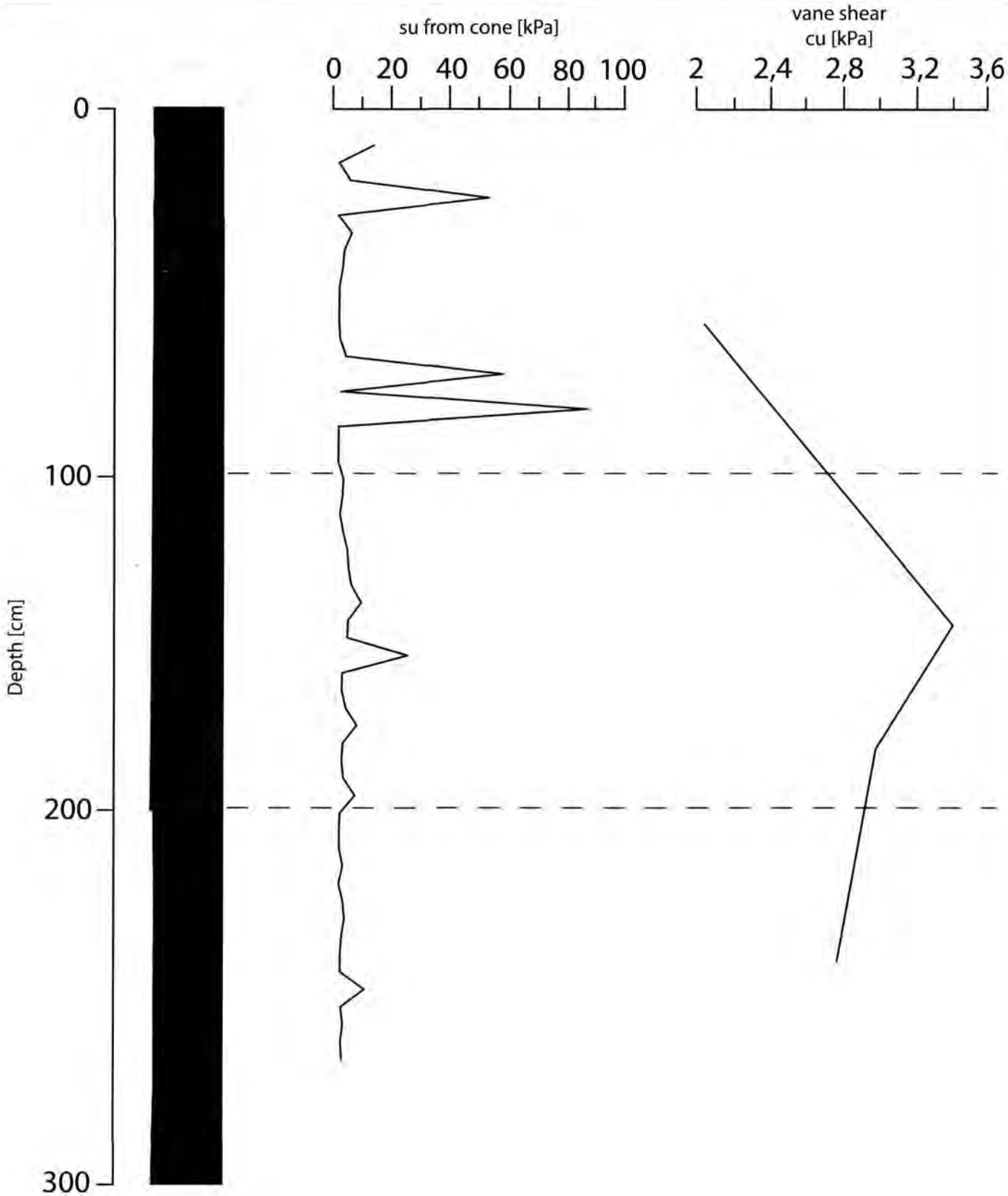

GeoB 15363

Date : 27.03.2011 07:46
Water Depth : 2078 m
Study Area : Milano

Position : 33° 44.116' N
24° 44.848' E
Core Length : 180 cm

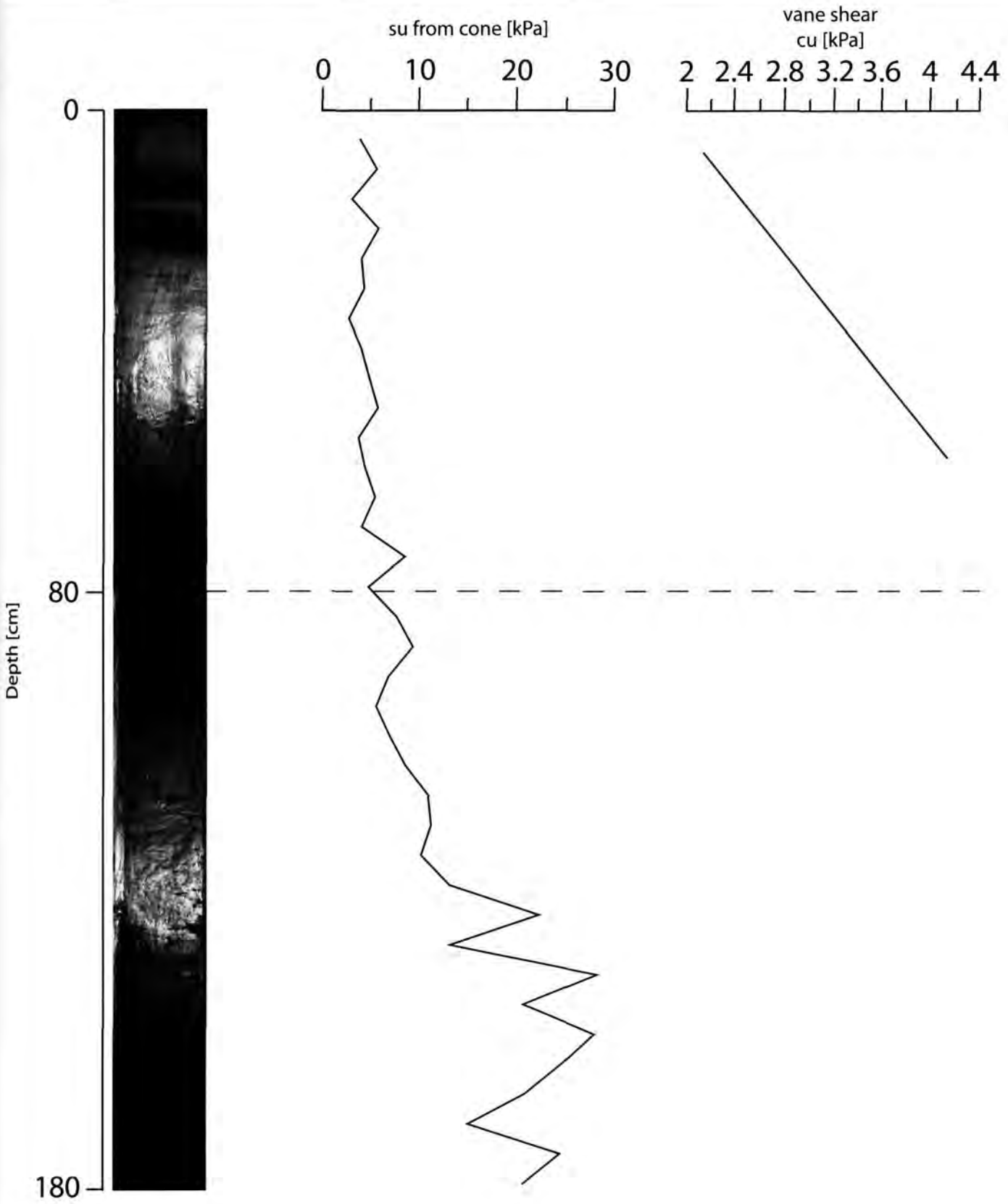

GeoB 15369

Date : 28.03.2011 6:45
Water Depth : 1800 m
Study Area : Maidstone ridge

Position : 33° 40.01' N
24° 32.80' E
Core Length : 324 cm

su from cone [kPa]

vane shear
cu [kPa]

GeoB 15370

Date : 28.03.2011 8:50
Water Depth : 1972 m
Study Area : Maidstone

Position : 33° 37.255' N
24° 40.309' E
Core Length : 200 cm

su from cone [kPa]

vane shear
cu [kPa]

Depth [cm]

0
50
100
150
200